UNIVERSIDAD COMPLUTENSE DE MADRID

FACULTAD DE CIENCIAS FÍSICAS

TESIS DOCTORAL

Assessing the Antarctic sea-level contribution from the Last Glacial Period to the future

Evaluación de la contribución de la Antártida al nivel del mar desde el Último Periodo Glacial hasta el futuro

MEMORIA PARA OPTAR AL GRADO DE DOCTOR

PRESENTADA POR

Javier Blasco Navarro

DIRECTORES

Alexander Robinson
Jorge Álvarez Solas

UNIVERSIDAD COMPLUTENSE DE MADRID
FACULTAD DE CIENCIAS FÍSICAS

TESIS DOCTORAL

Assessing the Antarctic sea-level contribution
from the Last Glacial Period to the future

Evaluación de la contribución de la Antártida al nivel del mar
desde el Último Periodo Glacial hasta el futuro

MEMORIA PARA OPTAR AL GRADO DE DOCTOR

PRESENTADA POR

Javier Blasco Navarro

DIRECTORES

Alexander Robinson

Jorge Álvarez Solas

This thesis was funded by the Spanish Ministry of Science and Innovation under the project MOCCA (Modelling Abrupt Climate Change, grant no. CGL2014-59384-R) and RIMA (Reducing the uncertainty in the evolution of ice sheets, grant agreement No CGL2017-85975-R). All model simulations analysed in this thesis were performed in Brigit (previously EOLO), the High-Performance computing of Climate Change of the International Campus of Excellence of Moncloa, funded by MECD (Ministerio de Eucación, Cultura y Deporte) and MICINN (Ministerio de Ciencias, Innovación y Universidades). Special thanks go to Catherine Ritz for providing the original ice-sheet-shelf model GRISLI (GRenoble Ice Shelf and Land Ice model), subsequently extended by our research group (PalMA) and named as GRISLI-UCM model to be used in the first study in this thesis.

A mi familia

VIII

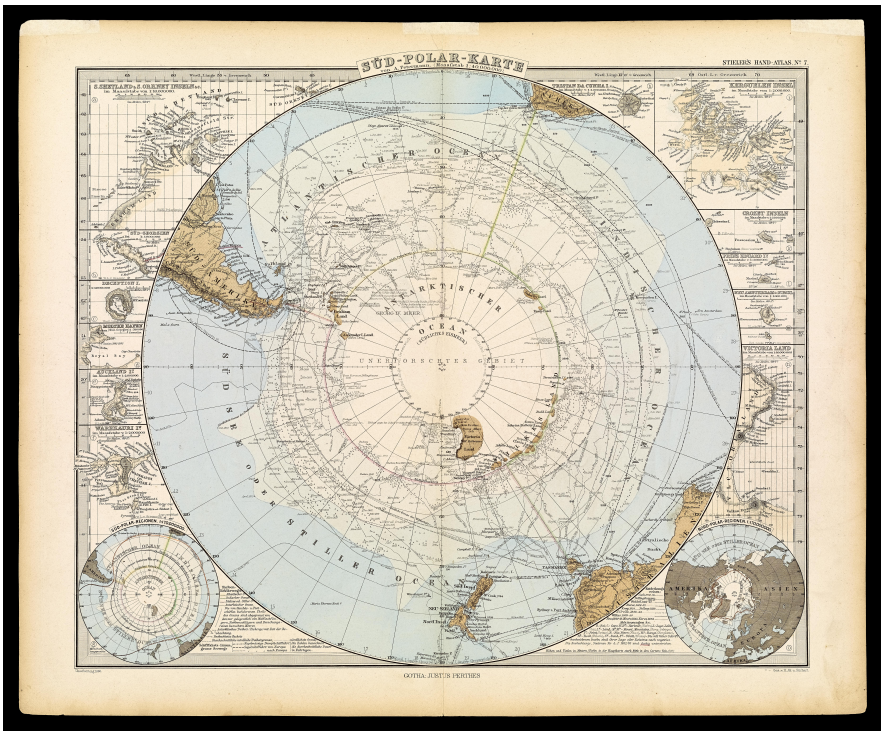

A 19th century south pole map from the German cartographer Augustus Heinrich Petermann. Brown color represents land-known areas, blue color open water, greenish color drift ice and white color permanent ice. In the very center it is written "Unerforschtes Gebiet", the unexplored region. From *Stieler's Hand-Atlas* (Gotha: Justus Perthes, 1890), 7.

Look, my liege. Camelot!
It's only a model.
Shhh.

Monty Python and the Holy Grail.

Contents

Agradecimientos

Esta tesis nace como un cúmulo de circunstancias y casualidades que difícilmente habría imaginado cuando terminé los estudios. Todo comenzó una mañana aleatoria donde tuve la fortuna de encontrarme con la que fue mi profesora Marisa. Y tras varios cafés y alguna charleta en la cafetería de Físicas un día me propuso la idea de realizar mi tesis doctoral. Es difícil describir en unas pocas líneas la gratitud que siento hacia Marisa. No solo por haberme mostrado un campo de la Física que desconocía y ha acabado por cautivarme, sino además por haberme enseñado a desarrollar un espíritu crítico, a no dejar de hacerme preguntas y a disfrutar de lo que hago. Por supuesto, nada de esto habría sido posible sin el trabajo y la constante ayuda de Jorge y Alex, a quienes admiro ya no sólo como científicos, sino también como compañeros y amigos. Jorge, tu pasión por la Ciencia y tu alegría natural son una constante fuente de inspiración. Alex, tu inagotable curiosidad científica y tu perseverancia frente a los problemas me han servido de guía durante todos estos años. Tampoco podré olvidar a Ilaria, mi inestimable vecina de trabajo y (tal y como describe ella) "pareja refunfuñona de 80 años". Como olvidar nuestra preciosa luna miel en Karthaus, nuestras felices bodas de plata en Grindelwald o nuestras fugaces escapadas a los congresos. Haber pasado por todas las fases de tesis juntos, codo con codo, ha hecho esta aventura mucho más fácil.

Por supuesto, tampoco puedo olvidarme de todos los compañeros y compañeras con los que he tenido el gusto y placer de compartir laboratorio y debates a la

hora de comer. Cris R., compañera de cervezas, grupo de consumo, festivales, vacaciones y alumna de guitarra. Dificilmente habría imaginado que nos uniría una amistad tan fuerte, estos años no habrían sido iguales sin ti. Cris V., echaré mucho de menos nuestros cafés a mediodía pero siempre nos quedarán los *telecofibreaks* de los viernes. Félix (¡Qué tío!), has hecho de la hora de comer mi tertulia favorita. ¡Mucha suerte con tu doctorado! Camilo, ojala podamos celebrar nuestras tesis juntos por todos estos años. ¡Que seais muy felices, familia! Dani, ajedrecista, músico y atleta. Tus ganas de aprender y mejorar son envidiables, seguro que te va a ir genial aquí. Norman, nos hemos recorrido España de norte a sur. Habrá que repetir por tierras germanas. Etor, siempre has estado ahí para dar algún consejo ingenioso y añadir tu faceta artística en las presentaciones. Disfruta mucho de tu nueva aventura en Hamburgo. Elena, se te echa de menos por el laboratorio. Gracias por darle ese toque de gracia al grupo con tus comparaciones tan extravagantes. Navarro, compi de la terreta, a ti también te mantienen retenido últimamente. Nos queda pendiente un duelo de paellas. Rubén, gracias por tu bendita paciencia en los inicios. Sin tu ayuda no habría podido llegar hasta aquí. Fidel, he podido aprender muchísimo de ti gracias a tu capacidad comunicativa y divulgativa así como tu forma de afrontar los problemas.

También querría acordarme de todos los colegas que (citando al Dr. Cirera-Salinas) "no ayudaron en absoluto a terminar este trabajo, más bien al contrario" pero me han acompañado durante estos años: Los Scouts (Fede, Pabli, Martín, Bob, Rita, Pau, María, Fabio, Aini, Akela, El Maa, Nabo, Juan, Yago, Charlie, Sebas, Iván, Martino), Los Erasmus (Borja, Piter, Toni, Mose, Luci, Isildur, Roland, Puertas, Maci, Berta, Santi), Los Físicos (Marina, Javi, Laura, Paloma, Chicho, Dani) y gente que he tenido la oportunidad de conocer durante la realización de la tesis (Marta, Cosme, Kili, Ana, Rocío, Serbio, Martí, Vulkan, Lara, María, Carlota, Marina, Aida, Pot, Dani).

Y por último, a mi familia. A tots els meus cosinets i cosinetes, per totes les nits que hem passat (i passarem!) a València menjant carxofes. A mis Yayas por su cariño y paciencia *amb el seu net perdut*. A mi Madre y Padre por apoyarme en todas las decisiones de mi vida y animarme a afrontar retos que creía imposibles. A mis hermanos por alegrarme cada día con sus ocurrencias y humor absurdo. Gracias a todos vosotros y vosotras por hacer de este camino una experiencia mucho más bonita.

List of acronyms

ACC	Antarctic Circumpolar Circulation
AIM	Antarctic Isotope Maxima
AIS	Antarctic Ice Sheet
AMOC	Atlantic Meridional Overturning Circulation
APIS	Antarctic Peninsula Ice Sheet
BP	Before Present
DO	Dansgaard-Oeschger (events)
EAIS	East Antarctic Ice Sheet
EIS	Eurasian Ice Sheet
ELRA	Elastic Litosphere-Relaxing Asthenosphere
EMIC	Earth system Model of Intermediate Complexity
FIS	Fennoscandian Ice Sheet
GCM	Global Circulation Model
GHG	Greenhouse Gas
GIA	Glacial Isostatic Adjustment
GrIS	Greenland Ice Sheet
HE	Heinrich Event
IRD	Ice-rafted debris
ka	Thousand years before present
LGM	Last Glacial Maximum

LGP	Last Glacial Period
LIG	Last Interglacial
LIS	Laurentide Ice Sheet
Ma	Million years before present
MIS	Marine Isotope Stage (e.g. MIS-3, Marine Isotope Stage 3)
MPT	Mid-Pleistocene Transition
NADW	North Atlantic Deep Water
NH	Northern Hemisphere
PD	Present Day
PDD	Positive Degree-Day
SH	Southern Hemisphere
SIA	Shallow Ice Approximation
SLE	Sea Level Equivalent
SO	Southern Ocean
SSA	Shallow Shelf Approximation
SST	Sea Surface Temperature
SSW	Southern Sourced Water
WAIS	West Antarctic Ice Sheet

List of parameters

A_0	Arrhenius Law constant (1.257 $10^{-5}\,a^{-1}\,Pa^{-3}$ for T $\leq$ 263.15 K; 6.042 $10^{-6}\,a^{-1}\,Pa^{-3}$ for T $>$ 263.15 K)
b	Base of the ice sheet (m)
B_{ref}	Reference submarine melting rate, assumed at the present-day ($m\,a^{-1}$)
B	Basal melt (B_{gl}, at the grounding line; B_{sh}, below the ice shelf; $m\,a^{-1}$)
c	Heat capacity of ice (146.3 + 7.253 T[K]) J $kg^{-1}\,K^{-1}$)
g	Gravitational acceleration (9.81 $m\,s^{-2}$)
H	Ice thickness (m)
M	Surface mass balance ($m\,a^{-1}$)
n	Flow law stress exponent
N_{eff}	Effective pressure between ice and water pressure (Pa)
p	Pressure (Pa)
P_{ann}	Annual precipitation ($m\,a^{-1}$)
Q	Activation energy (60 $kJ\ mol^{-1}$ for T $\leq$ 263.15 K; 139 kJ mol^{-1} for T $>$ 263.15 K)
R	Universal gas constant (8.314 $J\ mol^{-1}\ K^{-1}$)
S	Ice surface elevation (m)
T	Temperature (K)
T_{f}	Temperature at the freezing point (K)
T_{atm}	Atmospheric temperature (K)
T_{ocn}	Oceanic temperature (K)
t	time (a)

U	Depth-averaged horizontal ice velocity (=(U,V))
$\mathbf{v}$	Ice velocity (=(u, v, w))
α	Orbital climatic index
β	Millennial climatic index
ΔT_{atm}	Atmospheric temperature anomaly
ΔT_{ocn}	Oceanic temperature anomaly ($\Delta T_{\mathrm{ocn}}^{\mathrm{mil}}$, interstadial-stadial anomaly; $\Delta T_{\mathrm{ocn}}^{\mathrm{orb}}$, glacial-interglacial anomaly)
ϵ_{ij}	Strain rate
η	Ice viscosity
κ	Ice-ocean heat-flux coefficient (oceanic sensitivity; ($m\,a^{-1}\,K^{-1}$))
κ_i	Heat conductivity of ice (9.828 exp(-0.0057 T[K]) $W\,m^{-1}\,K^{-1}$)
ρ	Density of the ice (910 kg m^{-3})
ρ_w	Density of seawater (1028 kg m^{-3})
$\boldsymbol{\sigma}$	Cauchy stress tensor
τ_{ij}	Deviatoric stress
τ_{b}	Basal drag term
τ_{d}	Driving stress

Summary

Introduction

Sea-level rise is one of the biggest threats to modern humankind. The Antarctic Ice Sheet (AIS) plays an important role in future projection, as it is the largest ice sheet on Earth, and hence the potential major contributor. However, as put in the Intergovernmental Panel on Climate Change (IPCC) fifth report, the AIS is also the largest source of uncertainty to sea-level rise. Part of this uncertainty arises due to uncertain future projections. Another source relies on the underlying mechanisms that drive the evolution of large continental ice sheets. Basal friction as well as ice-ocean interactions are probably one of the most important, and yet unknown, building blocks in defining the evolution of the AIS. This occurs because basal and sub-shelf processes are compounded into complex systems which are highly unconstrained. Through satellite observations it is possible to infer properties of these features but it does not give information about how it evolved in the past or the future. A way to gain insight into sub-shelf melting and basal friction, as well as future projections, is through paleo-modeling studies. Paleo-modeling studies are essential tools, as they allow not only analysis of the behaviour of ice sheets under past climatologies, but also to investigate the role of different features, such as ice dynamics, and compare with proxy data. Thus, through such an analysis, a better understanding of basal friction as well as ice-

ocean interactions is possible and it is applicable to the future evolution of the AIS.

Aim of this thesis

The goal of this thesis is to study the potential Antarctic sea-level contribution since the Last Glacial Period (LGP) to the future. This issue has been already tackled by different studies, however, rather than to give a precise quantity, this thesis aims to assess the AIS sea-level uncertainty at these periods due to different boundary conditions, such as the ice-ocean interactions, climatologies and basal friction conditions. For this purpose, the thesis is structured in a chronological order. First, the role of the ocean at glacial millennial timescales is investigated. To this end, this first part of the study focuses on the LGP. Then, the role of friction at the marine regions, as well as the atmospheric boundary conditions, is investigated for the simulation of an Antarctic Last Glacial Maximum (LGM) state. Finally, the third study evaluates the role of different friction laws for the Antarctic deglaciation, from the LGM to present-day (PD) conditions, and then, how the ice sheet responds to different global warming scenarios using these different friction laws. These three studies allow the estimation of a range of plausible AIS sea-level contributions since the LGP to the future.

Results

The first study investigates the role of the ice-ocean interactions in the AIS during the LGP. Sea-level reconstructions during that period show rapid sea-level variations of around 20 meters at millennial timescales. This points to a rapid response of large continental ice sheets to abrupt climate changes The origin of these sea-level fluctuations has been classically assigned to North Hemisphere (NH) paleo-ice sheets as more ablation occurs. Millennial-timescale fluctuations are also found in Antarctic records in phase with sea-level fluctuations. Nonethe-

less, these warming event are less pronounced and modeling studies of the AIS have not paid much attention to this issue as the response is expected to be negligible. However, by invoking the bipolar seesaw mechanism, one could hypothesize that the ocean also warms in phase with the observed atmospheric warming. This first study analyses for the first time the impact of millennial-scale oceanic variation during glacial periods on the AIS. The results suggests that when oceanic forcing is considered, then the AIS is capable of producing a non negligible sea-level contribution during the LGP.

The second study explores the impact of two sources of uncertainty on simulating an Antarctic LGM state, mainly atmospheric boundary conditions and basal friction. Assessing the sea-level budget of large continental ice sheets at the LGM has proven to be challenging and proxy data are not fully in agreement with model reconstructions. Furthermore, Antarctic model results show large discrepancies. This occurs partly because boundary conditions during the LGM are not well known, adding a degree of difficulty. Whereas marine and terrestrial geological records serve to constrain the extension of ice sheets at this period, the total amount of ice volume remains unknown. The total ice content is strongly determined by the boundary conditions, such as the atmospheric climatology and basal friction conditions. Although the overall climatic conditions are expected to be colder and drier during the LGM, they remain uncertain for localized regions. Also basal friction plays a crucial role as it has the potential to generate more (or less) ice streams affecting the total ice volume. The results of this second work show that climatologies as well as dynamics have a similar impact on the uncertainty in the simulation of an AIS state contributing to an uncertainty range of 7 meters sea-level equivalent.

Finally, the third study investigates the role of different friction laws in the evolution of the AIS, since the LGM to the future, for different warming scenarios. Projections of the AIS for future global sea-level rise are highly uncertain to a large extent due to the potential collapse of the marine sectors. Whether such an instability is already underway or is far away from being triggered remains unclear, partly due to the lack of knowledge of basal dragging conditions. The impact of the friction law on the future evolution of the AIS has been recently

investigated other studies, but these experiments are run from an equilibrated PD, tuned to observational data. This procedure neglects the thermal memory of the AIS and a potential drift, driven by the onset of the last deglaciation. Thus, this work assesses the future evolution of the AIS with an ensemble of simulations using different friction laws that are constrained to be consistent with realistic LGM and PD states. The main results are that the warming scenario is the main driver of future sea-level rise, as expected. Nonetheless, at short timescales, the choice of friction law plays a critical role as more inland ice can be accelerated faster, producing more ice discharges into the ocean.

Main conclusions

All these studies point to the high sensitivity of the marine parts of the AIS to oceanic warming and friction configurations. On one hand, oceanic perturbations at short timescales can lead to an abrupt retreat on the marine parts of a fully extended LGM AIS. Also, oceanic warming is the main driver of future sea-level rise, leading to a potential collapse of the western part of the AIS. On the other hand, different friction configurations have the capability of simulating dynamically faster (or slower) ice sheets in agreement with proxy data. These configurations respond differently to future climate warming. Although there are large uncertainties associated to ice-ocean interactions, as well as to basal friction, this thesis assesses the influence of these two issues for simulating the evolution of the AIS.

Resumen

Introducción

Una de las consecuencias del aumento de temperaturas por emisiones antropogénicas es la subida del nivel del mar causada por el deshielo. La Antártida juega un papel importante en la predicción de estimaciones de aumento del nivel del mar ya que es el mayor manto de hielo de la Tierra. Sin embargo, según el quinto informe del Panel Intergubernamental de expertos del Cambio Climático, la Antártida es también la mayor fuente de incertidumbre a este respecto. Esta incertidumbre está asociada por una parte al aumento de las temperaturas atmosféricas y oceánicas en los próximos años y por otra parte al hecho de que los modelos de mantos glaciares no resuelven todos los mecanismos subyacentes con precisión. En particular, la fricción que ejerce el lecho rocoso sobre el glaciar, así como las interacciones hielo-océano constituyen dos componentes básicos que no están representados correctamente en modelos de hielo. A través de observaciones de satélite es posible inferir propiedades en la base de mantos glaciares, sin embargo, no permiten obtener información sobre la evolución pasada o futura. Una forma de profundizar las interacciones hielo-océano y fricción basal es a través de estudios de paleo modelización. Estos estudios constituyen herramientas esenciales ya que no solo permiten analizar la evolución de los mantos de hielos a otros climas, sino también la sensibilidad de diferentes parámetros y comparar con datos observacionales. A través de estos análisis se puede adquirir un mayor

conocimiento de las interacciones hielo-océano así como de la dinámica del hielo y aplicar a la evolución futura de la Antártida.

Objetivo de la tesis

El objetivo de esta tesis es estudiar la contribución antártica a la evolución del nivel del mar desde el Último Periodo Glacial (UPG) hasta el futuro. Esta tarea ya ha sido investigada en otros estudios, por ello, más que dar una cantidad específica, el objetivo es evaluar cómo varía la contribución antártica si se consideran diferentes condiciones de contorno. Concretamente, se investiga la sensibilidad oceánica, las condiciones climatológicas y las condiciones basales. Para ello, esta tesis se estructura en orden cronológico. La primera parte del estudio se centra en el papel que jugó el océano a escalas milenarias durante el UPG. La segunda parte del estudio se centra en el Último Máximo Glacial (UMG) y se evalúa cómo afecta la fricción en las zonas marinas de la Antártida, así como diferentes condiciones climatológicas. Por último, el tercer estudio evalúa con que precisión representan diferentes leyes de fricción la deglaciación desde el UMG al presente y cómo responden a diferentes escenarios de cambio climático antropogénico.

Resultados

El primer estudio investiga la influencia del océano en la Antártida durante el UPG. Las reconstrucciones del nivel del mar en ese periodo muestran variaciones de unos 20 metros a escalas de tiempo milenarias. El origen de estas fluctuaciones se atribuye a los grandes mantos de hielo situados en el hemisferio norte, ya que están expuestos a más procesos de ablación. Los testigos de hielo en la Antártida también muestran calentamientos en sintonía con los cambios del nivel del mar. Sin embargo, estos calentamientos son tan bajos que los estudios de modelización han considerado que la contribución de la Antártida al nivel del mar debe ser nula o insignificante. No obstante, mediante el mecanismo del balancín bipolar,

el océano se puede calentar también en fase con la atmósfera, provocando una respuesta del manto antártico no desdeñable. El primer estudio de esta tesis investiga por primera vez el impacto de las variaciones milenarias en épocas glaciales, y en particular de las variaciones oceánicas en la Antártida. Los resultados muestran que los calentamientos oceánicos pueden provocar un aumento del nivel del mar de hasta 6 metros durante el UPG.

El segundo estudio investiga el impacto de dos fuentes de incertidumbre, que son las condiciones atmosféricas y la fricción basal, para simulaciones de la Antártida en el UMG. Al examinar las reconstrucciones del nivel del mar durante el UMG y comparar con los resultados de diferentes modelos, se observa que existen discrepancias entre ellos. En el caso de la Antártida, a partir de los registros marinos y terrestres es posible determinar su extensión durante el UMG, sin embargo no es posible inferir la cantidad de hielo acumulado. Parte de esta diferencia entre modelos y reconstrucciones se debe a las condiciones de contorno, y más concretamente, las condiciones climatológicas y la fricción basal. Por un lado, respecto a las condiciones climatológicas, se sabe que era una época más gélida, aunque se desconoce cuál era la distribución espacial a lo largo de toda la Antártida. Por otro lado, la fricción basal juega un papel crucial en la evolución antártica, ya que afecta a la dinámica de las corrientes de hielo. No obstante, existen muy pocos indicadores que permitan conocer las condiciones dinámicas de la Antártida durante el UMG. Los resultados de este segundo trabajo muestran que tanto las climatologías como la dinámica del hielo son dos fuentes de incertidumbre importantes que contribuyen a variaciones de hasta 7 metros en el nivel del mar.

Por último, en el tercer estudio se investiga el papel de diferentes leyes de fricción en la evolución de la Antártida, desde el UMG hasta el futuro, para diferentes escenarios de emisión antropogénica. Las previsiones para el futuro de la Antártida son altamente inciertas debido a un posible colapso de las zonas marinas. Existen dudas sobre si el mecanismo que impulsa este colapso ya ha podido ser desencadenado o no. Parte de esta incertidumbre surge porque los modelos de criosfera utilizan diferentes leyes de fricción. Además, muchos estudios parten de una configuración presente idealizada donde diferentes parámetros han

sido optimizados para emular un manto de hielo casi perfecto. Sin embargo, estas optimizaciones ignoran una potencial deriva causada por la última deglaciación. Por ello, este trabajo investiga varias configuraciones de parámetros que simulan una deglaciación realista para diferentes leyes de fricción. Aquellos parámetros que simulan correctamente un estado glacial y un estado presente son forzados luego a diferentes escenarios de emisión antropogénico. La principal conclusión es que el futuro de la Antártida está dictaminado por el escenario de emisión antropogénico. Sin embargo, a escalas de tiempo cortas, la elección de ley de fricción es crucial ya que puede fomentar una mayor aceleración del hielo que a su vez fomenta una mayor descarga de hielo al océano y la consiguiente subida del nivel del mar.

Conclusiones generales

Estos tres estudios analizan la sensibilidad, especialmente de las zonas marinas de la Antártida, a cambios de temperaturas oceánicas y a diferentes configuraciones de fricción basal. Por un lado, se demuestra que perturbaciones oceánicas a escalas milenarias pueden provocar un retroceso de la línea de tierra en un estado glacial de la Antártida. También, que en las previsiones de futuro, el aumento de las temperaturas oceánicas es la principal causa del aumento del nivel del mar y un colapso de la Antártida occidental. Por otra parte, diferentes configuraciones de fricción basal tienen el potencial de simular corrientes de hielos, más o menos rápidas, acordes con las observaciones. Estas configuraciones responden de diferentes maneras a cambios climáticos. A pesar de las grandes incertidumbres que existen en las interacciones hielo-océano y fricción basal, esta tesis trata de arrojar algo de luz en la evolución de la Antártida.

Chapter 1
Introduction

This chapter introduces the Antarctic Ice Sheet (AIS) and discusses its role in the climate system. First, a general review of the AIS is made, where present-day conditions of the AIS and potential future scenarios are described (Section 1.1). Then, the past glacial history of Antarctica is reviewed based on proxy data (Section 1.2), focusing both on orbital and millennial-scale variability. Special focus is given to the bipolar-seesaw mechanism, as it plays an important role in the evolution of the AIS. Section 1.3 summarizes the development of ice-sheet models and describes specifically their state of the art applied to the AIS. Recent technical improvements, as well as limitations, and current major challenges are briefly described. Finally, the main motivations of this thesis are laid out (Section 1.4) and the overall structure of the work is outlined (Section 1.5).

1.1 The Antarctic Ice Sheet (AIS)

Though the AIS is the largest ice sheet on Earth, it was not until 1820, when Fabian Gottlieb von Bellingshausen discovered the vast icy continent. It covers ca. 14 million km^2 and stores a total ice volume of 26 million km^3, corresponding to a sea-level equivalent (SLE) of around 58 m (Fretwell et al., 2013). Geographically, the AIS is located at the south pole, surrounded by the Southern Ocean (SO). The SO is governed by the strong east-flowing Antarctic Circumpolar Current (ACC),

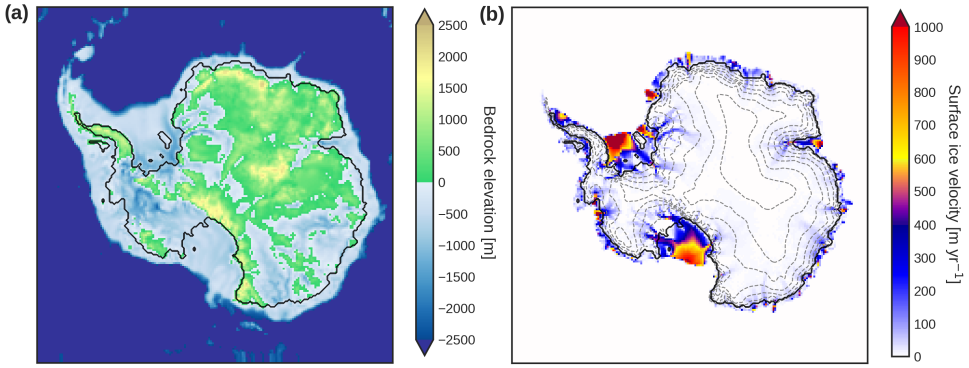

Fig. 1.1: **(a)** Bedrock elevation from Schaffer et al. (2016) interpolated onto the 32km x 32km grid used in this thesis. **(b)** Observed surface ice velocities from Rignot et al. (2013). Grey discontinuous lines are surface elevation contours drawn every 500 m up to 3500 m from Schaffer et al. (2016). The black lines shows the observed present-day grounding-line position.

which isolates the AIS from warmer penetrating waters (Martinson, 2012). In addition, the strong polar easterlies and katabatic winds make Antarctica one of the most arid regions and the coldest place on Earth, with the lowest natural temperature ever directly recorded (-98°C). Due to these hostile conditions, life is not as prevalent as on other continents.

The AIS plays a fundamental role in the Earth System and it is crucial to understand how it responds to climatic changes. First, the AIS has the potential to increase sea level substantially. Sea-level rise (SLR) is one of the main threats of global climate change, especially for the coastal regions and poorest countries (King and Harrington, 2018). Coastal regions are more densely populated than inland zones, which may lead to massive mobilization of population with high SLR (Neumann et al., 2015). In addition, in arid zones with low rainfall like Egypt or India, SLR could contaminate coastal aquifers with salt water (Sherif and Singh, 1999). Small islands, in the Pacific Ocean for instance, would also be in danger of disappearing (Ourbak and Magnan, 2018). Additionally, if the AIS loses ice, then the surface albedo diminishes at the margins and the Earth can

heat up even more. It is clear then, that understanding its role within the Earth System, especially in a world with risks of warming temperatures, is important.

The AIS can be divided into three parts: the East Antarctic Ice Sheet (EAIS), the West Antarctic Ice Sheet (WAIS) and the Antarctic Peninsula Ice Sheet (APIS). The EAIS is the largest part of the AIS and stores around 53 of its total 58 meters of sea-level equivalent (msle; Fretwell et al. 2013). It is, in its vast majority, a land-based ice sheet, i.e. the grounded ice lies on bedrock above sea level (Fig. 1.1a). Its coastlines are surrounded by small ice shelves (i.e. floating ice caps) in contact with ocean water. The total mass balance of ice sheets is determined by ice accumulation and ablation at the surface, calving of icebergs at the ice-shelf front and melting at the base of ice shelves. In the EAIS there is no ablation, hence only calving and basal melting can contribute to mass loss. The latest satellite data show a positive mass balance (i.e. ice gain), of 5 Gt yr^{-1} since 1992 (Martin-Español et al., 2016, 2017; Shepherd et al., 2018), however, on a longer timescale, since 1979, the EAIS shows a negative mass balance (i.e. mass loss) of 51 Gt yr^{-1} (Rignot et al., 2019). Separated by the Transantarctic Mountains lies the WAIS, the second largest ice sheet of the AIS with a sea-level content of around 4 msle. Contrary to the EAIS, the WAIS is in its vast majority a marine-based ice sheet, i.e. its grounded ice lies on bedrock below sea level (Fig. 1.1a). Mass balance measurements show that this is the region that is losing mass more rapidly from the AIS, with a total ice discharge of around 94 Gt yr^{-1} since 1992 and 159 Gt yr^{-1} since 1979. As in the EAIS, in this region, temperatures are not warm enough to produce ablation at the ice surface, therefore all the mass is lost due to calving at the ice front, and basal melt at the ice-shelf base. A remarkable characteristic of this ice sheet is that it contains the two largest ice shelves on Earth, the Filchner-Ronne and the Ross ice shelf, which have a combined extent of 1.5 million km^2 and rather high velocities, up to 4 km yr^{-1}($Fig.1.1b$). As confirmed by observations, all the mass is lost due to calving at the ice front, and basal melt at the ice-shelf base (Rignot et al., 2013; Paolo et al., 2015; Liu et al., 2015). It is clear then, that the ocean plays a crucial role for the WAIS. Finally the APIS, a mountainous region of Antarctica, is the smallest ice sheet of the three, and stores less than 1 msle. Summer temperatures in this

region are high enough to allow for ablation, and its net annual mass balance is also negative, around 20 Gt yr^{-1} since 1992. The overall resulting mass balance of the AIS gives a negative rate of nearly 500 Gt yr^{-1} which corresponds to a total SLR of nearly 13.9 mm since 1979 (Rignot et al., 2019), similar to the Greenland Ice Sheet (GrIS), whose mass loss has raised sea-level by 13.7 mm since 1972 (Mouginot et al., 2019).

Whether this mass loss of the AIS is caused by humankind or due to internal climatic variability is a matter of debate. In the Fifth Assessment Report of the United Nations Intergovernmental Panel on Climate Change (IPCC) (Bindoff et al., 2013) the rapid melting in Greenland is likely associated to anthropogenic emissions but remained inconclusive for the AIS. Recently, Holland et al. (2019) showed that internal climate variability cannot reproduce mass loss observations of the AIS if anthropogenic forcing is not taken into account.

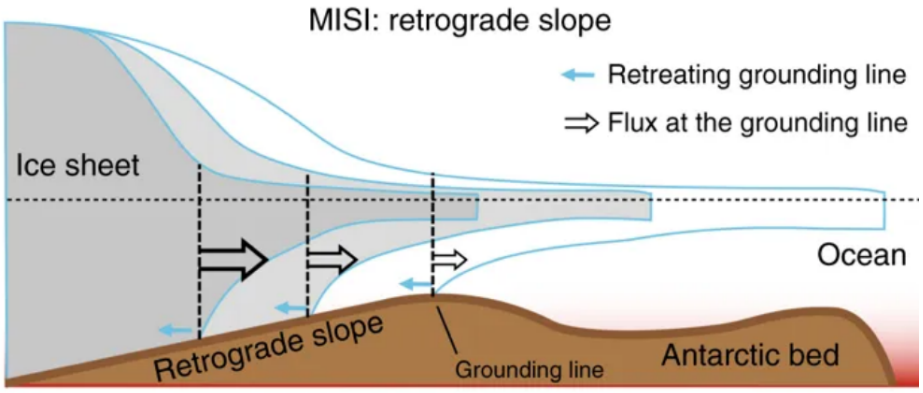

Fig. 1.2: Representation of the MISI mechanism. A grounding-line retreat in a retrograde slope can increase the flux at the boundary which then results in a positive feedback, displacing the grounding-line into deeper waters (from Pattyn, 2018).

In the last years special focus has been given to ice-ocean interactions, as it can lead to potential instabilities in the WAIS. First, an increase in oceanic tem-

peratures would boost melting at the base of the ice shelves and shrink their size (Schmidtko et al., 2014; Sallée, 2018). Floating ice does not directly contribute to sea-level rise. However, some ice shelves, depending on their degree of confinement, have a buttressing effect on the ice sheet (Fürst et al., 2016). If such ice shelves reduce their size, their buttressing effect diminishes and the outflow of inland ice is accelerated. Faster ice leads to increased ice discharge into the ocean which contributes to sea-level rise. This effect of inland ice accelerating after the collapse of an ice shelf was observed in Year 2002 after the collapse of the Larsen B ice shelf (Rignot et al., 2004; Scambos et al., 2004).

The AIS may furthermore be subject to an inherent instability specific to marine ice sheets (Fig. 1.2). A change in the ice flow also changes the ice flux at the grounding line, the border between the grounded and the floating ice or ocean. Variations in the grounding-line flux are the ultimate drivers of an ice sheet advance and/or retreat. If a marine-based ice sheet retreats on a downward-sloping (retrograde) bedrock, an internal positive feedback is triggered: Ice flux at the grounding line increases as the ice thickness becomes larger, causing a further retreat until the grounding line reaches a positive bedrock slope where it does not retreat. This mechanism is known as the marine ice sheet instability (MISI, Weertman (1974); Schoof (2007)). Mercer (1978) presaged that if the oceanic temperatures increase, this could lead to a potential collapse of the WAIS. A collapse of the WAIS is considered a tipping point in nature as it may involve an abrupt, irreversible transition between two states, which could be triggered by the loss of buttressing effect (Lenton et al., 2019). Grounding-line migrations as seen in the Pine Island Glacier have been claimed to hint that this mechanism could be underway (Jacobs et al., 2011; Favier et al., 2014). It is believed that it may have occurred in the past (Pollard and DeConto, 2009; Sutter et al., 2016) and that it could happen again in the future, contributing to a sea-level rise of 3 to 5 meters, depending how much inland ice will accelerate (Bamber et al., 2009; Joughin and Alley, 2011; Feldmann and Levermann, 2015; Golledge et al., 2015). Recent studies have begun to propose tactics to prevent future sea-level rise associated to the MISI mechanims using artificial snow accumulation (Feldmann et al., 2019) or geoengineering, such as creating an artificial sill (Wolovick and

Moore, 2018). In addition to this, some models predict that the future potential sea-level contribution from the AIS could be underestimated and that certain processes such as enhanced snowfall in the EAIS (Winkelmann et al., 2012) or the controversial ice cliff instability mechanism (MICI; DeConto and Pollard 2016) could raise the sea-level rise risk further.

For these reasons it is important to understand the response of AIS to climatic changes and its potential effects on the Earth System (Golledge et al., 2019). In order to better constrain AIS sensitivity, its important to quantify its past evolution and to identify the relevant underlying mechanisms of ice sheets. Proxy data, such as moraines, marine sediments and ice cores, provide information to estimate past boundary conditions, such as oceanic or atmospheric temperatures or the ice extent as well as the past configuration of the AIS. The comparison of ice-sheet model results together with proxy data, allows for a comprehensive understanding of the ice sheet behaviour. But first, its necessary to describe the past evolution of the AIS and what is known.

1.2 The history of the AIS

1.2.1 Formation of the Antarctic Ice Sheet

Ice formation in Antarctica is thought to have begun around 34 Million years ago (Myr BP), when atmospheric CO_2 concentrations lowered below a threshold of 750 parts per million (ppm) during the Eocene-Oligocene transition (Coxall et al., 2005; Pearson et al., 2009). Sedimentary records also support the onset of orbitally driven waxing and waning of the AIS, identified with the beginning of early glacial cycles in this time-period (Zachos et al., 1996). This initial ice sheet was at first restricted to the land-based zones of the EAIS and subsequently evolved to modern-like volumes in line with global CO_2 atmospheric drops (Galeotti et al., 2016). At around 25 Myr BP the Drake Passage, which connected the Antarctic continent to South America, opened up, facilitating a pathway for circumpolar currents, giving rise to the formation of the strong ACC at the

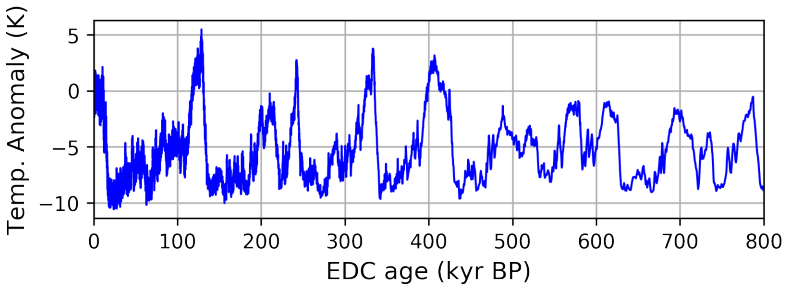

Fig. 1.3: Temperature reconstruction from the Dome C ice core (from Jouzel et al., 2007).

Southern Ocean (Barker and Burrell, 1977). These currents cooled and isolated thermally the Antarctic continent, which together with a continuous drop in CO_2 concentrations, enhanced the formation of a vast ice sheet (DeConto and Pollard, 2003). Since then, the AIS has fluctuated between cold and warm states, within glacial cycles.

1.2.2 The physics of the glacial cycles

The theory of the glacial cycles was proposed in the publication "Kanon der Erdbestrahlung und seine Anwendung auf das Eiszeitenproblem" of Milankovitch (1941). Milankovitch proposes three main cycles that control the occurrence of glaciation periods: Changes in precession (i.e. shifts in the orientation of the Earth's rotational axis) with a periodicity of around 23 kyr; changes in the axial tilt (i.e. the inclination of the Earth's axis with the plane of the Sun and the orbit), whose periodicity is about 40 kyr; and changes in eccentricity (i.e. the shape of the Earth's orbit), with a periodicity of around 100 kyr. However, it was not until 1976 when Hays, Imbrie and Shackleton finally confirmed in paleoreconstructions the periodicities predicted by Milankovitch, that the origin of the Quaternary glacial cycles were caused by changes of the Earth's orbit with respect to the

Sun, confirming the success of Milankovitch theory (Hays et al., 1976). Since then, it is broadly assumed that the origin of these glacial cycles is related to the incoming summer solar radiation at high northern latitudes. The imprints of glacial cycles have been observed in different records, from ice cores to marine sediments and terrestrial records, as well as in sea-level reconstructions (Paillard 2015 and references therein).

The recorded glacial cycles have a characteristic saw-tooth form signal. It begins with a warm state, defined as an interglacial period. An interglacial period is characterized by high concentrations of atmospheric greenhouse gases (GHGs), high global temperatures, and hence high precipitation, and high sea-level standings, as a result of the shrinking of the continental ice sheets. The warm state is followed by a slow cooling which lasts for several thousands of years, till it reaches its minimum, defined simply as glacial state. A glacial state is characterized by low concentrations of GHGs, low global temperatures, less precipitation and low sea-level standings, and hence a large ice-sheet extent (e.g. Bradley 1985; Crowley and North 1991; Paillard 2015 and many others). In the Antarctic ice core records, a temperature minimum corresponds to a drop of around 10 K with respect to the interglacial stage. A glacial cycle finishes with an abrupt warming, or deglaciation (lasting around 10 kyr), returning to a warm state.

The imprints of glacial cycles in Antarctica are registered in ice cores, where a total of ten deep cores have been extracted. In the year 2004, the deepest ice core was drilled, the Epica Dome C ice core (EDC, EPICA Community Members (2004)). This ice core extends back to 800 kyr BP and shows eight glacial cycles with the dominant frequency being the eccentricity component ($\sim$ 100 kyr periodicity). In the coming years, the Epica project "Beyond Oldest Ice" expects to extract an ice core with up to 1.5 Myr old ice (Schiermeier, 2019). This time period is of enormous interest as it coincides with the Mid-Pleistocene Transition, when the glacial cycles changed from a dominant frequency of 41 kyr (obliquity) to 100 kyr (eccentricity) (Clark et al., 2006). Of particular interest is the last glacial period (LGP). Being so recent, proxy records from that time period have a higher temporal resolution than previous glacial cycles. Because deeper ice core

layers can melt at the base, merge with other layers and even fold, reconstruction of the rest of glacial cycles are more uncertain (Steig, 2008).

1.2.3 The Last Glacial Period (LGP)

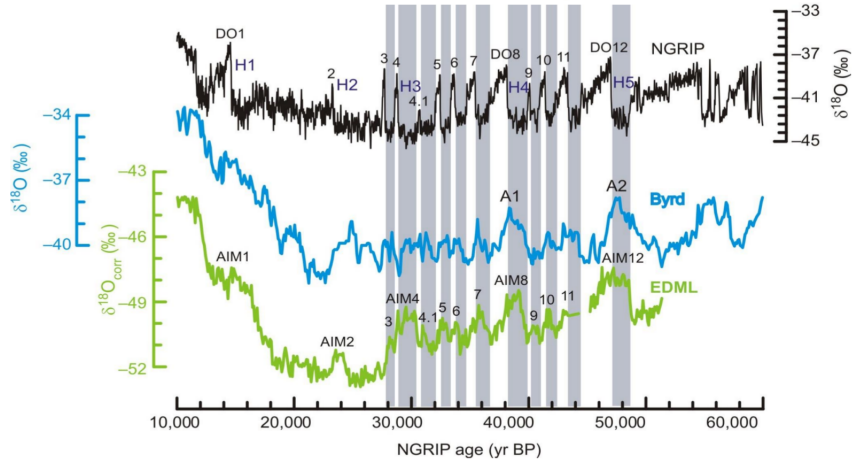

Fig. 1.4: Oxigen isotope δO^{18} record from NGRIP (black curve), Byrd (Blue curve) and EDML (green curve) ice core. The shaded grey areas represent the stadial conditions before a Dansgaard-Oeschger event (DO numerical labeled), whilst the Antarctic ice cores show a gradual warming. Antarctic Isotope Maxima (AIM) coincide with the DO interstadials (from EPICA, Community Members, 2006).

The LGP extents from 115 ka BP (just after the end of the Last Interglacial; LIG) to 10 ka BP (the onset of the Holocene). The LIG is of particular interest as it is a slightly warmer climate than present day (PD), which could increase understanding of future rising-temperature scenarios. The LIG began about 130 ka BP and was a warmer period than the Holocene, by around 2 degrees globally

(Otto-Bliesner et al., 2013; Bakker et al., 2014), with sea-level estimates between 6 to 9 m higher than present day (Siddall et al., 2003; Kopp et al., 2009; Dutton and Lambeck, 2012). This pronounced sea-level high stand is mainly caused by ice-sheet loss with a marginal contribution from land glaciers and thermal expansion (McKay et al., 2011; Marzeion et al., 2012; Dutton et al., 2015). Different studies suggest a collapse of the WAIS as the main contributor to this estimate, between 3-4 msle (Scherer et al., 1998; Sutter et al., 2016) as sea-surface temperatures in the Southern Ocean were likely warmer than today (Capron et al., 2014). This issue has aroused special interest, as climatic conditions were similar to the present, pointing to a potential WAIS collapse in the future (DeConto and Pollard, 2016). However, Holloway et al. (2016, 2017) concluded that an increase in δ^{18}O in Antarctic ice cores at the LIG, which was associated with a WAIS collapse, could also be explained by sea-ice retreat, leaving the WAIS configuration intact. Furthermore, Wilson et al. (2018) provided evidence from marine sediments and terrestrial records, that the Wilkes sub-glacial basin in the EAIS retreated in warm interglacials. Thus, whereas it is well established that the AIS contributed to sea-level rise, its precise origin remains unknown. However the high sea-level stand at the Eemian is generally attributed to marine based regions and oceanic temperature changes.

The LGP started with a gradual cooling which lasts 80 kyr, till it reaches its minimum at around 21 kyr BP, known as the Last Glacial Maximum (LGM) with an Antarctic temperature drop of about 10 K (Jouzel et al., 1987, 2007; Kawamura et al., 2007). At the LGM, the measured sea-level stands, derived from fossil corals, was between 120 m to 130 m lower than PD (Hanebuth et al., 2000; Clark and Mix, 2002; Austermann et al., 2013; Yokoyama et al., 2018). The dominant part of these lowstands come from Northern Hemisphere (NH) paleo ice sheets, mostly from the Laurentide Ice Sheet (LIS) and the Fennoscandian Ice Sheet (FIS), which stored more than 90 msle (Simms et al. (2019) and references therein). On the other hand, the accumulated ice content of Antarctica must have oscillated between 10-20 msle (Simms et al., 2019). Dating methods and field mapping as well as our knowledge of glacier physical processes allow precise ice extension measurements of paleo ice-sheets. However, assessing the sea-level

budget at the LGM of individual ice sheets is still a challenging task (Clark and Tarasov, 2014; Simms et al., 2019).

The LGP finished with an abrupt warming which lasted around 10 kyr, into PD-like conditions. This warming is accompanied by an abrupt increase in sea level pointing to a fast response of ice sheets to climate changes (Fairbanks, 1989; Clark et al., 2004). The reason for the asymmetry between a smooth and gradual cooling, and a fast warming, is that several positive feedbacks are involved during the deglaciation. As ice sheets shrink, their albedo lowers. In addition to this, CO_2 from the ocean is released as temperatures increase, further increasing the GHG effect (Galbraith et al., 2007; Schmitt et al., 2012; Shakun et al., 2012). Additional potentially relevant feedbacks are the increase of freshwater fluxes into the ocean, which perturbs the Atlantic Meridional Overturning Circulation (AMOC). This enhances heat transport from the Atlantic ocean towards higher latitudes promoting melting (Manabe and Stouffer, 1995; Thornalley et al., 2010). All these processes together have a cascade effect with a strong impact on the global climate.

This LGP orbitally-driven signal has not only been observed in Antarctic ice cores, but also Greenland ice cores, as well as benthic-foraminifera $\delta^{18}O$ records from marine sediments and terrestrial records, suggesting that it is a global phenomenon (Bond et al., 1992; Allen et al., 1999; Johnsen et al., 2001). Additionally, despite the climatic changes related to the Earth's orbit, the LGP records also show a quasi-periodic millennial-scale variability. Contrary to the orbital changes, the millennial-scale imprints do not look the same in the North and in the South pointing to different climatic responses (Fig. 1.4).

1.2.4 Millennial-scale variability

Glacial millennial-scale variability are rapid climate transitions that are found both, in the NH as well as the SH. These events are of tremendous interest as they give information of the response of large continental ice sheets to rapid climatic changes. These events are found both, in the NH as well as SH. Nonetheless,

its imprint is not equal in the Antarctic and Greenland records and its important to highlight these differences. Greenland ice cores show a characteristic signal during the LGP known as Dansgaard-Oeschger (DO) events, first identified by Dansgaard et al. (1984) and Oeschger et al. (1983). These events are characterized by an abrupt warming from a cold glacial state (the stadial state) by more than 10 K on decadal timescales into a relatively warm glacial state (the interstadial state), followed by a slow cooling, which can last from hundreds to thousands of years, and ending with a sudden temperature drop again within decades, returning to its stadial state (North Greenland Ice Core Project members, 2004; Kindler et al., 2014). In the GrIS LGP records, 24 of these events have been found (Vasskog et al., 2015), showing a stochastic dominant periodicity component of around 1500 years (Alley et al., 2001; Schulz, 2002). The imprint of these events is not only recorded in Greenland ice cores, but Northern Hemisphere proxies such as marine sediments (Bond et al., 1993; Cacho et al., 1999; Kissel et al., 1999; Shackleton et al., 2000), lake sediments (Benson et al., 1996; Allen et al., 1999; Stockhecke et al., 2014) as well as speleothem-derived proxies (Asmerom et al., 2010; Kanner et al., 2012) also show DO signals, pointing to a global impact in the NH. The underlying mechanism behind this periodic signal is associated with a reorganization of the AMOC (Broecker et al., 1985) as supported by reconstructions (McManus et al., 2004; Barker et al., 2015; Böhm et al., 2015; Henry et al., 2016) and modeling studies (e.g., Ganopolski and Rahmstorf (2001); Rahmstorf (2002); Shaffer et al. (2004)). The main hypothesis is that changes in the AMOC trigger DO events. During stadials, a weak AMOC persists, which means that the Atlantic Ocean transports less heat northwards towards higher latitudes. This reduces the North Atlantic Deep Water formation (NADW), a deep and warm water mass formed in the North Atlantic Ocean. The AMOC strengthens before the occurrence of a DO event (and hence an interstadial stage), enhancing heat transport towards the North (Lynch-Stieglitz, 2017). However, the origin of the AMOC transitions remains poorly understood and their ultimate cause is still under debate. A freshwater forcing produced by changes in the Northern Hemisphere ice sheets, such as the LIS, FIS or even the GrIS, could trigger such a reorganization (Ganopolski and Rahmstorf, 2001, 2002; Clark et al., 2002; Men-

viel et al., 2014). Other type of freshwater sources from the Antarctic Ice Sheet (Stocker, 2003; Weaver et al., 2003) or solar induced changes (Braun et al., 2005) have been suggested. Banderas et al. (2012, 2015), proposed that a southward shift of the intertropical convergence zone (ITZ) could enhance the upwelling of CO_2 at the SO, invigorating the AMOC. Others claim changes in moisture transport as a trigger of potential feedback mechanism of these oceanic transitions (Leduc et al., 2007; Zhang et al., 2017).

An alternative mechanism for triggering Greenland warming without necessarily invoking strong oceanic current changes points to wind field changes (Wunsch, 2006; Li and Born, 2019) and sea-ice retreat (Li et al., 2005, 2010). Modeling studies and reconstructions suggest that the northern Arctic sea ice plays a key role, as it acts as an insulator between ocean and air. The reduction of sea ice preceded the abrupt warming, facilitating the formation of a deep oceanic heat reservoir (Sadatzki et al., 2019). Consequently, when this sea ice retreated, due to small changes in wind stress controlled either stochastically (Kleppin et al., 2015), by ice elevation changes (Zhang et al., 2014), by stratification of the Nordic Seas (Dokken et al., 2013; Jensen et al., 2016) or by heat transport through small AMOC changes (Gildor and Tziperman, 2003; Kaspi et al., 2004), a massive heat exchange between ocean and atmosphere occurred. This hypothesis was expanded by adding an ice shelf which could explain the gradual and slow cooling of the DO events (Petersen et al., 2013; Boers et al., 2018). However, latest studies from the NGRIP ice core do not support the collapse of sea ice as initial trigger of interstadial warming (Erhardt et al., 2019) and the ultimate cause for DO events remains unknown.

In addition, during some glacial stages, North Atlantic marine sediments show layers of periodic deposition of large amounts of grained sediments from land (Bond et al., 1992). These layers, are commonly known as Heinrich events (H), named after the work of the paleoclimatologist Heinrich (1988). The ultimate cause of this phenomenon is associated with iceberg transport of land particles eroded by the Laurentide Ice Sheet (LIS), therefore these layers are also defined as ice-rafted debris (IRD). H events are found to precede the major DO events after long stadials, confirming so-called Bond-cycles (Bond et al., 1993). How-

ever, not all stadial epochs were punctuated by the presence of IRD deposition. In total, seven of these events are found to occur during the LGP (Rashid et al., 2003). Initially, these quasi-periodic iceberg discharges were considered as a consequence of internal binge-purge oscillations (MacAyeal, 1993). This could have been a potential source of freshwater which could trigger AMOC changes and ultimately cause DO events. Nonetheless, modeling studies and accurate proxy measurements showed that a strong AMOC had already started before the IRD deposition and that sub-shelf oceanic warming may have led to the origin of these iceberg discharges (Hemming, 2004; Alvarez-Solas et al., 2013; Andrews and Voelker, 2018; Alvarez-Solas et al., 2019).

Antarctic ice-core records do not show the abrupt warming found in GrIS ice-core records, but rather slow warming in surface air temperatures during Greenland stadials, with cooling during the interstadials, where the peaks of the signal, known as Antarctic Isotope Maxima (AIM), almost coincide with those in Greenland (Blunier and Brook, 2001; EPICA, Community Members, 2006) (Fig. 1.4). This difference between both hemispheres can be explained by the bipolar-seesaw mechanism (Crowley, 1992; Stocker, 1998). The underlying idea relies on heat conservation. With a strong AMOC, more heat is transported to higher northern latitudes. On the other hand, a weak AMOC transports less heat northward and hence more heat is stored in the South. Stocker and Johnsen (2003) showed that the difference in timescales between northern and southern records could be explained if the Southern Ocean acts as a thermal heat reservoir during Greenland stadials. The SO accumulates the heat slowly and integrates the signal into the Antarctic ice cores. When a strong AMOC resumes, heat is transferred to the NH and the SO begins to cool down. However, the existence of a single heat reservoir is still controversial. Pedro et al. (2018) argue that the heat reservoir is distributed partially between the global atmosphere, the Pacific Ocean and part of the north of the Antarctic Circumpolar Current (ACC) rather than the complete SO. They hypothesize that the recorded Antarctic warming occurs as a consequence of enhanced southwards atmospheric heat and moisture transport combined with periodic penetration of eddy-heat fluxes into the SO. These heat fluxes would amplify the AIM warming enhancing the sea-ice retreat

and sea-ice-albedo feedbacks. Thus, although the existence of a thermal heat reservoir is accepted by the scientific community, its location is under debate. Therefore, whether the origin of the smooth Antarctic warming is due to oceanic or atmospheric heat transport is elusive.

The response of the AIS to AIM warming events remains furthermore largely unknown. The amplitude of an AIM surface air temperature (SAT) warming lies between 2-3 K (Jouzel et al., 2007). Because these millennial-scale fluctuations occur within a glacial background climate, it is highly unlikely that a SAT warming of this magnitude can induce Antarctic major changes. However, to the extent that the AIM warming events have an oceanic counterpart, an Antarctic response cannot be excluded. Sea-level proxies show high variability during the LGP at millennial timescales. These are very likely associated with NH ice sheets because they are located at more equatorial latitudes and DO events are abrupt warmings of more than 10 K. Nonetheless, sea-level fluctuations show a synchronous coupling to Antarctic records rather than those registered in northern proxies (Rohling et al., 2009) pointing to a potential response of the AIS. Another possible way to clarify the response of the AIS to millennial warming would be to study IRD layers of enhanced iceberg discharge as in the Heinrich events. However, so far no conclusive deposition of IRD in the Southern Hemisphere (SH) has been found (Weber et al., 2012, 2014; Kim et al., 2018). If a periodic and continuous deposition of IRD could be found associated with millennial scales, then the bipolar seesaw mechanism and the heat storage in the SO could be demonstrated. In order to study the response of the AIS to past and future climatic changes for different timescales, ice-sheet models are needed.

1.3 Ice-sheet modeling

Models are used to predict and understand the underlying mechanisms of complex processes. They simulate, through mathematical formulations, simplified representations of reality. Because the Earth System encompasses land, ocean, atmosphere, biosphere and ice sheets, it is complicated to account for all the

involved natural processes and it is necessary to use such tools. Whereas the first scientific Earth models used rather simple parameterisations, technical improvements, as well as a more profound understanding of the fundamental physics and gradually increasing computational power, have greatly advanced the state of the art.

Ice-sheet models are no exception, but they were developed later than other climatic models. However, ice-sheet models are necessary building blocks to study and understand the past, present and future evolution of ice sheets to climatic changes. Initially, ice models were conceptual two-dimensional flow models used for dating ice cores (i.e. Dansgaard and Johnsen (1969)). Nowadays, there is a large variety of sophisticated ice-sheet models which account for three-dimensional representations, thermo-mechanical coupling and increased spatial resolution among other technical advances (i.e. Gagliardini and Zwinger 2008; Lipscomb et al. 2009; Winkelmann et al. 2011; Cornford et al. 2013; Pattyn 2017; Quiquet et al. 2018).

Modeling of the Antarctic Ice Sheet, more specifically, started at the beginning of the 1980s when Budd and Smith (1982) developed a first model to study its PD state. It was a simple two-dimensional grid model with a rather rough resolution (100km x 100km). This first model already accounted for features like bedrock depression through glacial isostatic adjustment (GIA), surface velocity based on the basal-shear stress, a constant ice-shelf thinning rate and ablation and accumulation fields dependent on the ice elevation. It was then extended to a three-dimensional numerical model of the WAIS (Budd et al., 1984). However, it was not until the 1990s when large continental-scale ice-sheet models fully emerged (e.g., Huybrechts (1990); Huybrechts and Oerlemans (1990); Greve (1997)). Resolution was still low (around 50km), but a more precise formulation for the ice deformation was employed via the Shallow Ice Approximation (SIA; Hutter (1983)). Initially, these models were used for long timescale simulations, like glacial-interglacial cycles (Ritz et al., 2001), or for investigating the Antarctic glacial inception (DeConto and Pollard, 2003). However, one of the first limitations of these models was related to the grounding-line treatment of marine ice sheets and its incapability to respond to climatic changes on shorter timescales

(Vieli and Payne, 2005). Due to the SIA treatment and the lack of coupling between floating and grounded ice, these first ice models were unable to reproduce the theoretically proposed and validated MISI mechanism (Weertman, 1974; Schoof, 2007), which made them ill-suited for future projections.

As the years passed, the importance of coupling the grounded ice to floating ice shelves became obvious. Ice-sheet models evolved into more sophisticated tools and included the Shallow Shelf Approximation (SSA, MacAyeal 1989) for solving fast flowing ice shelves and ice streams. Also, refinements in grounding-line treatments and sub-gridding processes were achieved. In addition, new necessary physical processes were considered, such as the so-called buttressing effect of floating ice shelves restraining the inland ice flow (Fürst et al., 2016), or the effect of accelerated ice retreat due to hydrofracturing (DeConto and Pollard, 2016) leading to MICI, although its influence within the Antarctic evolution is still under debate (Edwards et al., 2019). Moreover, technical advances from satellite data allowed for more realistic representations of surface elevation, bedrock depth, SMB estimates, basal melting rates and the geothermal heat-flux. All this meant a breakthrough for Antarctic ice-sheet modelling, improving the response on decadal timescales and thus moving towards strong future predictions (Golledge et al., 2015; Ritz et al., 2015; DeConto and Pollard, 2016; Pattyn, 2018).

Nowadays, the number of ice-sheet models has greatly increased, which has enabled the creation of intercomparison groups. ISMIP6 for instance is a recent consortium of several ice-sheet models which aims to explore and constrain the potential contribution of the AIS and GrIS to sea-level rise in the following century. Within this scope, the importance of initialization methods has been studied (Seroussi et al., 2019). It also aims to study more profoundly the effect of buttressing through idealized configurations were ice shelves are removed from Antarctica (ABUMIP). Nonetheless, despite all the recent advances, there are still open problems. For instance, basal conditions, such as the bedrock topography in localized regions (Gasson et al., 2015), the exerted basal friction (Gladstone et al., 2017) and the GIA response (Whitehouse et al., 2019) are poorly constrained in the present day and play a fundamental role in understanding the

past and future ice sheet evolution. Depending on the employed basal-friction law or the bedrock topography, the WAIS instability can be enhanced (or suppressed) (Joughin et al., 2019), thereby increasing the uncertainty of future sea-level studies. In addition, ice-ocean interactions, as well as the influence of oceanic currents are considered in a simple way. Hence there is a need to use precise mathematical formulations and physical laws as well as robust ice-sheet-shelf models for understanding the past, the present and the future evolution of the AIS for different climatic scenarios.

1.4 Motivation

A potential WAIS collapse is a clearly defined tipping point in nature (Lenton et al., 2008, 2019). Furthermore, compared to other tipping elements in the climate, its probability of occurrence is not negligible even within the Paris agreement (Schellnhuber et al., 2016; Pattyn et al., 2018). In fact, the grounding-line retreat currently observed for the Pine Island Glacier, Thwaites Glacier and surrounding glaciers could indicate the the MISI mechanism is already underway (Jacobs et al., 2011; Favier et al., 2014; Rignot et al., 2014). However, this is still controversial. On one hand, the response of large continental ice sheets to abrupt climate changes is uncertain. The AIS has been classically considered as a slowly reactive ice sheet, which responded rather to slow orbital changes. Nonetheless, in the last year, the intrusion of deep warm waters onto the continental shelf has been identified as an important mechanism, resulting in accelerated ice loss (Thoma et al., 2008; Dutrieux et al., 2013). Therefore, several attempts have been made to study the response of the AIS to a warming ocean (Golledge et al., 2015; Ritz et al., 2015; DeConto and Pollard, 2016; Pattyn et al., 2018). A key problem is that the evolution of oceanic temperatures and how they translate into basal-melting rates is uncertain. Ice-sheet models use different approaches for representing basal-melting rates to obtain accurate PD states relative to observations (Seroussi et al., 2019). This represents a big handicap in sea-level projections as these laws require different model calibrations and will potentially

respond differently to oceanic warmings. A potential way to study the reaction of large ice sheets to climate change is through paleo studies. Furthermore, because of the rapid timescales involved in future warming scenarios, the response of the AIS to past abrupt climate changes represents an ideal benchmark scenario. In the literature this issue has been addressed for NH ice sheets, such as the LIS (Alvarez-Solas et al., 2013), the EIS (Alvarez-Solas et al., 2019) and the GrIS (Tabone et al., 2019) during the LGP. However, such a study is lacking for the AIS. A profound study and assessment of the ice-ocean interaction in the past evolution of the AIS will help to constraining model-dependent parameters in future scenarios.

Another source of uncertainty in ice-sheet models is related to ice dynamics and, more concretely, basal friction. It is clear that a soft bedrock, either due to the presence of sediments or water, will facilitate faster ice flow than bedrock frozen to the ice, leading to different ice discharges. However, it is a hard task to determine the flow regimes of ice for different regions in Antarctica. Satellite data allow for a profound analysis of PD bedrock conditions, however, whether these conditions hold for other time periods is unknown. Furthermore, future warming scenarios are typically based on an AIS with steady-state thermodynamics, with optimized bedrock conditions. Constraining the friction, based on itstransient, past evolution, could have a different response for future estimates. For these reasons, understanding the response of the AIS to different oceanic warming events as well as friction conditions is necessary. Therefore this thesis aims to investigate the past evolution of the AIS focusing on the role of the ocean on abrupt climate changes, as well as on the impact of different friction choices. Then, this will be applied for studying the future evolution, based on its past. The following scientific questions will be addressed:

Does the AIS respond to glacial millennial-scale climatic variability?

Sea-level rise is one of the major threats in the future. Rising oceanic and atmospheric temperatures will presumably have a strong impact on ice caps and large ice sheets. Antarctica plays a fundamental role within the Earth System as it is the largest ice sheet and potentially the dominant sea-level rise contributor. However the time response of the AIS to these climatic changes is not well constrained and the predictions from different ice-sheet models vary widely. The increase of oceanic temperatures represents its major hazard. Because ablation in Antarctica is almost negligible and accumulation will potentially increase with warming air temperatures, and thus increase the total amount of ice volume, the potential inherent marine instability (MISI) of the WAIS represents its biggest danger. An increase of oceanic temperatures will very likely reduce the size of ice shelves, accelerating inland ice when the buttressing effect is removed. Understanding the response of the AIS to rapid variations is crucial for the study of future warming. AIM events of the LGP represent an ideal benchmark as they represent rapid warming events on millennial timescales. Furthermore, the response of the NH paleo ice sheets to glacial millennial-scale variations has been addressed in several studies. In fact, reconstructions of sea-level estimates during the LGP attribute the majority of these fluctuations mainly to the waxing and waning of the LIS, EIS and GrIS, although their individual contributions are still controversial. Of course, because they rest at lower latitudes than the AIS, they are subject to ablation and are more likely to melt under warming, hence it is expected that they respond with greater amplitude. However, the response of the AIS to glacial millennial-scale variability and its potential sea-level contribution has not been directly addressed in the literature. In fact, sea-level variations follow an Antarctic fluctuation rhythm rather than an abrupt DO signal, suggesting a non-negligible contribution from the AIS. Furthermore, according to the bipolar seesaw mechanism, the Southern Ocean potentially stored heat during weak AMOCs. Because of the marine character of the AIS, especially during glacial stages when it tends to advance towards the continental-shelf break, a

periodic intrusion of warm waters could have the potential to produce a response of Antarctica in the form of ice discharge. This would have profound implications for assessing the sea-level budget of individual ice sheets during the LGP, as well as confirming the success of the bipolar seesaw mechanism theory.

To what extent do different boundary conditions affect the simulated LGM AIS?

From marine and terrestrial geological records it is believed that the grounded ice of the AIS advanced close to the continental-shelf break. Nonetheless, this extension still remains controversial in localized areas. Whereas this advance is well defined in the Amundsen Sea region, the advance in the southern Weddell sea, for instance, is more arguable. In addition to the grounding-line extent, the sea-level budget of Antarctica is even less defined. Models range from predicting more conservative contributions, less than 10 msle, to a large ice storage of more than 15 msle. Assessing the Antarctic sea-level budget in the LGM would help to constrain the ice content of other continental ice sheets as well. One reason for the ambiguity in results lies in the choice of basal friction. Basal conditions, even at present day, are poorly constrained and exert a strong control on the large-scale dynamics, which in turn affect the size of the ice sheet. Thus, a comprehensive study of the role of basal friction in simulating an Antarctic glacial state is needed. But, in addition to this, atmospheric conditions are also poorly known. While some modeling studies apply a simple scheme of a spatially homogeneous decrease in temperature and precipitation, based on ice proxy records, other studies use climatic fields generated from general circulation models (GCM). But even the simulated LGM conditions estimated from GCMs differ greatly between them, adding more uncertainty. Therefore, in order to improve estimates of the AIS sea-level budget, it is necessary not only to constrain the basal friction conditions, but also the role of the climatic fields during the LGM.

How does the AIS respond to anthropogenic warming for different friction laws?

The fifth IPCC report points out that the AIS is the largest source of uncertainty in future sea-level projections, mainly due to the potential threat of a collapse of the marine sectors of the AIS. Whether the MISI mechanism is already underway or far from being triggered remains elusive. Knowing this is crucial for developing mitigation strategies. Ice dynamics, and more concretely basal friction, plays a crucial role in driving the MISI mechanism. However, basal conditions are poorly constrained even for PD. Furthermore, no universal friction law has been defined for the Antarctic domain and models use many different representations, adding uncertainty to future sea-level projections. Whereas some friction laws allow for faster sliding promoting a potential WAIS collapse, other laws are more conservative, slowing the grounding-line retreat. But, in addition, future model sea-level projections from the AIS are generally run from an equilibrated PD state that matches with observational data. However, this procedure does not take into account the thermal inertia of the ice sheet and there is no apparent reason for ruling out that the PD may be subjected to a natural drift since the deglaciation onset ($\sim$20 kyr BP) which could potentially play a crucial role for different basal conditions. Hence, it is not only necessary to study the response of the AIS to different climatic scenarios but also to different friction laws as they play a fundamental role in the timing of reaching sooner (or later) Antarctic tipping points. Furthermore, the friction law can have profound implication by facilitating, or impeding, a return to its PD state.

1.5 Overview

This thesis aims to study the sensitivity of the AIS to past oceanic changes and basal friction conditions, from large orbital-driven changes to variations on short timescales. Simulations of the AIS will be analyzed for past, present and future conditions. The importance of the ocean and basal sliding in the AIS has

been explained in this chapter. For studying the ice sheet response to climatic changes and different basal conditions, the three-dimensional thermo-mechanical ice-sheet-shelf Yelmo model, described in Chapter 2, will be used. This model has been developed in the PalMA research group of the Complutense University of Madrid (UCM) in parallel with this thesis. The particular contribution of this work includes extensive testing of calibration parameters, as well as a comprehensive study of the basal-melting and basal dragging parameterisations used in the code. The model solves for the dynamics of grounded ice as well as for floating ice shelves. First, the role of the ice-ocean interaction is studied in the context of millennial-scale glacial variability (Chapter 3). Next, the impact of the friction and atmospheric forcing is addressed for an Antarctic glacial state representative of LGM conditions (Chapter 4). Lastly, Chapter 5 builds on the results of both previous studies of basal friction and the ice-ocean interaction to assess the future evolution of the AIS. Chapter 6 discusses the broader context of the main scientific results presented in this thesis and finally Chapter 7 summarizes the main conclusions.

Scientific publications related to this thesis:

The Antarctic Ice Sheet response to glacial millennial-scale variability (published)

Blasco, J., Tabone, I., Álvarez-Solas, J., Robinson, A. and Montoya, M., 2019: The Antarctic Ice Sheet response to glacial millennial-scale variability. *Climate of the Past*, **15**, 121-133. DOI 10.5194/cp-15-121-2019.

This work is reported in Chapter 3. Here, for the first time, the response of the AIS to millennial-scale variability is studied, with a particular focus on its interaction with the SO. Although it is assumed that the source of global millennial sea-level fluctuations during the LGP is the waxing and waning of NH paleo ice sheets, a contribution from Antarctica cannot be excluded. Further-

more, due to the marine character of the AIS, a warming of the SO driven by the bipolar seesaw mechanism can potentially trigger a response of the AIS. This work investigates, through a sensitivity study, the response of the AIS to millennial scale variability, focusing on the potential role of the ocean for an Antarctic glacial state. For this purpose, a hybrid thermo-mechanical ice-sheet-shelf model is used. Oceanic temperature variations are converted into submarine basal melting rates through a linear function. The transient simulations are forced through an index method, extracted from Dome C, and orbitally filtered to account only for the millennial impact. Atmospheric temperature and precipitation variations, related to millennial-scale variability, do not have an appreciable impact on the size and shape of the AIS. On the other hand, oceanic warming can trigger a strong response from Antarctica. The results show that substantial grounding-line migrations and sea-level rises up to 6 m on millennial timescales are possible. These results point to a rapid Antarctic response, rather than the widespread assumption that the AIS is a slow reactive and static ice sheet that responds to orbital timescales only. These results point to the necessity to improve our knowledge of the role of the AIS in millennial-scale climate changes and its role within the Earth System.

Exploring the impact of atmospheric forcing and basal boundary conditions on the simulation of the Antarctic ice sheet at the Last Glacial Maximum (submitted)

Blasco, J., Álvarez-Solas, J., Robinson, A. and Montoya, M., 2020: Exploring the impact of atmospheric forcing and basal boundary conditions on the simulation of the Antarctic ice sheet at the Last Glacial Maximum. *The Cryosphere Discussion*, 1-27. DOI 10.5194/tc-2020-28.

This work is reported in Chapter 4. The aim of this section is to explore the uncertainty in friction and atmospheric conditions in the simulation of an Antarctic glacial state. Marine and terrestrial geological constraints point to a fully advanced ice sheet up to the continental-shelf break, with considerable un-

certainties at certain locations. The total sea-level content, on the other hand, is less constrained. Simulated sea-level estimates from ice models differ greatly. Ice dynamics play a crucial role, as a more dynamically active ice sheet will potentially store less ice than a slower ice sheet. In addition, the applied climatic boundary conditions determine the total mass of the ice sheet through accumulation. This work investigates the simulated Antarctic LGM state forced with different basal dragging choices and glacial background climatic conditions obtained from the third phase of the Paleoclimate Modelling Intercomparison Project (PMIP3). For this purpose, a hybrid ice-sheet-shelf model forced with constant glacial background conditions is used. From a set of parameters which simulate realistic PD states, the relative LGM state is studied. Then, for a reference basal configuration, the effect of the uncertainty in climatic conditions is explored by using different climatologies from the PMIP3 groups. The results show that the uncertainty of the total sea-level storage due to the friction choice is equivalent to that of the climatic boundary conditions. More dynamically active ice sheets can lead to small sea-level contributions but despite fully expanding up to the continental-shelf break, whereas less dynamically active ice sheets lead to larger volumes. In addition, the surface boundary temperature field determines the ice extent, controlled by viscosity. For equally extended ice sheets, the total ice volume depends on the boundary precipitation field. The simulated sea-level and ice-extension differences between the PMIP3 models are about 6 msle and $1{\cdot}10^6$ km2, respectively.

The Antarctic sea-level contribution since the LGM to the future for different basal-dragging laws ()

Blasco, J., Robinson, A., Álvarez-Solas, J., Tabone, I. and Montoya, M., 2020: The Antarctic sea-level contribution since the LGM to the future for different basal-dragging laws. *submitted*.

The main results of this work are described in Chapter 5. The aim of this section is to study the potential response of the AIS to anthropogenic climate

change and the simulated spread due to basal friction uncertainty. To infer the future sea-level contributions from large continental ice sheets is a difficult task as it depends not only on the uncertainty of future climate projections, but also on the dynamic response of the ice sheets to these changes. Regarding the AIS, the largest uncertainty associated with future sea-level estimates relies on the triggering of a MISI mechanism in the WAIS. However, such instability is highly dependent on the used friction law, but as already discussed, no universal friction law has been defined for the AIS. Ice-sheet models range from hard bedrock parameterisations, which diminishes basal sliding, towards weak tills, enhancing basal sliding, and hence a rapid WAIS collapse. Moreover, other studies focused on the Antarctic response to future scenarios start from an equilibrated PD state. However, there is no apparent reason to rule out an internal drift driven since the deglaciation onset (∼20 kyr BP). Here, a hybrid ice-sheet-shelf model is used to investigate the AIS uncertainty in sea-level contributions since the LGM to the future for four different basal-dragging laws. Future sea-level rise projections are investigated for different Representative Concentration Pathway (RCP) scenarios. The deglaciation spin-up allows not only for a qualitative assessment of past LGM ice volume, but also to ensure that the model has thermal memory for future projections. Results show that the future SLR is mainly dependent on the RCP scenario, with a maximum contribution of 8.1 msle for RCP8.5 and a minimum contribution of 2.1 msle for RCP2.6. However the choice of friction law is highly relevant on short timescales, as inland velocity perturbations propagate differenly for each friction law.

Chapter 2
The Yelmo ice-sheet-shelf model

Yelmo is a three-dimensional, hybrid themomechanical ice-sheet-shelf model (Robinson et al., 2020). Because of its novelty, this thesis includes the first published results using this model. It is an open source model accessible for everyone. Yelmo has evolved from the GRISLI (Ritz et al., 1996) and SICOPOLIS (Greve, 1997) models, which have been already used for simulating the paleo and future evolution of the NH ice sheets (Alvarez-Solas et al., 2013, 2019; Tabone et al., 2018) as well as the AIS (Ritz et al., 2015; Quiquet et al., 2018). Important differences with respect to other models include its division into four independent blocks: topography, dynamics, material properties and thermodynamics. This division allows for a clear and clean way of defining variables. In addition, boundary conditions such as atmospheric or oceanic temperature fields, precipitation or sea-level variations are defined outside of Yelmo, greatly facilitating ice-sheet coupling to other models.

Here, the most fundamental equations and approximations used in Yelmo will be described. Many of these physical processes are already described in depth in Greve and Blatter (2009). Special focus will be given to the parameterisation used for the ice-ocean interaction and the basal drag routine because of their important role within this thesis. Further details can be found in the Yelmo model description (Robinson et al., 2020).

It is worth mentioning that results in Chapter 3 are obtained with the ice-sheet-shelf GRISLI-UCM model, an intermediate version preceding Yelmo's de-

velopment. Although the applied physics are the same, there are some slight differences with the employed parameterisations with respect to Yelmo. For the sake of simplicity, this chapter only describes the main features of the Yelmo model. The relevant differences of GRISLI-UCM will be explained in the experimental set up of Chapter 3 (more detail about GRISLI-UCM can be found in Tabone et al. 2018, 2019; Alvarez-Solas et al. 2019).

2.1 Topography

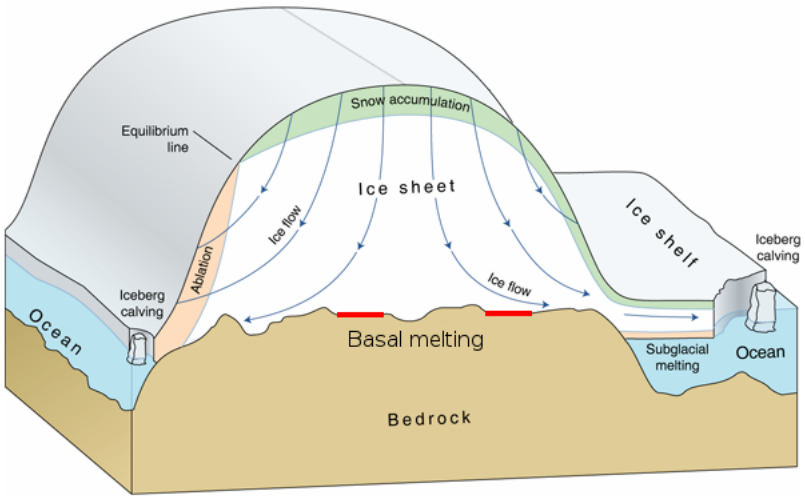

Fig. 2.1: Sketch of an ice sheet interacting with the climate system (from Landsat Image Mosaic Of Antarctica, 2008). At the surface, accumulation and ablation take place through interaction with atmosphere. At the ice base, the ice sheet interacts with the bedrock via geothermal heat flux exchange. Mass loss takes places at the ice front via calving and at the shelf base due to subglacial melting.

Mass conservation is expressed via the continuity equation as:

$$\frac{\partial \rho}{\partial t} + \boldsymbol{\nabla} \cdot (\rho \mathbf{v}) = 0, \tag{2.1}$$

where ρ represents the ice density and $\mathbf{v}$ the ice velocity vector. Assuming that enough time has passed, so that ice has been pressed towards an incompressible state under its own weight, the mass conservation equation (Eq. 2.1) can be rewritten as:

$$\boldsymbol{\nabla} \cdot \mathbf{v} = \frac{\partial u}{\partial x} + \frac{\partial v}{\partial y} + \frac{\partial w}{\partial z} = 0, \tag{2.2}$$

where u, v and w represent the x,y and z components of the velocity vector $\mathbf{v}$ (being x and y the horizontal component, and z the vertical component). Integrating Eq. 2.2 vertically and considering boundary conditions, determined by mass gain and mass loss, gives:

$$\frac{\partial H}{\partial t} = a - b - c - \left(\frac{\partial (H \cdot \bar{u})}{\partial x} + \frac{\partial (H \cdot \bar{v})}{\partial y} \right). \tag{2.3}$$

This equation describes the mass conservation of the ice column. The ice thickness evolution ($\frac{\partial H}{\partial t}$) is obtained from the surface mass balance (a; difference of ice accumulation and ice ablation), the basal melting at the ice base (b; valid for grounded and floating ice), the advected ice flux ($\frac{\partial (H \cdot \bar{u})}{\partial x}$ and $\frac{\partial (H \cdot \bar{v})}{\partial y}$) and the calving rate ($c$), that applies at the ice front of ice shelves. In this thesis, the method of Peyaud et al. (2007) and Lipscomb et al. (2019) is followed, where calving occurs if the ice thickness decreases below an imposed threshold (H_{ref}) and the upstream ice flux is not large enough to provide the necessary ice for maintaining the reference thickness on a characteristic calving time τ_c:

$$c = \frac{H_{ref} - H}{\tau_c}. \tag{2.4}$$

An ice sheet is in equilibrium if the ice loss from the dynamics is compensated by the total accumulation and melting from the boundary conditions and hence $\frac{\partial H}{\partial t} = 0$. Melting of floating ice-shelves depends on the oceanic heat-flux exchange, which in turn depends on oceanic temperatures and salinity. Melting of grounded ice occurs if the bed temperature is at the pressure melting point. Because the

melting rates are imposed as boundary conditions, they will be discussed more extensively in Section 2.6.

2.2 Material

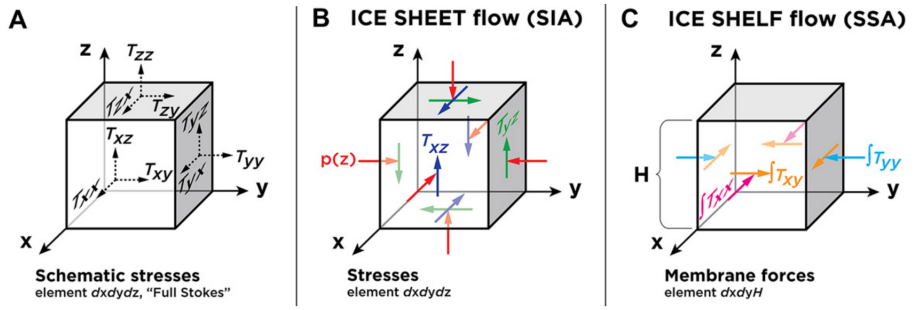

Fig. 2.2: Schematic representation of the stresses acting over a virtual ice box. (A) shows all the stress components as in a full Stokes problem. (B) represents the acting stresses for the SIA solution and (C) for the SSA solution (figure based on Kirchner et al. (2011)).

The material component of Yelmo computes the strain rate tensor and effective strain rate (amount of deformation as a consequence of stress), the rate factor, and the effective viscosity (fluidity of a material). Additionally, Yelmo offers the possibility of computing the ice age through an Eulerian tracer advection model (Robinson et al., 2020) . The material component is the link between thermodynamics and ice dynamics. The grid cells of ice can be imagined as a virtual ice box. The Cauchy stress tensor (or simply stress tensor) $\boldsymbol{\sigma}$ defines the state of stress of ice and is expressed as:

$$\boldsymbol{\sigma} = \begin{pmatrix} \sigma_{xx} & \sigma_{xy} & \sigma_{xz} \\ \sigma_{yx} & \sigma_{yy} & \sigma_{yz} \\ \sigma_{zx} & \sigma_{zy} & \sigma_{zz} \end{pmatrix} = \sigma_{ij}. \tag{2.5}$$

Note that the diagonal components (σ_{xx},σ_{yy},σ_{zz}) represent the normal stresses (i.e. perpendicular to the referred plane), whereas the other six components (σ_{xy}, σ_{xz}, σ_{yx}, σ_{yz}, σ_{zx}, σ_{zy}) are called shear stress (i.e. act parallel to the referred plane; Fig. 2.2a). This stress tensor can be split up into a deviatoric part (τ_{ij}), which tends to distort the ice box, and a hydrostatic stress component, which tends to change the size, and hence the volume. The hydrostatic stress components are commonly referred as pressure p:

$$\sigma_{ij} = \tau_{ij} - \frac{1}{3}\tau_{kk}\delta_{ij} = \tau_{ij} - p, \tag{2.6}$$

where Einstein's tensorial notation is followed. This deviatoric stresses can be split up into an effective viscosity component (η) and a strain rate tensor ($\dot{\epsilon}_{ij}$):

$$\tau_{ij} = 2\eta\dot{\epsilon}_{ij}, \tag{2.7}$$

where the strain rate tensor itself is:

$$\dot{\epsilon}_{ij} = \frac{1}{2}\left(\frac{\partial u_i}{\partial x_j} + \frac{\partial u_j}{\partial x_i}\right). \tag{2.8}$$

The second invariant of the stress deviatoric tensor defines the effective strain:

$$\dot{\epsilon} = \left(\frac{1}{2}\dot{\epsilon}_{ij}\dot{\epsilon}_{ij}\right)^{\frac{1}{2}}. \tag{2.9}$$

Using Glen's flow law (Glen, 1955), which relates creep and stress, the effective viscosity is calculated as:

$$\eta = \frac{1}{2}\left(\dot{\epsilon}^2\right)^{\frac{1-n}{2n}} A^{-\frac{1}{n}}, \tag{2.10}$$

where n is the Glen's flow law exponent, set to $n = 3$ within this thesis. A is the rate factor, which is computed as a function of ice temperature following the Arrhenius law:

$$A\left(T_i\right) = E_f A_0 \exp\left(-\frac{Q_a}{RT_i}\right), \tag{2.11}$$

where $R = 8.314$ [J mol^{-1} K^{-1}] is the universal gas constant. Q_a is the activation energy and A_0 the rate factor coefficient. E_f is the enhancement factor, which

captures the impact of ice anisotropies on the ice flow. Because this effect is not captured by Glen's flow law, this variable is often set as a tuning parameter (Ma et al., 2010; Pollard and DeConto, 2012b; Maris et al., 2014; Albrecht et al., 2019). Yelmo distinguishes between three flow regimes: shear, stream and shelf. Wherever there is floating ice, the shelf value is set. The enhancement factor for inland grounded ice is then the weighted average between the shear and stream enhancement factors, depending on the shear fraction of total deformation at a given location.

2.3 Dynamics

The dynamics of the ice sheet are deduced from the momentum conservation equation:

$$\rho \frac{d\mathbf{v}}{dt} = \boldsymbol{\nabla} \cdot \boldsymbol{\sigma} + \rho \mathbf{g}, \tag{2.12}$$

where $\mathbf{g}$ is the Earth's gravitational acceleration. At the involved timescales, the acceleration term of ice is considerably smaller than the ice deformation. Thus, neglecting $\frac{d\mathbf{v}}{dt}$, Eq. 2.12 can be rewritten as:

$$\boldsymbol{\nabla} \cdot \boldsymbol{\sigma} + \rho \mathbf{g} = 0, \tag{2.13}$$

which constitutes the steady-state (Stokes) equation. Written in components equation, this becomes:

$$\frac{\partial \sigma_{xx}}{\partial x} + \frac{\partial \sigma_{xy}}{\partial y} + \frac{\partial \sigma_{xz}}{\partial z} = 0 \tag{2.14}$$

$$\frac{\partial \sigma_{yx}}{\partial x} + \frac{\partial \sigma_{yy}}{\partial y} + \frac{\partial \sigma_{yz}}{\partial z} = 0 \tag{2.15}$$

$$\frac{\partial \sigma_{zx}}{\partial x} + \frac{\partial \sigma_{zy}}{\partial y} + \frac{\partial \sigma_{zz}}{\partial z} = -\rho g. \tag{2.16}$$

Solving this system of equations is computationally very expensive, hence, for the sake of simplicity, several assumptions are made.

2.3.1 Hydrostatic approximation

This approximation relies on the assumption that the horizontal extent of the ice sheet (and more particularly Antarctica) is much greater than its height (Antarctica's horizontal extension reaches up to 4000 km, whereas its largest ice column is around 4 km thick). Hence the vertical shear stresses σ_{xz} and σ_{yz} are much smaller than σ_{zz} and can be neglected. Thus integrating over z in Eq. 2.16 gives:

$$\sigma_{zz} = \rho g \left(H - z \right), \tag{2.17}$$

which is the hydrostatic pressure. Substituting Eq. 2.17 into Eq. 2.14 and Eq. 2.15 (following Greve and Blatter (2009)):

$$2\frac{\partial \tau_{xx}}{\partial x} + \frac{\partial \tau_{yy}}{\partial x} + \frac{\partial \sigma_{xy}}{\partial y} + \frac{\partial \sigma_{xz}}{\partial z} = \rho g \frac{\partial z_s}{\partial x} \tag{2.18}$$

$$2\frac{\partial \tau_{yy}}{\partial y} + \frac{\partial \tau_{xx}}{\partial y} + \frac{\partial \sigma_{yy}}{\partial y} + \frac{\partial \sigma_{yz}}{\partial z} = \rho g \frac{\partial z_s}{\partial y}, \tag{2.19}$$

where z_s is the surface elevation. Inserting in these equations the deviatoric stress definition (Eq. 2.7) the hydrostatic approximation is obtained:

$$\begin{aligned} 4\frac{\partial}{\partial x}\left(\eta \frac{\partial u}{\partial x}\right) + 2\frac{\partial}{\partial x}\left(\eta \frac{\partial v}{\partial y}\right) + \frac{\partial}{\partial y}\left(\eta\left(\frac{\partial u}{\partial y} + \frac{\partial v}{\partial x}\right)\right) & \\ + \frac{\partial}{\partial z}\left(\eta\left(\frac{\partial u}{\partial z} + \frac{\partial w}{\partial x}\right)\right) & = \rho_i g \frac{\partial z_s}{\partial x} \end{aligned} \tag{2.20}$$

$$\begin{aligned} 4\frac{\partial}{\partial y}\left(\eta \frac{\partial v}{\partial y}\right) + 2\frac{\partial}{\partial y}\left(\eta \frac{\partial u}{\partial x}\right) + \frac{\partial}{\partial x}\left(\eta\left(\frac{\partial u}{\partial y} + \frac{\partial v}{\partial x}\right)\right) & \\ + \frac{\partial}{\partial z}\left(\eta\left(\frac{\partial v}{\partial z} + \frac{\partial w}{\partial y}\right)\right) & = \rho_i g \frac{\partial z_s}{\partial y}. \end{aligned} \tag{2.21}$$

2.3.2 Shallow Ice Approximation

Yelmo is a hybrid model which includes the Shallow Ice Approximation (SIA) and Shallow Shelf Approximation (SSA). In this thesis, it treats the horizontal

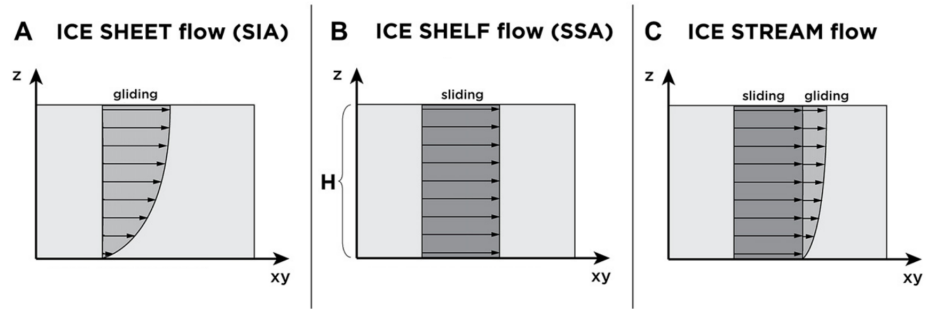

Fig. 2.3: Velocity profile of the SIA solution (A) and the SSA solution (B). In the SIA solution gliding processes prevail, the SSA solution is dominated by sliding. Yelmo computes all inland ice points as ice streams (C). Ice closer to the dome regions will have a small sliding velocity contribution, whereas it will increase towards the coast. Ice shelves velocities are solved only with the SSA solution (figure based on Kirchner et al. (2011)).

velocities ($u(x, y, z)$ and $v(x, y, z)$) as a sum of the internal shear stress computed by the SIA solution (denoted with a sub-index *sia*) and sliding at the base calculated by the SSA solution (denoted with a sub-index *ssa*), hence:

$$u = u_{sia} + u_{ssa} \tag{2.22}$$

$$v = v_{sia} + v_{ssa}. \tag{2.23}$$

The SIA solution (Hutter, 1983) is a further simplification from the hydrostatic approximation. It only considers deformation terms, hence $\tau_{xx} = \tau_{yy} = 0$, and assumes that the shear component in the z direction is dominant over the xy plane, thus $\sigma_{xy} = 0$. It thus describes slow flowing ice, dominated by the shearing regime (see Fig. 2.3a). With this Eq. 2.18 and Eq. 2.19 simplify to:

$$\frac{\sigma_{xz}}{\partial z} = \rho g \frac{\partial z_s}{\partial x} \tag{2.24}$$

$$\frac{\sigma_{yz}}{\partial z} = \rho g \frac{\partial z_s}{\partial y}. \tag{2.25}$$

If these equations are integrated taking into account that here no basal sliding is allowed within the SIA solution, as it is assumed that the SIA solution is frozen to bedrock ($u_{sia}(x, y, z_b) = v_{sia}(x, y, z_b) = 0$), and that the ice surface is stress-free ($\sigma_{xz}|_{z_s} = \sigma_{yz}|_{z_s} = 0$), then the zero-order depth-dependent SIA solutions are obtained:

$$u_{sia}(z) = -\left[2\left(\rho g\right)^n \left|\nabla z_s\right|^{n-1} \int_{z_b}^{z} A(z_s - z)^n\right] \frac{\partial z_s}{\partial x} \tag{2.26}$$

$$v_{sia}(z) = -\left[2\left(\rho g\right)^n \left|\nabla z_s\right|^{n-1} \int_{z_b}^{z} A(z_s - z)^n\right] \frac{\partial z_s}{\partial y}, \tag{2.27}$$

where n is the Glen exponent and A the material rate factor described in the Material module (Section 2.2; Eq. 2.11).

2.3.3 Shallow Shelf Approximation

The SSA solution (MacAyeal, 1989) is applied to fast flowing areas, characteristic of ice shelves and ice streams, dominated by the stretching regime (see Fig. 2.3b). Again, it is an extension of the hydrostatic approximation, but now vertical components are neglected. Following Greve and Blatter (2009) the vertical shear stresses are simplified to:

$$\sigma_{xz} = \eta \frac{\partial w}{\partial x} \tag{2.28}$$

$$\sigma_{yz} = \eta \frac{\partial w}{\partial y}. \tag{2.29}$$

Inserting these equations into the hydrostatic approximation and integrating over depth, the SSA solution is obtained:

$$\frac{\partial}{\partial x}\left[\bar{\eta}_d\left(4\frac{\partial u_{ssa}}{\partial x}+2\frac{\partial v_{ssa}}{\partial y}\right)\right]+\frac{\partial}{\partial y}\left[\bar{\eta}_d\left(\frac{\partial u_{ssa}}{\partial y}+\frac{\partial v_{ssa}}{\partial x}\right)\right]=\rho g H\frac{\partial z_s}{\partial x}-\tau_{b,x} \tag{2.30}$$

$$\frac{\partial}{\partial y}\left[\bar{\eta}_d\left(4\frac{\partial v_{ssa}}{\partial y}+2\frac{\partial u_{ssa}}{\partial x}\right)\right]+\frac{\partial}{\partial x}\left[\bar{\eta}_d\left(\frac{\partial u_{ssa}}{\partial y}+\frac{\partial v_{ssa}}{\partial x}\right)\right]=\rho g H\frac{\partial z_s}{\partial y}-\tau_{b,y}. \tag{2.31}$$

Note that $\bar{\eta}_d$ is the depth-integrated ice viscosity described as:

$$\bar{\eta}_d=\frac{1}{2}\bar{B}\left(\dot{\varepsilon}_d^2+\dot{\varepsilon}_0^2\right)^{\frac{1-n}{2n}}, \tag{2.32}$$

where

$$\bar{B}=\frac{1}{H}\int_{z_b}^{z_s}A^{-1/n}dz, \tag{2.33}$$

is the vertically averaged ice hardness. $\dot{\epsilon}_0$ is a regularization factor to avoid singularities and $\dot{\epsilon}_d$ the effective strain rate computed as a reduced form of the second invariant of the strain rate tensor without vertical shear terms, hence:

$$\dot{\epsilon}_d^2=\left(\frac{\partial u_b}{\partial x}\right)^2+\left(\frac{\partial v_b}{\partial y}\right)^2+\frac{\partial u_b}{\partial x}\frac{\partial v_b}{\partial y}+\frac{1}{4}\left(\frac{\partial u_b}{\partial y}+\frac{\partial v_b}{\partial x}\right)^2. \tag{2.34}$$

$\boldsymbol{\tau_b}$ is the basal stress applied at the base to the SSA solution. For ice shelves its value is set to zero, while for grounded ice, Yelmo offers different treatments.

2.3.4 Basal friction

Friction on a surface is based on Newton's third law, where the bedrock responds with an opposite reaction to the applied force. Hence, the simplest way to relate the basal stress $\boldsymbol{\tau_b}$ with the horizontal basal velocity vector $\mathbf{u_b}$ is with the so-called basal friction coefficient β

$$\boldsymbol{\tau_b}=-\beta\mathbf{u_b}. \tag{2.35}$$

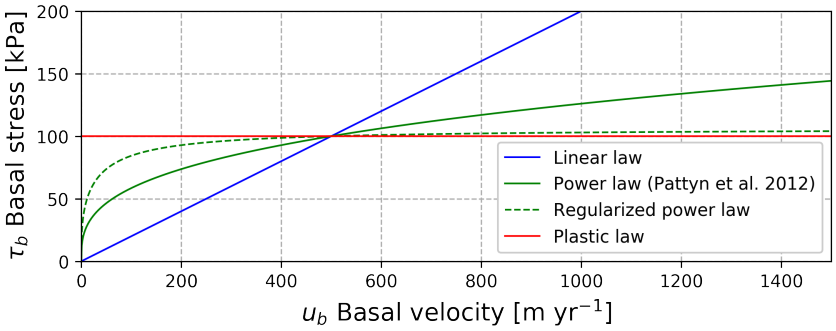

Fig. 2.4: Graphical illustration of the basal shear stress function ($\boldsymbol{\tau_b}$) for different friction laws (linear, Coulomb, regularized Coulomb and plastic). Friction coefficients have been tuned to obtain 100 kPa for a basal velocity of 500 m yr−1 (figure based on Joughin et al. (2019)).

Note that the horizontal basal velocity vector is expressed in [m yr^{-1}] and the basal stress in [Pa], thus β has units of [Pa yr m^{-1}] (e.g. MacAyeal et al. (1995); Cuffey and Paterson (2010)). This representation allows for an indirect inference of basal friction at the ice base through inversion methods based on surface velocities (e.g. Morlighem et al. (2013); Le clec'h et al. (2019)). Nonetheless, these inversion methods show a particular configuration of PD conditions which is not necessarily valid for other time periods. The actual resistance relation $\boldsymbol{\tau_b}(\mathbf{u_b})$ depends on local properties, such as the presence of sediments or basal water. Therefore, to account for bedrock characteristics, Yelmo splits the friction coefficient into a a bedrock coefficient (c_b), which accounts for several bedrock properties, a threshold velocity (u_0), which will be discussed later, and a velocity function $f(\mathbf{u_b})$:

$$\beta = \frac{c_b}{u_0} f(\mathbf{u_b}) . \tag{2.36}$$

Note that $f(\mathbf{u_b})$ is unitless, thus c_b has units of [Pa] and the threshold speed u_0 [m yr^{-1}]. The velocity function accounts for the sliding character of the ice sheet. Different frictions apply at the ice base depending on the velocity regime. Whereas at *hard beds* resistance will become stronger with increasing velocity,

as a consequence of null water presence or no sediments, at *weak/soft beds* the presence of water can enhance basal sliding. Yelmo accounts for these features through different basal friction laws.

Basal friction laws

The choice of the velocity function, $f(\mathbf{u_b})$, as described above, and thereby the friction law is relatively arbitrary and unconstrained in ice modelling, as no universal law has been defined. It is poorly constrained but plays a fundamental role within the dynamics of continental ice-sheets. Several observational studies are beginning to identify the most realistic friction-laws from satellite observations (e.g. Joughin et al. (2019)). Still it is not clear whether a unique friction law can be used for large ice-sheets and whether the same friction-law holds for cold and warm periods. Although Yelmo offers the possibility to couple with a hydrological model, in this thesis the presence of basal water is assumed through different friction representations. The presented friction laws are intended to cover the whole range of possibilities as well as the most common laws used in the literature.

Power law

Any power law can generally be expressed as $f(\mathbf{u_b}) = u_0^{1-q} |\mathbf{u_b}|^{q-1}$ (Robinson et al., 2020). This yields when substituted into Eq. 2.35 (Schoof, 2010; Aschwanden et al., 2013)

$$\boldsymbol{\tau_b} = -c_b \left(\frac{|\mathbf{u_b}|}{u_0} \right)^q \left(\frac{\mathbf{u_b}}{|\mathbf{u_b}|} \right), \tag{2.37}$$

where u_0 is the regularizing velocity term and $q\epsilon[0,1]$ is the non-dimensional pseudo-plastic exponent. From here, three of the most common friction laws used in ice-sheet models can be obtained: linear power-law, pseudo-plastic power law and a purely plastic law. If $q = 1$, then a linear power law is obtained:

$$\boldsymbol{\tau_b} = -c_b \frac{\mathbf{u_b}}{u_0}. \tag{2.38}$$

Due to its simplicity, this law is very popular in ice-sheet models (e.g. Alvarez-Solas et al. (2013); Quiquet et al. (2018)). It is especially relevant for *hard beds* as the basal stress scales proportionally to basal velocity (blue curve; Fig 2.4). Hence, unless the presence of water or sediments is taken into account, higher velocities generate a larger bedrock friction. Because velocity increases towards the margins, this provides a very stable solution for ice sheets in fast flowing regions. However, as friction increases one could expect that frictional heat increases, resulting in more basal water production, which facilitates ice flow. This law hence does not include cavitation effects at the ice base which could limit the total friction.

At the other extreme, if q =0, then a purely plastic behaviour results from Eq. 2.37

$$\boldsymbol{\tau_b} = -c_b \frac{\mathbf{u_b}}{|\mathbf{u_b}|}. \tag{2.39}$$

This friction law applies the same basal stress independent of the flowing regime (red curve; Fig. 2.4). It represents a *weak bed* where the presence of basal water lubricates the ice flow and hence friction is independent of the basal velocity. This provides a more dynamic ice sheet than a linear law. This can have profound implications. For instance, a MISI mechanism will most likely occur earlier for a plastic law than for a linear law as fast velocities are not suppressed with a corresponding high friction. On the other hand, for a plastic law more friction is applied in slow regimes.

A typical value used in ice-sheet modeling for a middle case scenario is $q = \frac{1}{3}$, which will be defined hereafter as the pseudo-plastic power law

$$\boldsymbol{\tau_b} = -c_b \left(\frac{|\mathbf{u_b}|}{u_0} \right)^{\frac{1}{3}} \frac{\mathbf{u_b}}{|\mathbf{u_b}|}. \tag{2.40}$$

This solution also increases with increasing basal velocity but is not as pronounced as the linear case (green curve; Fig 2.4). This law intends to capture the phenomenon by which a high friction in fast flowing regimes releases more heat, melting the ice base, and enhances the ice flow. It resembles a *hard bed* better than a *weak bed* as it does not fully saturate and hence cavitation effects are not completely taken into account, but it clearly provides a lower friction than the linear case. A particular case is $u_0 = 1$ m yr^{-1} and $c_b = 3.165176\ 10^4$

Pa which are the friction parameters used in the MISMIP experiments (Pattyn et al., 2012).

Regularized-Coulomb law

The Regularized-Coulomb law is defined as $f(\mathbf{u_b}) = u_0 \left(|\mathbf{u_b}| + u_0\right)^{-q} |\mathbf{u_b}|^{q-1}$ and thus:

$$\boldsymbol{\tau_b} = -c_b \left(\frac{|\mathbf{u_b}|}{|\mathbf{u_b}| + u_0} \right)^q \frac{\mathbf{u_b}}{|\mathbf{u_b}|}. \tag{2.41}$$

This friction law allows for a power-law behaviour for low velocities (*hard bed* below u_0) and saturates afterwards if ice becomes too fast (*weak bed*), taking into account potential cavitation effects (green discontinuous line; Fig. 2.4). Recently, observations suggest that this solution may be the most adequate one for representing ice-sheet dynamics (Joughin et al., 2019). Because it combines low friction for both, slow and fast velocities, this solution provides the most dynamic ice sheet. This has profound implications for future sea-level projections. If the basal friction saturates beyond a threshold velocity, then the MISI instability for instance is more likely to occur than for a linear friction law and more inland ice will be discharged than for a plastic law.

2.3.5 Basal friction coefficient

The bedrock friction coefficient c_b is intended to provide information about bedrock characteristics such as basal temperature, the presence of basal sediments or the effective pressure for instance. The friction coefficient is split into a universal friction coefficient for the whole ice sheet (c_f), a topographic scaling parameter (λ) and the effective pressure (N_{eff})

$$c_b = c_f \lambda N_{eff}. \tag{2.42}$$

The effective pressure does not explicitly account for the presence of basal water and the potential intrusion through crevasses. It is instead parametrised following the Leguy et al. (2014) formulation

$$N_{eff}(p) = \rho_i g H \left(1 - \frac{H_f}{H}\right)^p, \tag{2.43}$$

where ρ_i stands for the ice density. H_f represents the floating portion of the grounded ice column. If ice is grounded above sea level, then it is set to zero, if it is grounded below sea level, the portion of floating ice depends on the bed depth and the sea-water density (ρ_w), thus:

$$H_f = max\left[0, -\frac{\rho_w}{\rho_i}\left(z_{sl} - z_b\right)\right], \tag{2.44}$$

where z_b denotes the bedrock elevation (positive/negative numbers above/below sea level) and z_{sl} the sea-level elevation. If the exponent p in Eq. 2.43 is set to zero, then the pressure exerted at the ice base is the weight of the ice column. If p =1 then full water pressure is applied at the marine zones. This means that the effective pressure is corrected subtracting the overburden pressure. Intermediate values allow for a partial connectivity to the ocean.

The scaling parameter $\lambda\epsilon$[0,1] is used to scale the universal friction coefficient c_f depending on bedrock characteristics. A lower λ allows for faster basal sliding because of the existence of a temperate bedrock base (i.e. $T_b = T_{fp}$) or because of the presence of sediments, for instance. In this thesis either a constant value will be used for the whole domain, hence $\lambda = 1$ (Chapter 3), or either through a depth dependent parameterisation, which enhances ice flow in topographic lows (Chapters 4,5). For this last case λ is defined through an exponential function dependent on bedrock elevation (z_b):

$$\lambda = \begin{cases} 1 & \text{if } z_b > z_1 \\ \max\left[\exp\left(\frac{z_b - z_1}{z_1 - z_0}\right), \lambda_{\min}\right] & \text{if } z_b < z_1. \end{cases} \tag{2.45}$$

Here z_0 and z_1 are internal parameters prescribed in the code, where $z_1 > z_0$. For a bedrock elevation above z_1 the scaling factor λ saturates to 1. This represents a bedrock depth where sliding is hampered (see Fig. 2.5). At z_0 the bedrock coefficient is always $1/e$ (the e-folding depth). Thus, if z_0 is set close to z_1 then the friction decreases more abruptly with decreasing depth than if these parameters are set more distanced. $\lambda_{\min}$ determines a threshold which allows for a faster or slower sliding. This parameterisation is intended to capture the nature of the fast sliding zones especially of the marine parts in Antarctica. It is ultimately based on the approach of Martin et al. (2011). They use a till friction angle which facilitates sliding as the bedrock decreases in the marine regions. They find that this formulation for the bedrock friction simulates more realistic PD states than a bedrock temperature approach, when a basal hydrology model is not present.

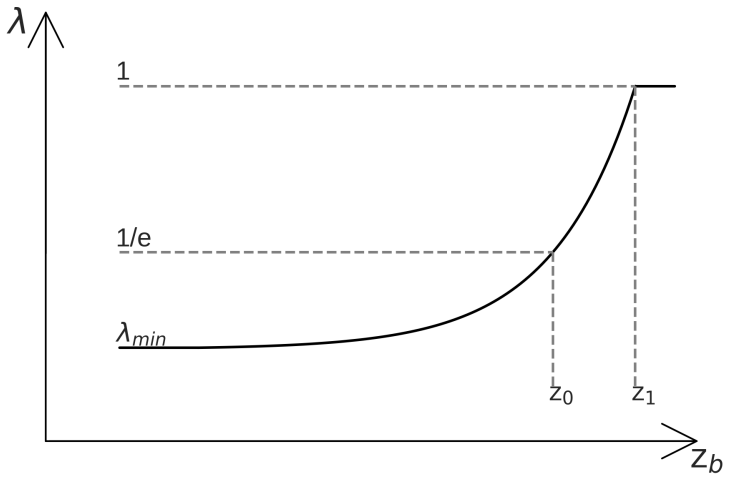

Fig. 2.5: Sketch of the scaling parameter λ for a depth dependent parameterisation.

2.4 Thermodynamics

Finally, the thermodynamics of the model are defined through energy conservation:

$$\rho_i c \left(\frac{\partial T}{\partial t} + \mathbf{v} \cdot \boldsymbol{\nabla} T \right) = \boldsymbol{\nabla}(k \boldsymbol{\nabla} T) + \Phi. \tag{2.46}$$

Here, c is the heat capacity of ice, T the ice temperature, k the heat conductivity of ice and Φ the internal deformation, also called strain heating. The ice temperature is necessary for solving the Arrhenius law as seen in Eq. 2.11 which determines the ice deformation through viscosity. Again, for solving the heat equation some assumptions are made for the sake of simplicity. First, the strain heating can be expressed as:

$$\Phi = 4\eta\dot{\epsilon}^2. \tag{2.47}$$

where $\dot{\epsilon}$ is the effective strain rate described in Eq. 2.8. Heat diffusion within the ice is considered purely vertical (only the ice column), as horizontal diffusion is considered negligible (Greve and Blatter, 2009). Thus, the energy conservation equation can be rewritten as

$$\frac{\partial T}{\partial t} = \frac{k}{\rho_i c} \frac{\partial^2 T}{\partial z^2} - u \frac{\partial T}{\partial x} - v \frac{\partial T}{\partial y} - w \frac{\partial T}{\partial z} + \frac{4\eta\dot{\epsilon}^2}{\rho_i c}. \tag{2.48}$$

Ice surface temperature

To solve the Equations2.48, boundary conditions are necessary. These are set separately and are commented on in Section 2.6. Nonetheless it is worth mentioning, that at the ice surface, the ice temperature is limited to a maximum value of $T_0 = 273.15$K, the freezing-point temperature.

Grounded ice basal temperature

At the ice-bedrock interface Yelmo distinguishes between two cases: a frozen bedrock and a temperate bedrock. If the ice base is frozen ($T_i < T_{fp}$), then the

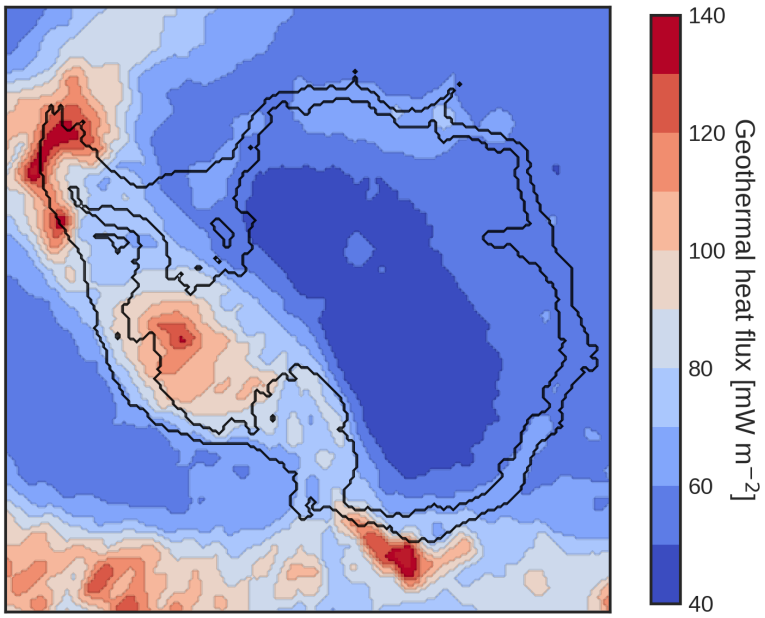

Fig. 2.6: Geothermal heat flux from Shapiro and Ritzwoller (2004). Inner black contour line represents the observed grounding-line position. External black line the continental-shelf break.

boundary condition for the vertical gradient of temperature is prescribed as

$$\left.\frac{\partial T}{\partial z}\right|_{z=z_b} = -\frac{Q_{geo}}{k}, \tag{2.49}$$

where Q_{geo} is the geothermal heat flux, which is set as a boundary condition. In this thesis a spatial map from Shapiro and Ritzwoller (2004) is used (Fig. 2.6). If the basal temperature is at the pressure melting point, then the bed is temperate and the melting rate (B) is diagnosed as (Cuffey and Paterson, 2010):

$$B = -\frac{1}{\rho L}\left(Q_b + k\left.\frac{\partial T}{\partial z}\right|_{z=z_b} + Q_{geo}\right). \tag{2.50}$$

Here L is the latent heat for fusion for ice and Q_b the basal heat production due to sliding friction. Melting of ice shelves is not computed through the thermodynamics module and is set as a boundary module (a detailed description can be found in Section 2.6).

2.5 Grounding-line diagnosis

The grounding-line is the limit between the marine grounded ice and the ocean or floating ice. Yelmo diagnoses the grounding-line through the overburden ice thickness, which is computed as

$$H_{grnd} = H_i - \frac{\rho_w}{\rho_i} \max\left(z_{sl} - z_b, 0\right), \tag{2.51}$$

where z_{sl} represents the sea level. Thus, if $H_{grnd} >0$, then the ice is grounded and if $H_{grnd} <0$ then the ice is floating (or an ocean grid point). The grounding line is diagnosed as the last grounded point before floating and is therefore considered fully grounded.

2.6 Boundary conditions

Yelmo includes a module which loads all the necessary fields that the model requires as boundary conditions. The required boundary conditions can be set manually or from other model outputs. This construction also allows for a potential coupling of the ice model with other Earth System models for instance. Here the most relevant boundary conditions in this work are discussed.

2.6.1 Surface mass balance

The surface mass balance is computed as the sum of the mass gain through accumulation and the mass loss via ablation. Accumulation is derived from the total snowfall from a mean climatic precipitation field. In this thesis, for PD boundary conditions, temperatures and precipitation are given from the regional climate model RACMO 2.3 (Van Wessem et al., 2014) forced by the ERA-Interim reanalysis (Dee et al., 2011). Ablation is computed through the Positive-Degree Day Scheme (PDD; Reeh (1989)). This method is very popular in ice models since it only requires surface temperatures as input. It calculates the number of days that temperatures are sufficiently high to melt ice from a normal statistical distribution around a mean, thus

$$PDD = \frac{1}{\sigma\sqrt{2\pi}} \int_{1\mathrm{yr}} \int_{0}^{\infty} \exp\left(\frac{-(T - T_d)^2}{2\sigma^2}\right) dT dt. \tag{2.52}$$

Here, σ is the standard deviation, assuming that daily temperatures (T_d) follow a normal distribution ($\sigma = 5$ K). The temperature evolution during one year follows a cosine function scaled with the mean summer and mean annual temperature. There are more complex methods that account for an energy-balance through short-wave radiation for instance (Robinson et al., 2011). Nevertheless, the PDD scheme is commonly used in ice models in the Antarctic domain, because ablation at these latitudes is almost negligible and there is no need for more sophisticated methods (Winkelmann et al., 2011; Pollard and DeConto, 2012b; Pattyn, 2017).

2.6.2 Ice-ocean interaction

As already mentioned before, floating ice shelves lose mass through melting at the surface, which is almost negligible on the Antarctic domain, calving at the ice front, and basal melting below the ice shelves. Ice-ocean interactions have played an important role in the past evolution of the AIS and, very likely, will do so in the future. Because an increase of oceanic temperatures can diminish

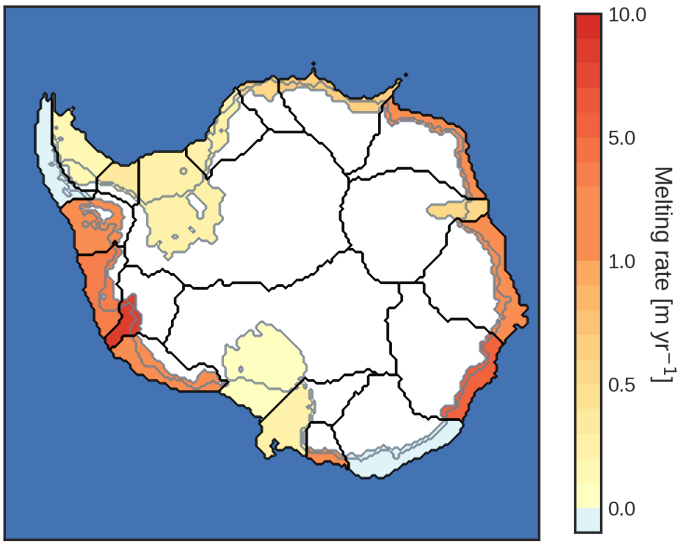

Fig. 2.7: The measured basal melting rates of Rignot et al. (2013) averaged into 19 basins based on Zwally et al. (2012) and Reese et al. (2018). Positive numbers represent basal melting whereas negative represent refreezing. At the grounding-line these values are scaled by a factor ten and averaged over its floating part. Dark blue colors represent the deep ocean (i.e. bedrock depths below -2000m).

the buttressing effect, or even trigger a MISI mechanism, its representation in ice-sheet models is crucial. However, ice models differ greatly in the way ice-ocean interaction is taken into account, as oceanic processes are difficult to asses. The oceanic waters at the continental shelf are mainly composed of cold and dense shelf waters, warm circumpolar deep waters and colder Antarctic surface waters (Dinniman et al. (2016) and references therein). The penetration of warm circumpolar deep waters onto the continental-shelf break is what drives melting at the base of ice shelves. However, the process by which these waters enter onto the continental shelf is complex. Changes in the tropics shift wind currents southwards, promoting upwelling at the SO and enhancing the penetration of these waters (Steig et al., 2012). In addition, three-dimensional ocean circulation

models are computationally expensive making it difficult to couple to ice-sheet models.

In addition to the oceanic currents, the freezing point temperature depends on the oceanic salinity, which in turn depends on the ice depth. This adds another degree of difficulty. However, not all ice-sheet models account for salinity changes and for simplicity it is generally set to T_{fp} =-1.8 C. Also, when the ice melts, turbulent buoyant plumes are formed at the ice-ocean interface which are propagated from the grounding-line towards the ice front (Jenkins, 2011). Because accounting for all these processes is a complicated task for ice-sheet models, the choice of basal-melting law is somewhat arbitrary. Several laws have been proposed and all succeed in simulating a realistic PD state with accurate parameter tuning (Seroussi et al., 2019, 2020).

In this thesis, in order to transfer the oceanic temperatures into basal melting rates (B_m) a linear law derived from Beckmann and Goosse (2003) is used

$$B_m(t) = \kappa \left(T^{\mathrm{ocn}}(t) - T_f \right), \tag{2.53}$$

where $T^{\mathrm{ocn}}(t)$ is the time evolving ocean temperature and T_f the freezing point temperature. The oceanic temperature can be obtained from models. κ is the heat flux exchange coefficient between ice and ocean, expressed in [m yr^{-1} K^{-1}]. A linear law is a common approach in ice models (Philippon et al., 2006; Martin et al., 2011; Alvarez-Solas et al., 2013; Golledge et al., 2015), however other studies use a quadratic approach (Holland et al., 2008; Pattyn, 2017; Pollard and DeConto, 2012b). Pollard and DeConto (2012b) went a step forward and included a scaling factor to account for changes in the oceanic currents depending on the embayment shape. Nowadays even more sophisticated models are available which include box models of the ocean and/or buoyant plume melt rate parameterisation (Lazeroms et al., 2018; Reese et al., 2018; Pelle et al., 2019). However, whether these relations hold for other time periods is unknown. In this work special focus is made on the past evolution of the AIS. Because the past oceanic temperature and salinity is not clearly defined, it is convenient to use a parameterisation more suitable for paleo studies. Hence, the basal melting rates will be computed the through temperature anomalies. To this end the oceanic

temperatures are split into the PD climatologies and the anomaly with respect to the referred time-period.

$$T^{\mathrm{ocn}}(t) = T^{\mathrm{ocn}}_{clim} + \Delta T^{\mathrm{ocn}}(t). \tag{2.54}$$

Hence Eq. 2.53 results in

$$B_m(t) = \kappa \left(T^{\mathrm{ocn}}_{clim} + \Delta T^{\mathrm{ocn}}(t) - T_f\right) = \kappa \left(T^{\mathrm{ocn}}_{clim} - T_f\right) + \kappa \Delta T^{\mathrm{ocn}}(t). \tag{2.55}$$

$\kappa \left(T^{\mathrm{ocn}}_{clim} - T_f\right)$ is equivalent to the present-day basal melting rates B_0 and so the definitive basal-melting equation used in this thesis is obtained

$$B_m(t) = B_0 + \kappa \Delta T^{\mathrm{ocn}}(t). \tag{2.56}$$

From satellite measurements these PD melting rates (B_0) can be estimated (Depoorter et al., 2013; Liu et al., 2015). For this work the inferred basal-melting rates from Rignot et al. (2013) are used, extrapolated over the Antarctic basins identified by Zwally et al. (2012) and Reese et al. (2018) (Fig. 2.7). Rignot and Jacobs (2002) found a linear relationship between the measured melt-rates and the temperature difference between the closest oceanic point and the freezing-point temperature, estimating a κ value of 10 [m yr^{-1} K^{-1}]. In this thesis a spatially homogeneous κ value is used, however this is a vast simplification. For instance, at the Amery or the Pine Island shelf a heat coefficient of 10 [m yr^{-1} K^{-1}] is very likely too high (Holland et al., 2008). Also, if it is used in transient simulations, it should be highly dependent on ocean salinity and currents. However, as already mentioned, there is high uncertainty in the ice-ocean interactions. This parameterisation allows for a comprehensive sensitivity study of the ocean's role in the evolution of the AIS.

The intrusion of warm salty bottom waters into the shelf and the plume formation ensure that the melting rates close to the grounding line are higher than at the ice front (Dutrieux et al., 2013; Reese et al., 2018). Rignot and Jacobs (2002) also show that these melting rates are about one order of magnitude larger at the grounding line. In Yelmo, an order of magnitude higher melt rates are prescribed

for floating ice points adjacent to the grounding line. Another common approach in ice models is to weight the grounded fraction at the grounding-line and apply its correspondent melt rate. However, this option is found to potentially overestimate sea-level estimates (Seroussi and Morlighem, 2018).

2.6.3 Glacial Isostatic Adjustent (GIA)

Yelmo is coupled to a simple glacial-isostatic adjustment (GIA) model to account for bedrock changes. The GIA describes the evolution of the solid Earth through the growth or decay of large ice sheets. It has profound implications for the AIS as it can hamper (or enhance) ice advance and facilitate the intrusion of warm water onto the continental-shelf (Whitehouse et al., 2019). However, although the physical basis is now well established (Whitehouse, 2018), ice models use rather simple schemes for long timescale simulations. In this thesis, the Elastic Lithosphere-Relaxed Asthenosphere method is used (Le Meur and Huybrechts, 1996). This model assumes that due to the elasticity of the lithosphere a deposition of ice weight has to result in a non-local response caused by a lateral shift (Greve and Blatter, 2009). The asthenosphere below, on the other hand, relaxes to its equilibrium in a defined characteristic time which is set as a parameter (in this work, set to 3000 yr). However, it is worth mentioning that this method does not capture differences in the asthenosphere viscosity and rheological properties as in the WAIS for example, where bedrock responses may occur on a different timescale.

Chapter 3
The Antarctic Ice Sheet response to glacial millennial-scale variability*

As already commented before, in Chapter 1, a significant sea-level contribution of the AIS at millennial timescales during the LGP cannot be discarded. The LGP shows episodes of rapid sea-level changes, up to 20 m at millennial timescales. The origin of these fluctuations is associated to northern paleo ice-sheets, such as the GrIS, FIS, EIS and LIS. However, no attempt has been made to study a potential contribution of the AIS. Compared to NH ice sheets, Antarctica is a much more isolated ice sheet, specially at glacial stages, and hence studies have not focused on its potential contribution. Nonetheless, it is well known from reconstructions, that during glacial times, the AIS advanced more than its present-day position encompassing a large portion of marine-based zones. Based on the bipolar seesaw mechanism, the SO could have acted as a heat reservoir during slow AMOCs. This converts Antarctica into a potentially vulnerable region and therefore the potential role of the ocean should be assessed.

Such a study allows to gain insight in the response of large continental ice sheets to abrupt oceanic warming, which is specially relevant for the future predictions. Hence, in this chapter the response of the AIS to glacial millennial-scale variability, focusing on its interaction with the ocean, is investigated. Contrary to the other works presented in this thesis, here the Grisli-UCM model is used.

* The main contents of this chapter are published in:
Blasco, J., Tabone, I., Alvarez-Solas, J., Robinson, A., and Montoya, M., 2019: The Antarctic Ice Sheet response to glacial millennial-scale variability. *Climate of the Past*, **15**, 121–133. DOI https://doi.org/10.5194/cp-15-121-2019, 2019.

It is a version of the thermomechanical three-dimensional ice-sheet-shelf Grisli model (Ritz et al., 2001) and precursor of the definitive Yelmo model described in Chapter 2 with some differences regarding boundary conditions and auxiliary modules. To investigate the response of the AIS to oceanic warming a sensitivity study of different heat-flux coefficients is performed. Results show that, contrary to the widespread idea that Antarctica is a slow reactive ice sheet which responds only to orbital scale forcing, the AIS is capable to react rapidly to abrupt oceanic changes. Important sea-level contributions (up to 6 m) and grounding-line migrations can take place at the involved timescales. This, furthermore, changes the potential role of the AIS during glacial stages and suggest that future reconstruction of sea-level variations, specially during MIS-3, should take Antarctica into account.

The chapter is structured as follows: first a theoretical background is introduced to describe millennial-scale variability during the LGP (Section 3.1); then the experimental setup is described (Section 3.2). In Section 3.3 the obtained results are shown and its potential implications and range of realness are discussed in Section 3.4. Finally, the main conclusions of this work are summarized (Section 3.5).

3.1 Millennial-scale variability and the role of the AIS

Understanding the response of the large ice sheets to abrupt climate changes is crucial to constrain future sea-level projections (Bakker et al., 2017a,b). A major concern of the glaciological community is the reaction of Antarctica to the penetration of warm circumpolar deep water (CDW) onto the continental shelf (Schmidtko et al., 2014; Sallée, 2018). On one hand, the thinning of ice shelves, as reported by Paolo et al. (2015), represents a global threat as it diminishes the buttressing effect that the floating ice exerts on the ice sheet (Fürst et al., 2016), accelerating inland ice flow into the ocean. This process has been observed in Larsen C ice shelf (Rignot et al., 2004) and Pine Island Glacier and Thwaites Glacier (Jacobs et al., 2011; Favier et al., 2014; Rignot et al., 2014). These two

last glaciers in addition suppose a critical component of the WAIS. Conceptual models suggest an inherent instability, the MISI, in the marine zones of the WAIS due to its retrograde bed slope, as in the Amundsen sea region (Weertman, 1974; Schoof, 2007). Such a mechanism could imply a sea-level rise of more than 3 m in a short timescale (Bamber et al., 2009; Feldmann and Levermann, 2015; Sutter et al., 2016). However, whether such a mechanism is already underway remains elusive. Thus, it is essential to improve our understainding of the AIS sensitivity, to constrain future projections (Bakker et al., 2017b). Some of the most remarkable abrupt climate changes of the near past are those of the last glacial period (LGP;110–10 ka). Thus, one way to gain insight in this respect is to assess the response of the AIS to these past rapid climate changes

MIS-3 sea-level reconstructions show rapid variations of more than 20 m at millennial timescales (Frigola et al., 2012; Grant et al., 2012; Rohling et al., 2014) and during meltwater pulse (MWP) 1A (at around 14.5 ka) rapid rises of 4 m per century occurred (Liu et al., 2016). The origin of these variations is associated to NH paleo ice-sheets (Arz et al., 2007; Ganopolski et al., 2010). Because the AIS is located at higher latitudes, and hence less exposed to mass losing processes through atmospheric forcing (ablation), no focus has been attended to the AIS. However, Siddall et al. (2008) already pointed to a potential source from the SH. Moreover, the sea-level fluctuations as recorded by coral fossils reveal an Antarctic-like rhythm, rather than an abrupt DO-like event, suggesting that a considerable contribution from the AIS cannot be excluded (Siddall et al., 2008; Rohling et al., 2009; Grant et al., 2012).

Because atmospheric variations alone seem rather an unrealistic mechanism to provoke a response of the AIS, focus has to be done in the ocean. This work is based on the bipolar-seesaw mechanism by which, during glacial stages, the AMOC slows down and more heat is transferred into the SO, acting as a heat reservoir (Stocker, 1998). Because of the marine character of the AIS, a warmer ocean could potentially have a strong effect in the marine parts. In fact, Kusahara et al. (2015) modelled the basal-melt rate of the Antarctic LGM ice shelves with a coupled ice-shelf–sea-ice–ocean model. Their results showed that LGM basal-melting rates of ice shelves were larger than PD values as a result of more warm

waters originating from Circumpolar Deep Water (CDW) caused by changes in the salinity. These warm waters could potentially penetrate onto the AIS cavities by the strengthen of circumpolar winds, enhancing upwelling (Banderas et al., 2012; Holland et al., 2019). Therefore, the impact of the SO during glacial stages has to be assessed as it could have strong implications on driving millennial-scale variability.

3.2 Experimental setup

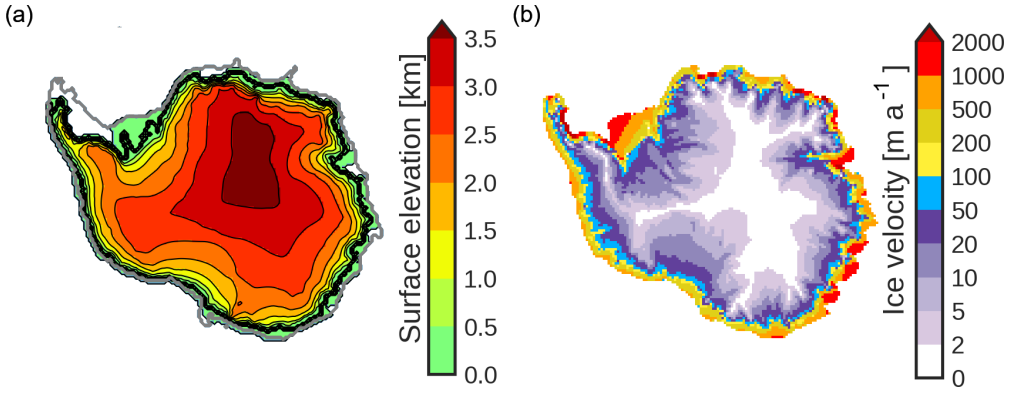

Fig. 3.1: Simulated ice-sheet (a) surface elevation (in km) and (b) ice velocities (in m a^{-1}) after the spin-up procedure. The thick black line indicates the simulated grounding line position. The thick grey line represents the continental shelf break (depth 2000 m).

For this study the three-dimensional thermomechanical ice-sheet-shelf Grisli-UCM model is used. Ice dynamics and thermodynamics are solved on a 40 km x 40 km grid of 21 vertical adaptive layers, covering a space of 157 x 147 grid points. The initial surface and bedrock elevations (and thus ice thickness values) are provided from the RTopo-2 dataset (Schaffer et al., 2016), an improved bedrock map of Bedmap2 (Fretwell et al., 2013) with corrected ice-shelf cavities. The

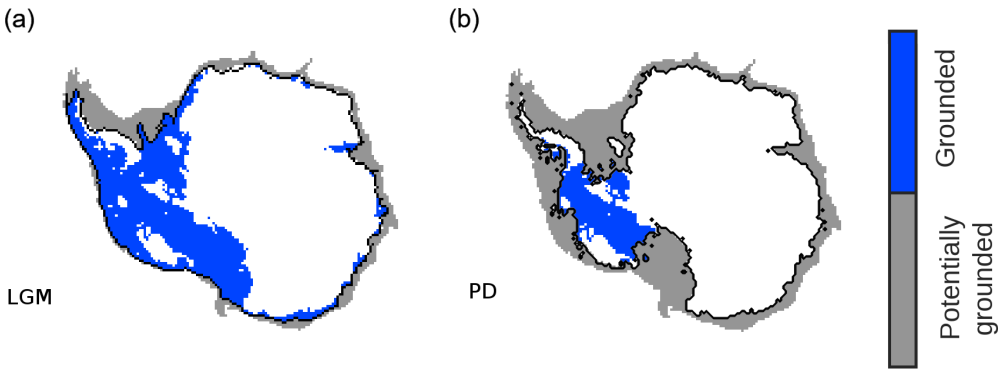

Fig. 3.2: Mask used to evaluate grounding line migration. (**a**) Ice extent after glacial spin-up and (**b**) PD ice extension. Blue zones are model grid cells with grounded ice in marine zones. Grey zones are model grid cells without grounded ice in marine zones but the underlying bathymetry is shallow enough to potentially become grounded (i.e., marine zones with depths less than 2000 m). The thick black line indicates the grounding line position.

Parameter	Units	Value(s)
LGM submarine melting B_{LGM}	m yr^{-1}	0
AIM temperature anomaly $\Delta T_{\mathrm{min}}^{\mathrm{ocn}}$	K	0.5
Heat flux coefficient κ	m yr^{-1} K^{-1}	0,1,3,5,7,10,15

Table 3.1: Summary of the studied parameter values used in each sensitivity test.

hybrid scheme used in this work is different than in Yelmo. If the temperature at the base is below the pressure-melting point, then no basal sliding is considered and internal dynamics are solved via its SIA solution. Zones of fast flowing areas are activated if the bedrock temperature is at the pressure-melting point and the exerted effective pressure at the ice base exceeds an imposed threshold. Only then basal sliding is allowed and dynamics are solved as a sum of the SIA and the SSA solution. Floating ice shelves are solved via the SSA solution without any basal friction.

As described in Chapter 2, the total mass balance is given by the total net accumulation and ablation at the surface, the melted ice at the base of the ice sheet and ice shelves, and calving at the ice front. The SMB is computed via the positive degree-day approach (PDD; Reeh 1989). Sub-shelf basal-melting rates are computed through the linear anomaly method described in 2.

3.2.1 Forcing method and experimental design

Based on Banderas et al. (2018), transient simulations are forced with two climatic indices, an orbital index α(t) (where $\alpha = 0$ represents the LGM state and $\alpha = 1$ the PD state) and a millennial index β(t) (where $\beta = 0$ represents the glacial state and $\beta = 1$ the AIM state). Because this work focuses on the response of an Antarctic glacial state to millennial-scale variability, $\alpha = 0$ is set, to maintain constant glacial background conditions. The β index is extracted from the Dome C temperature reconstruction (Jouzel et al., 2007) and filtered between 1 and 19 ka to avoid any spurious noise and orbital contribution (Fig. 3.3c). Hence, the evolution of the temperature ($T^{\mathrm{atm}}(t)$) and precipitation field ($P(t)$) is given by the following equation:

$$T^{\mathrm{atm}}(t) = T^{\mathrm{atm}}_{\mathrm{LGM}} + \beta(t)\, T^{\mathrm{atm}}_{\mathrm{mil}} \tag{3.1}$$

$$P(t) = P_{\mathrm{LGM}}\left[(1-\beta(t))\,\delta P_{\mathrm{orb}} + \beta(t)\,\delta P_{\mathrm{mil}}\right], \tag{3.2}$$

where the LGM climatologies ($T^{\mathrm{atm}}_{\mathrm{LGM}}$ and P_{LGM}) are computed from the PD ERA-Interim reanalysis (Dee et al., 2011) and corrected with the LGM-PD anomaly obtained from the climatic model of intermediate complexity Climber-3α (Montoya and Levermann, 2008). The anomaly fields between the LGM and the AIM state ($T^{\mathrm{atm}}_{\mathrm{mil}}$ and P_{mil} respectively) are provided from the same climatic model.

Following this same procedure to Eq. 2.56, the applied basal melting rates (B_m) can be rewritten as:

$$B_m(t) = B_{\mathrm{LGM}} + \kappa\beta(t)\,\Delta T^{\mathrm{ocn}}_{\mathrm{mil}}. \tag{3.3}$$

B_{LGM} represents the basal melting rate at the LGM and $\Delta T_{\mathrm{mil}}^{\mathrm{ocn}}$ the oceanic temperature anomaly during an AIM stage. κ is the heat-flux exchange coefficient between ice and ocean. To avoid unrealistic accretion rates, the melting parameterisation cannot become negative. Rignot and Jacobs (2002) showed that basal-melting rates close to the grounding-line are by one order of magnitude larger than at the rest of the ice shelf. Thus, Grisli-UCM computes basal-melting rates of floating points in contact with a grounding-line point ten times larger than at the rest of floating points. The election of a linear basal melting law is somewhat arguable. Although this is a common approach in ice models (Philippon et al., 2006; Alvarez-Solas et al., 2013; Golledge et al., 2015; Tabone et al., 2018), other studies use quadratic forms for instance (Pollard and DeConto, 2009; DeConto and Pollard, 2016; Pattyn, 2017). However, these approximations are not necessary more sophisticated and as the aim of this work is to investigate the oceanic sensitivity, no higher order dependence for this purpose is required.

In this experimental setup, first the ice model is spun up for 120 kyr under constant glacial conditions. Terrestrial and marine geological records indicate that the AIS most likely fully advanced towards the continental-shelf break at the LGM (Anderson et al., 2002; Denton and Hughes, 2002; Hillenbrand et al., 2012; Whitehouse et al., 2012a; The RAISED Consortium, 2014), thus, in order to allow for a maximum extension B_{LGM} =0 m yr^{-1} is set. The continental-shelf break is found to be at a bedrock depth of 2000 m. Grounded ice does not advance further because the continental slope is too steep. To avoid an unrealistic ice-shelf extension, an artificially large melting rate is set outside the continental-shelf break to kill the floating ice. This is motivated by the intrusion of warm circumpolar waters into the ice-shelf cavities at the LGM (Kusahara et al., 2015). The oceanic millennial temperature anomaly signal is extracted from the DomeC ice core (Jouzel et al., 2007). The amplitude of the AIM events is found to be ca. $\Delta T_{\mathrm{mil}}^{\mathrm{atm}}$ =2 K. Following the same approach as in Golledge et al. (2015), based on Collins et al. (2013), per every degree that the atmosphere warms/cools, the ocean warms/cools to one fourth. Hence $\Delta T_{\mathrm{mil}}^{\mathrm{ocn}}$ =0.5 K. For simplicity, oceanic variations are applied spatially homogeneous. Due to the uncertainty associated to the ice-ocean interaction, different oceanic sensitivities are tested. For this

purpose, a set of κ values is assigned, ranging from no ice-ocean interaction (0 m yr^{-1} K^{-1}) to a high sensitivity (15 m yr^{-1} K^{-1}). Table 3.1 summarizes all the tested parameters within this work. Sea-level variations are prescribed from Rohling et al. (2014).

3.3 Results

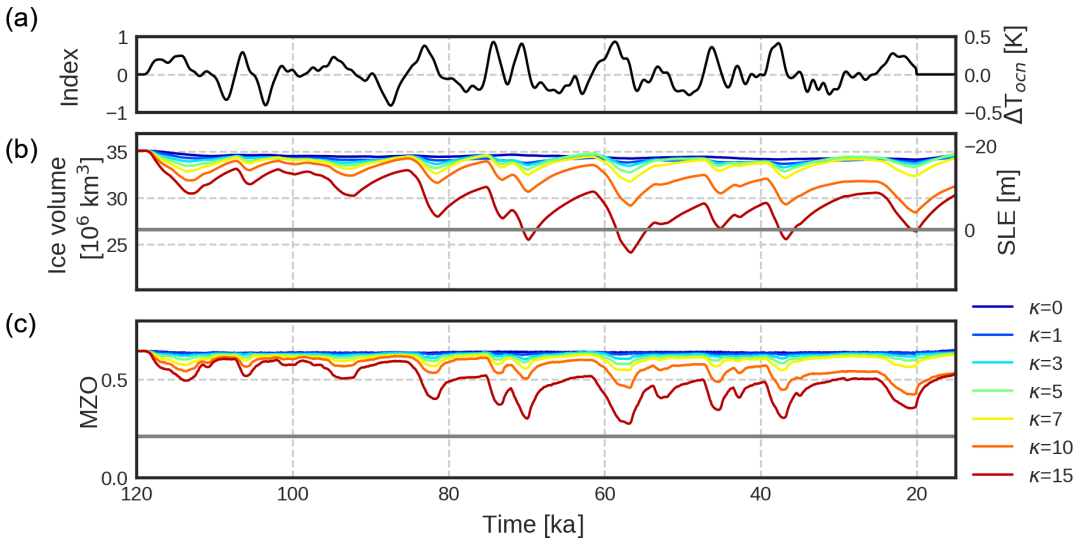

Fig. 3.3: (**a**) Millennial-scale forcing index (β). On the right-hand side the equivalent oceanic temperature anomaly is shown (in K). (**b**) Ice volume (in million km^3) and SLE contribution (in m). (c) MZO evolution for different oceanic sensitivities. Colors go from no ice-ocean interaction ($\kappa = 0$ m a^{-1} K^{-1}, dark blue) to large oceanic sensitivity ($\kappa = 15$ m a^{-1} K^{-1}, red). The solid grey line in (**b**) and (**c**) indicates the present-day value of the ice volume and MZO, respectively.

Figure 3.3a shows the applied forcing index in this work, Figure 3.3b the response of the AIS in terms of SLE and Figure 3.3c the grounding-line migration

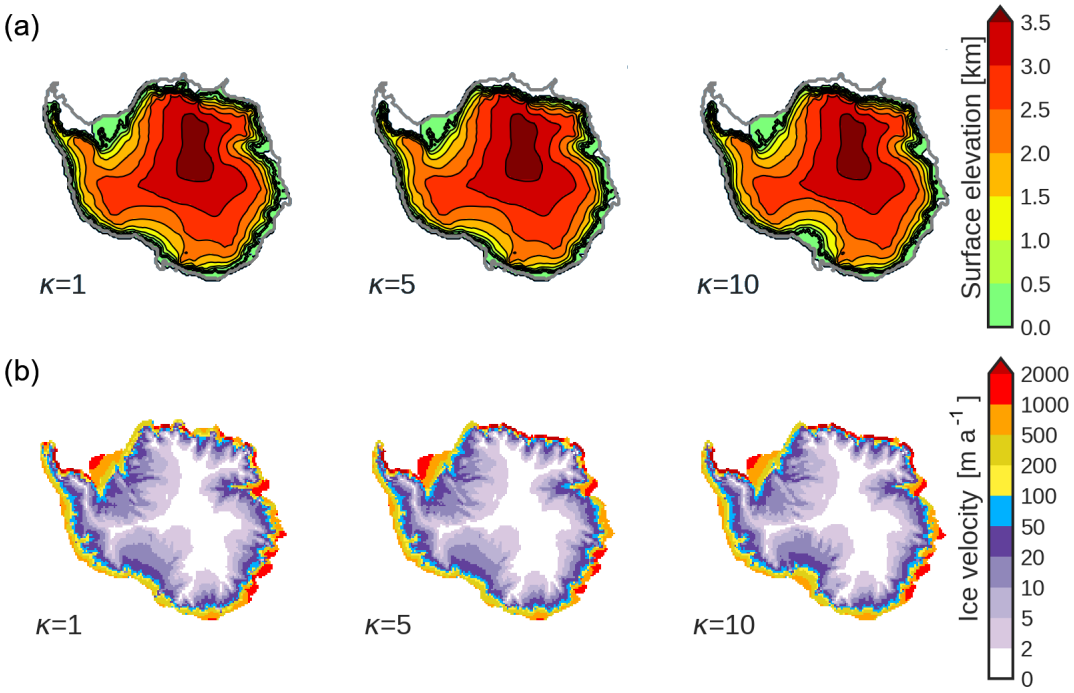

Fig. 3.4: Snapshots of the AIS simulations at a cold phase (61 ka) for three different oceanic sensitivities ($\kappa = 1, 5, 10$ m a^{-1} K^{-1}). (**a**) Surface elevation (in km). The thick black line indicates the grounding line position, and the thick grey line is the continental shelf break. (**b**) Ice velocities (in m a^{-1}).

for different oceanic sensitivities. If no ice-ocean interaction is considered (κ =0 m yr^{-1} K−1), then no sea-level changes nor grounding-line migrations are observed. This means that the atmospheric forcing (temperature and precipitation changes) alone are not sufficiently large to have a direct impact on the size of the AIS. Only when ice-ocean interactions are considered, ice volume, as well as ice area changes, occur. The amplitude of these variations increases with increasing oceanic sensitivity (κ values). Because basal-melting rates are set to zero (B_{LGM} =0 m yr^{-1}) ice discharges and ice retreat only occur when the β

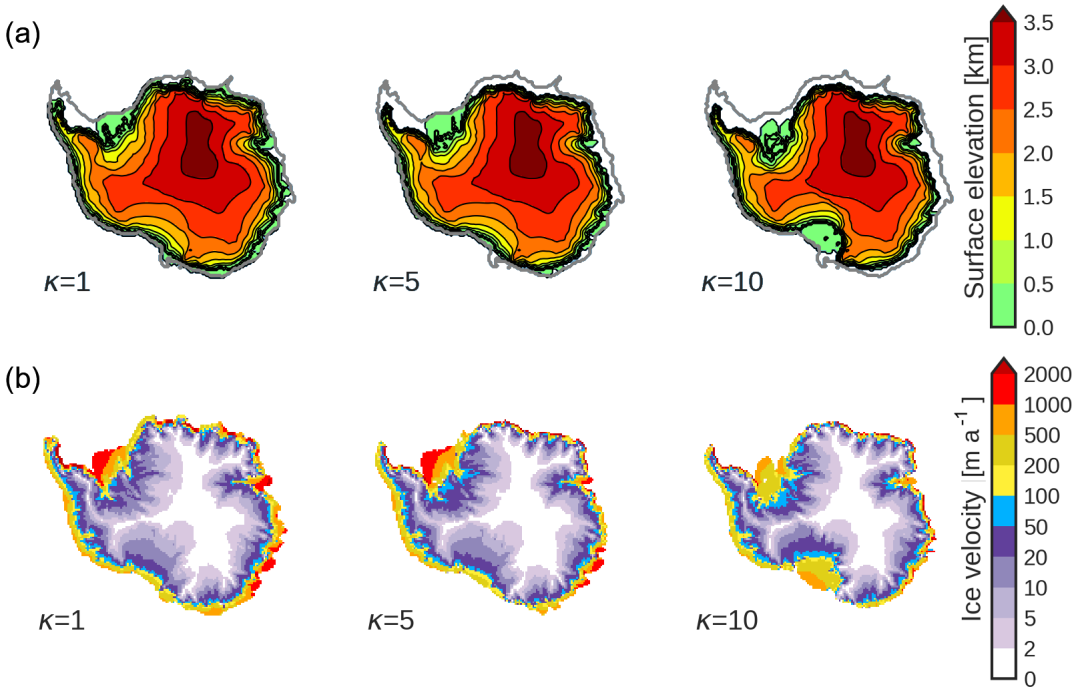

Fig. 3.5: Snapshots of the AIS simulations at the end of a warm phase (AIM) event (57 ka) for three different oceanic sensitivities ($(\kappa = 1, 5, 10$ m a^{-1} K^{-1}). (**a**) Surface elevation (in km). The thick black line indicates the grounding line position, and the thick grey line is the continental shelf break. (**b**) Ice velocities (in m a^{-1}).

index becomes positive. When the forcing index becomes negative no melting (nor refreezing) happens and the AIS expands and increases.

To quantify the ice extension the parameter "Marine Zone Occupation" (MZO) is introduced, defined as:

$$\mathrm{MZO} = \frac{N_\mathrm{G}}{N_\mathrm{G} + N_\mathrm{P}}, \tag{3.4}$$

where N_G is the total number of modeled grid cells with grounded ice in marine zones (i.e., zones where the ice is grounded below sea-level; blue zones in Fig. 3.2a,b). N_P is the total amount of marine grid cells which potentially could

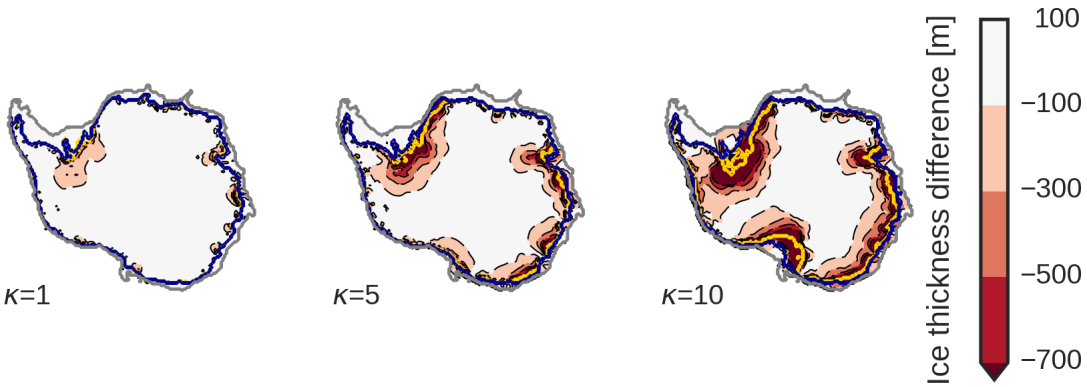

Fig. 3.6: Ice thickness difference between the AIM and the cold phase (AIM minus cold) for different values of oceanic sensitivity ($\kappa = 1, 5, 10$ m a^{-1} K^{-1}). Zones with an intense red color illustrate a larger ice difference and hence a major ice loss. The thick blue line illustrates the grounding line position at the cold phase and the thick yellow line the grounding line position at the AIM phase. The thick grey line illustrates the position of the continental shelf break.

become grounded (i.e. regions where the ice is not grounded and its bathymetry is shallow enough to become grounded but below sea-level; in this work these regions are identified as bedrock depths above -2000 m; grey zones in Fig. 3.2a,b). Thus, a fully expanded ice sheet would imply a MZO value of 1. PD values are about MZO=0.21 (Fig. 3.2b), hence lower values imply a more retreated ice sheet than PD. After the spin-up procedure a LGM value of MZO=0.71 is simulated (Fig. 3.2a). The simulated LGM ice sheet did not fully advance towards the continental-shelf break. The Pine Island zone or George Land for instance remain ungrounded (Fig. 3.1a). If no oceanic sensitivity (κ =0 m yr^{-1} K−1), then the MZO value remains at its LGM state. Otherwise, when oceanic variability is considered, then AIS waxing and waning events at millennial timescales are found (Fig. 3.3c).

An intermediate simulated glacial state (at 61 ka) for different heat-flux coefficients (κ =1, 5, 10 m yr^{-1} K^{-1}) shows similar surface elevations (Fig. 3.4a) and ice velocities (Fig. 3.4b). The Ronne shelf as well as the EAIS show an almost identical grounding-line position. A slightly more retreated grounding line

is found in the Ross shelf for κ =10 m yr^{-1} K^{-1}. This is also reflected in the ice stream activity. The Ross shelf is more dynamically active with ice streams penetrating further inland. On the other hand, during an AIM event (at 57 ka), different heat-flux have strong effects on the ice sheet (Fig. 3.5). Whereas a low sensitivity case (κ =1 m yr^{-1} K^{-1}) presents an extensive ice sheet, similar to its glacial state, as the oceanic sensitivity increases (κ =5 m yr^{-1} K^{-1}) marine zones in the Ronne or part of the EAIS begin to retreat and ice velocities increase. For higher sensitivities (κ =10 m yr^{-1} K^{-1}), substantial grounding-line migrations are found in the Ronne and Ross shelf. This allows ice streams to penetrate further inland promoting ice discharge into the ocean. Figure 3.6 shows the ice thickness difference between the glacial state and the AIM state. This highlights the regions where more ice is discharged. Although the grounding-line position for κ =1 m yr^{-1} K^{-1} is almost the same, small ice thickness anomalies are found at the Ronne embayment. As the oceanic sensitivity increases, the anomaly becomes larger and the grounding-line position is more retreated, especially in the Ronne, Ross and Amery shelf.

If the oceanic sensitivity is too large, then the AIS is not capable to return to its glacial state during regrowth periods (β <0). The cooling phases between 70 and 60 ka and 40 and 20 ka represent two good benchmark regrowth periods for instance. Whereas medium to low sensitivities (up to κ =7 m yr^{-1} K^{-1}) return almost to the LGM state (see MZO evolution in Fig. 3.3c), higher sensitivities (κ >7 m yr^{-1} K^{-1}) do not return back to its glacial state suggesting a hysteresis behaviour from the AIS. Thus, a readvance of the grounding-line is only possible if oceanic forcing is suppressed long enough.

Finally, what determines the amplitude of the discharging events is a combination of amplitude and duration of the warming signal. A profound analysis of the detrended ice volume signal between 75 and 15 ka allows to focus only on the basal-melting mechanism (Fig. 3.7a). During this time period six significant discharging events are found in accordance with enhanced submarine melting phases (β >0; grey shaded areas in Fig. 3.7a). The absence of ice-ocean interaction (κ =0 m yr^{-1} K^{-1}) produces no ice discharging events, pointing again to the negligible effect of the atmospheric variability into the AIS size. As the ice-

ocean sensitivity increases (increasing κ) not only larger sea-level contributions for every discharging event occur, but also a wider spread between the events is found, meaning that the sea-level difference between the maximum and minimum event increases. Furthermore, what determines the total amount of sea-level rise of an AIM event is the total heat exchange between the ice and ocean (i.e. the integrated area of β, Fig. 3.8c). If the amplitude is large, but the time interval is short, then the ice sheet has not enough time to respond to the applied warming (Fig. 3.8a). On the other hand, if the AIM period is long, but its warming is smooth, then less melting and retreat will occur (Fig. 3.8b). Thus, the total ice discharge is a sum of both effects.

3.4 Discussion

This experimental design is mainly based on the bipolar seesaw mechanism (Crowley, 1992; Stocker, 2003). The underlying hypothesis states that during millennial-scale reorganizations of the AMOC (slow AMOC) the SO acts as a heat reservoir, warming up. However, this mechanism is under debate as it is not clear yet how much the SO heats. Pedro et al. (2018) for example argue that the strong ACC impede the penetration of warm waters, acting as a barrier and isolating the Antarctic continent. They suggest that the heat reservoir is provided by the southern subtropical Atlantic, rather than the ocean, and transferred into the AIS proxy records through atmospheric currents. In addition, oceanic heat transport changes could be compensated to a large extent by changes in heat transport by the atmosphere and the Pacific Ocean.

On the other hand, Kusahara et al. (2015) show that during the LGM, due to strong stratification in the SO, CDW are warmer and sub-shelf melting rates of overhunged ice shelves are larger than at PD. If these warm waters could penetrate onto the continental-shelf break, it could provoke a rapid response of the AIS at millennial timescales. An increase in wind strength for instance could enhance the intrusion of warm CW causing more melting (Thoma et al., 2008). There is strong evidence of changes in the Antarctic wind changes driven by El

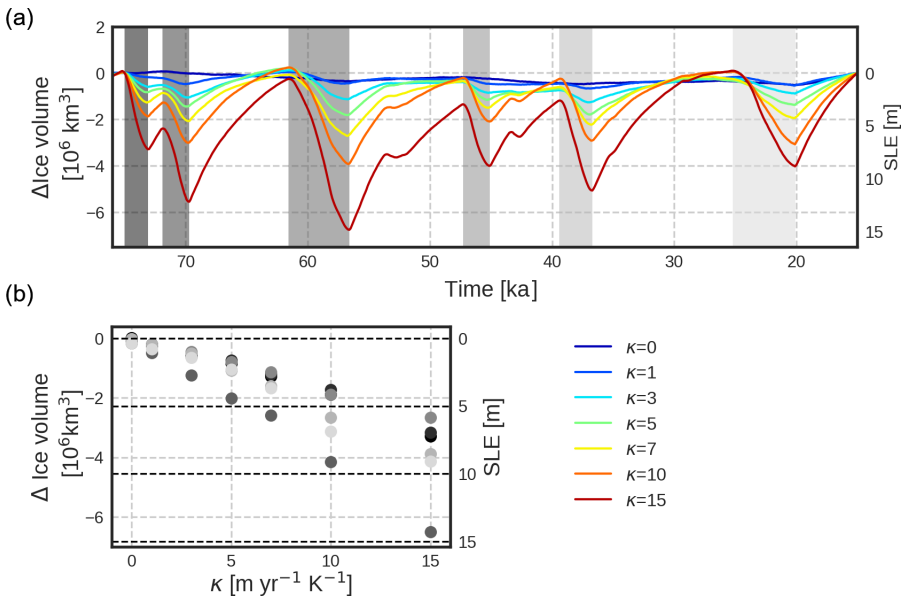

Fig. 3.7: (**a**) Simulated ice volume anomaly between 75 and 15 ka for different values of oceanic sensitivities. Anomalies are calculated relative to the state at 15 ka and detrended between 75 and 15 ka. Grey illustrates significant ice discharging events with increasingly darker grey colors for older events. (**b**) Scatterplot of the sea-level contribution of every discharging phase with respect to κ.

Niño events (Holland et al., 2019) causing changes in West Antarctica (Lachlan-Cope and Connolley, 2006; Steig et al., 2012). Thus, if at a stadial epoch the SO westerly wind intensify, as in Banderas et al. (2015), this could potentially explain a transport of warmer CDW onto the continental-shelf validating the proposed mechanism in this work. Finally, changes in the SO overturning and/or convection can lead to much larger, localized warming (e.g. Martin et al. 2013, 2014). And, in addition, positive feedbacks, as a result from enhanced sea-ice and ice-shelf melting, could further increase warming of the subsurface by enhanced stability of the water column (Weber et al., 2014).

Oceanic temperatures for past periods are highly uncertain due to the scarcity of available data. Thus, because the aim of this work was to study the millen-

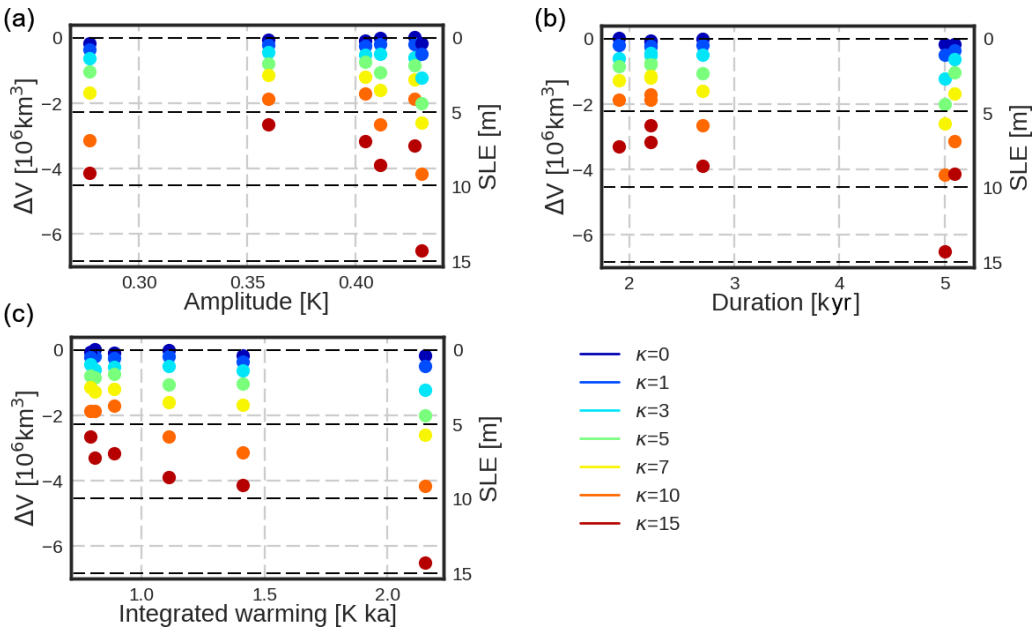

Fig. 3.8: Ice-volume discharge and SLE contribution of every event against (**a**) the amplitude of the warming, (**b**) the duration of the warming phase, and (**c**) the integrated warming defined as the peak warming times the duration. Colors represent the different ice-ocean sensitivities.

nial response of the AIS to a hypothetical glacial oceanic warming, a spatially homogeneous warming in phase with the atmospheric temperature anomaly was considered for simplicity. This anomaly was deduced from an atmospheric temperature reconstruction of DomeC ice core (Jouzel and Masson-Delmotte, 2007). Based on Collins et al. (2013), the estimated oceanic temperature anomaly of an AIM event was about 0.5 K. Of course, a lower amplitude of the AIM signal would smoother the response of the AIS to millennial-scale oceanic temperature variability. Nonetheless, because the heat-flux coefficient κ is still somewhat arguable, it could also be reinterpreted as a weighting parameter of the transferred heat into the SO. Timing differences between the Greenland ice core signal and Antarctic ice cores show a north-to-south directionality supported for a slow

(oceanic) rather than a fast (atmospheric) propagation mechanism (WAIS Divide Project Members, 2015). Thus, it is unclear how much the SO warms up during AIM events, highlighting the need of precise oceanic temperature reconstructions which are unavailable yet.

In this experimental setup, if the heat flux coefficient was larger or equal κ =10 m yr^{-1} K^{-1}, then the ice sheet could not recover to its glacial spin-up state, neither in ice volume nor in extent. This could be highlighting that this conductivity parameter may be too large for the employed ice-sheet model as it is well known, that during the LGM the AIS reached its maximum size from models and reconstructions (Anderson et al., 2002; Denton and Hughes, 2002; Hillenbrand et al., 2012; Whitehouse et al., 2012a; The RAISED Consortium, 2014). Because a κ value of κ =10 m yr^{-1} agrees with observations (Rignot and Jacobs, 2002)., another possible explanation for this hysteresis behaviour could be the fact, that a spatially homogeneous warming may be overestimating melting in specific zones, simulating an unrealistic response of the ice sheet.

In addition to the sea-level changes, grounding-line migrations at the involved timescales are found. The exposed results show that at relatively short timescales, compared to glacial-interglacial cycles, the AIS could retreat and even advance to its glacial configuration rapidly. On one hand, this points to a potentially rapid response of the AIS to future warming scenarios, but this could have also a strong effect on driving climate changes in fact. As proposed by Paillard and Parrenin (2004) brine rejection over the continental-shelf break can have a profound effect on the Earth System. During sea-ice formation, salty water is released defined as brine. Salty waters descend to the bottom of the ocean, affecting the stratification of the water column. This stratification can enhance carbon uplift, which in turn can rise into the atmosphere changing the climate. A periodical retreat and advance of the grounding-line towards the continental-shelf, as in the exposed results, is a potential mechanism to explain periodical brine deposition into deep waters. This may explain DO events as well as glacial-interglacial shifts at orbital timescales.

Finally, sea-level reconstruction during MIS-3 show millennial fluctuations of more than 20 msle (Siddall et al., 2008). The origin of these variations are at-

tributed to paleo NH ice sheets (Arz et al., 2007). This work shows that a considerable sea-level contribution of the AIS cannot be neglected. In fact, none of the results did exceed more than 20 m, thus the results stay within the range of realness. If the heat-flux coefficient is set low (κ <5 m yr^{-1} K^{-1}), sea-level fluctuations are lower than 5 m, which means that the NH ice sheets are the major contributor to these variations, as expected. On the other hand, if κ >10 m yr^{-1} K^{-1} then more than 10 m of sea-level rise happens, which would imply that more than a half of the MIS-3 sea-level changes are due to the AIS contribution. However, as seen before, these values are quite unrealistic, as the ice discharges were probably overestimated. An intermediate case, such as κ =7 m yr^{-1} K^{-1} leads to an ice discharge of 6 msle. This work highlights the importance to gain more knowledge into the Antarctic response to millennial-scale variability as it has a direct impact on reconstructing the size of other paleo ice sheets.

3.5 Conclusions

In this chapter the response of the AIS to millennial-scale variability was studied. For this purpose the hybrid ice-sheet-shelf Grisli-UCM model was used, a previous model version of Yelmo. The climatologies of the model are forced through an index method described in Banderas et al. (2018). Oceanic temperatures, which are transferred into the model as basal melting rates, are forced through an anomaly method as in Tabone et al. (2018). Due to the uncertainty in ice-ocean interactions several oceanic sensitivities are tested. Based on the bipolar seesaw mechanism from Stocker and Johnsen (2003) its assumed that oceanic temperatures covary with atmospheric temperature variations at millennial timescales. These results highlight that, contrary to the widespread assumption that the AIS is rather a slow reactive ice sheet, the AIS is capable to respond to millennial-scale climate variability. Also, whereas atmospheric variation at millennial timescales have no appreciable effect on the size and extension of AIS, SO temperature warming plays a crucial role. Increased basal melting rates lead to substantial ice discharges and grounding-line migrations which could potentially drive cli-

mate transitions. In the range of realness considerable grounding line retreat in the Ronne, Ross, and Wilkes Land embayment, as well as sea-level discharge of around 6 msle at millennial timescales, can occur. This work highlights the possibility, that if the SO acts as a heat reservoir of a slowdown of the AMOC, then, through the bipolar seesaw mechanism, significant sea-rises recorded by proxy records can be attributed to the AIS.

Chapter 4

Exploring the impact of atmospheric forcing and basal boundary conditions on the simulation of the Antarctic ice sheet at the Last Glacial Maximum *

Sea-level changes on long timescales are driven by the waxing and waning of large continental ice sheets, mainly the LIS, EIS, GrIS and the AIS. Studying the sensitivity to past climate changes allows to identify the underlying mechanisms that force an ice sheet to respond and gain insight into future climatic scenarios. Understanding large sea-level variations has been proven to be crucial not only for quantifying sea-level rise (Nicholls and Cazenave, 2010; Defrance et al., 2017; King and Harrington, 2018; Golledge et al., 2019; Robel et al., 2019), but also to asses the risk of crossing potential tipping points in nature, such as a collapse of the WAIS (Kopp et al., 2009; Sutter et al., 2016; Pattyn, 2018).

The role of the AIS within the Earth System is clear as it is the largest ice sheet on Earth, with a total sea-level content of about 58 m (Fretwell et al., 2013). Potentially it will dominate future sea-level rise projections, however assessing its contribution is challenging as its response is unclear in terms of timing and quantity (Collins et al., 2013). One important benchmark period of sea-level standings is the Last Glacial Maximum (LGM, ca, 21 ka), a period of large ice sheet exposure where sea level was about 130 m lower than PD (Clark and Tarasov, 2014; Simms et al., 2019). Evaluating the total sea-level content of each

* The main contents of this chapter are published in:
Blasco, J., Alvarez-Solas, J., Robinson, A., and Montoya, M., 2020: Exploring the impact of atmospheric forcing and basal boundary conditions on the simulation of the Antarctic ice sheet at the Last Glacial Maximum. *The Cryosphere Discussions*, 1-27. DOI https://doi.org/10.5194/tc-2020-28, 2020.

continental ice sheet is crucial to assess the total sea-level budget during the LGM (Simms et al., 2019). Regarding the AIS, from marine and terrestrial geological records it is well assumed that the ice sheet advanced up to the continental-shelf break, however its exact position as well as the total ice volume remains somewhat elusive.

This chapter is structured as follows: first the Antarctic LGM state is introduced through previous reconstructions and modelling studies (Section 4.1); then the experimental design of this work is described (Section 4.2) and results are shown (Section 4.3); finally the results and its implications are discussed in Section 4.4 and the main conclusions of this work are summarised (Section 4.5).

4.1 The Antarctic LGM state

Marine and terrestrial geological records permit to infer the extension of the AIS at the LGM. In some regions measurements are more accurate and allow for a precise reconstructions as it is the case of the Bellingshausen Sea and the Antarctic Peninsula. On the other hand, the position of the grounding-line in other zones, as the Ross Sea and the East Antarctic region remains more controversial (Stolldorf et al., 2012; The RAISED Consortium, 2014). Overall, these records indicate that, at the LGM, the AIS advanced up to the continental-shelf break (Anderson et al., 2002, 2014; Hillenbrand et al., 2012, 2014; Mackintosh et al., 2014; The RAISED Consortium, 2014). The total ice volume on the other hand is even less well constrained, as these records do not give any direct information on the past ice content (Simms et al. 2019 and references therein). Several approaches have been used to estimate the LGM sea-level content of the AIS. The most common approach is to simulate the AIS with an ice-sheet model by imposing LGM background climatic conditions (e.g. Huybrechts 2002; Golledge et al. 2012; Whitehouse et al. 2012a; Gomez et al. 2013; Briggs et al. 2014; Maris et al. 2014; Quiquet et al. 2018). An alternative method is to infer the sea-level content through Glacial Isostatic Adjustment (GIA) modelling. Theses models describe the Earth's bedrock response to changes in the surface load by ice and

water (e.g. Ivins and James 2005; Bassett et al. 2007). Latest models have gone one step further and coupled ice-sheet with GIA models (e.g. Whitehouse et al. 2012a) and in order to obtain more accurate results, these models were constrained with GPS observations of current uplift and paleo reconstructions based on exposure age dating (Whitehouse et al., 2012b; Ivins et al., 2013; Argus et al., 2014b). The first Antarctic LGM estimates simulated rather large contributions above 15 m (e.g. Nakada et al. 2000; Huybrechts 2002; Peltier and Fairbanks 2006; Philippon et al. 2006; Bassett et al. 2007) and more recent modelling studies as well as reconstructions have lowered these contributions to 7.5-13.5 m (e.g. Mackintosh et al. 2011; Whitehouse et al. 2012a; Golledge et al. 2012, 2014; Gomez et al. 2013; Argus et al. 2014b; Briggs et al. 2014; Maris et al. 2014; Sutter et al. 2019). On one hand, considerable technical improvements have been achieved in the latter years through the inclusion of more complex physics, increased spatial resolution and sub-grid scale grounding-line treatment (e.g. Goelzer et al. 2017; Pattyn 2018). Also, external physical processes as the ice-ocean interaction or the GIA response are represented with more accurate parameterisations and/or models (e.g. Reese et al. 2018; Whitehouse et al. 2019). Nonetheless, models still differ by more than 10 m.

Boundary conditions are essential building blocks on driving the evolution of an ice sheet. In particular, ice-dynamics as well as atmospheric climatologies, through accumulation changes, must have played a leading role during the LGM. Because of the involved long timescales and the size of the ice sheets, paleo studies are based on hybrid schemes which rely on the Shallow Ice Approximation (SIA) and Shallow Shelf Approximation (SSA). These approximations do not account explicitly for the basal friction and models parametrise basal conditions through friction laws generally based on a Weertman type (Weertman, 1974). Friction choices range from linear laws, typically of ice flowing over hard bedrocks (e.g. Quiquet et al. 2018), to plastic and regularized power-laws representative of soft bedrocks or saturated tills (e.g. Aschwanden et al. 2013; Joughin et al. 2019), with intermediate cases as purely power-laws (e.g. Pattyn et al. 2012). All these laws have internal unknown friction coefficients, generally dependent on bedrock characteristics, which need to be tuned in order to obtain realistic simulations. The

simplest case is to prescribe a spatially friction coefficient (Golledge et al., 2012). However, state of the art model incorporate now dependencies on the effective pressure exerted by the ice, through hydrology, as well as bedrock characteristics by making use of assumed till properties or basal temperature conditions (Winkelmann et al., 2011; Pattyn, 2017; Quiquet et al., 2018; Albrecht et al., 2019; Sutter et al., 2019). Nonetheless, capturing more physical processes adds a degree of uncertainty and complexity to the estimates. Briggs et al. (2014) for example obtained more than 5 msle of difference for AIS LGM states only for different friction coefficients between hard and soft beds. To avoid the uncertainty associated to a larger amount of tunable parameters some studies have chosen to optimize friction coefficients through the use of inverse methods to obtain accurate PD states (Morlighem et al., 2013; Le clec'h et al., 2019). Nonetheless it is not obvious that these optimizations are valid for other time periods or if it is rather a particular configuration of present conditions. All in all, basal conditions are poorly characterized and represent a big milestone in ice models.

Another uncertainty source relies in the past climatologies at the Antarctic continent, which are also poorly constrained. Of course, it is well assumed from ice core records that the LGM period must have been colder and drier at the large continental scale (Frieler et al., 2015; Fudge et al., 2016). In order to simulate these conditions ice models use two approaches. The simplest way to prescribe LGM conditions is imposing a spatially homogeneous temperature anomaly (around 10 K) and reduction in precipitation (generally by 40% to 50% compared to PD) based on ice core data (Huybrechts, 2002; Golledge et al., 2012; Whitehouse et al., 2012b; Gomez et al., 2013; Quiquet et al., 2018). It is clear however that this approach is a vast simplification of reality. Although temperature anomalies may show spatially a similar shape, estimated precipitation changes are less homogeneous, misrepresenting climatologies in localized areas (Frieler et al., 2015; Fudge et al., 2016). Also, because ice cores are obtained from ice domes far inland, the recorded changes are not necessary the same than for coastal regions. In summary, applying a simple homogeneous method may be an oversimplification of the LGM climatologies where localized changes of precipitations may play an important role.

A more sophisticated method is to prescribe LGM conditions based on climate model outputs (Briggs et al., 2013; Maris et al., 2014; Sutter et al., 2019). Different outputs from simulations have been used in the literature, from global general circulation models (GCMs) (Sutter et al., 2019), sometimes downscaled with regional models (Maris et al., 2014) to Earth System Models of Intermediate Complexity (EMICs) as in Chapter 3. More complex approaches include the effect of inter-model variance through an empirical orthogonal function (EOF) analysis (Briggs et al., 2013). Nonetheless, the realism of these models is called into question as temperature and precipitation anomalies are not simulated correctly in specific sites driving to over/underestimates in certain regions (Cauquoin et al., 2015).

Because of all these reasons, the uncertainty in friction as well as in climatologies needs to be assessed. Understanding the potential uncertainty of these two boundary conditions seems a relevant piece to gain insight into the sea-level reconstructions at the LGM.

4.2 Experimental design

For this work the hybrid Yelmo ice-sheet-shelf model is used over a domain with 190x190 grid cells with a spatial resolution of 32km x 32km with 10 adaptive vertical layers (detailed description in Chapter 2; Robinson et al. (2020)). As in the experimental setup of Chapter 3, initial topographic conditions are provided from the RTopo-2 dataset (Schaffer et al., 2016). Grounded ice velocities are computed as a sum of the SIA and SSA solution corrected with basal drag. Ice shelves are solved through the SSA solution without any basal dragging correction. Enhancement factors are tuning parameters in ice models supposed to capture the impact of ice anisotropies on the ice flow (Ma et al., 2010; Pollard and DeConto, 2012b; Maris et al., 2014; Albrecht et al., 2019). Consistent values were found for E_{grounded} =1 and E_{floating} =0.7. The surface mass balance (SMB) is computed through the PDD method (Reeh, 1989).

To study the impact of bedrock friction on an Antarctic LGM state a linear friction law is employed as described in 2.38:

$$\tau_{\mathbf{b}} = -\beta \mathbf{u_b} \tag{4.1}$$

with

$$\beta = c_b N_{\text{eff}} \tag{4.2}$$

Here, $\tau_{\mathbf{b}}$, given in kPa, represents the corrected basal drag added to the SSA solution. $\mathbf{u_b}$, given in m yr^{-1}, is the basal velocity and β, kPa yr m^{-1}, the basal-drag coefficient. The basal-drag coefficient is split up into the effective pressure N_{eff}, in kPa, and friction coefficient, given in yr m^{-1}, which reflects bedrock characteristics. As described in Chapter 2, c_b is described as follow

$$c_b = \begin{cases} c_{\max} & \text{if } z_b \geq 0 \\ \max\left[c_{\max}\exp\left(-\frac{z_b}{z_0}\right), c_{\min}\right] & \text{if } z_b < 0 \end{cases}. \tag{4.3}$$

This parameterisation captures the phenomenon by which the occurrence of sliding is favoured in topographic lows and specifically within the marine sectors of the ice sheet. For land-based regions (i.e. bedrock above sea level) the friction coefficient becomes $c_{\max}$. z_0 represents the e-folding depth, thus higher values of z_0 favour a more abrupt fall of the friction coefficient with depth. As in Martin et al. (2011) and Albrecht et al. (2019), sliding is favoured in low elevation zones (scaled through the "till friction angle").

Based on Leguy et al. (2014), the effective pressure is computed as the weight of the ice load corrected with its overburden pressure (i.e. how far the ice column is to become floating), thus:

$$N_{\text{eff}} = \rho_i g \left(H - H_{\text{f}}\right) \tag{4.4}$$

Note, that the flotation thickness is expressed as $\max\left(0, -\frac{\rho_w}{\rho_i}\left(z_{sl} - z_b\right)\right)$. This ensures that at the grounding line the effective pressure is equal to zero and thus the basal drag $\tau_{\mathbf{b}}$ becomes continuous.

Atmospheric forcing

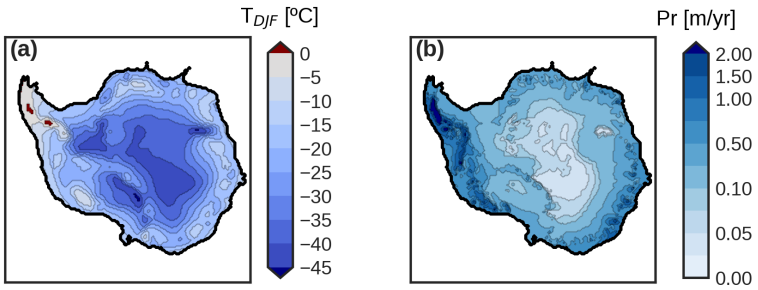

Fig. 4.1: PMIP3 ensemble mean **(a)** surface summer temperature (in °Celsius) and **(b)** annual precipitation (in m yr^{-1}) at sea level. The thick black line shows the 2000 m-depth contour.

Based on the index evolution, the orbital component is set to α =0 to create constant glacial background conditions. The LGM climatologies are hence rewritten as:

$$T^{atm}_{\text{LGM}} = T^{atm}_{\text{PD}} + \Delta T^{atm}_{\text{LGM-PD}} \tag{4.5}$$

$$P_{\text{LGM}} = P_{\text{PD}} \delta P_{\text{LGM/PD}} \tag{4.6}$$

The sub-index PD stands for the present-day climatic conditions for temperature (T^{atm}_{PD}) and precipitation (P_{PD}) respectively obtained from RACMO2.3 forced by the ERA-Interim reanalysis data (Van Wessem et al., 2014). $\Delta T^{atm}_{\text{LGM-PD}}$ is the temperature anomaly and $\delta P_{\text{LGM/PD}}$ the relative precipitation anomaly between the LGM and the PD. The sum of the PD fields with its anomaly gives the actual LGM climatologies (Fig. 4.1). The temperatures are corrected through a lapse rate correction that accounts for changes in elevations (0.008 K m^{-1} for annual temperatures and 0.0065 K m^{-1} for summer temperatures). Precipitations are also corrected through Clausius-Clapeyron scaling, which assumes more accumulation for warmer temperatures.

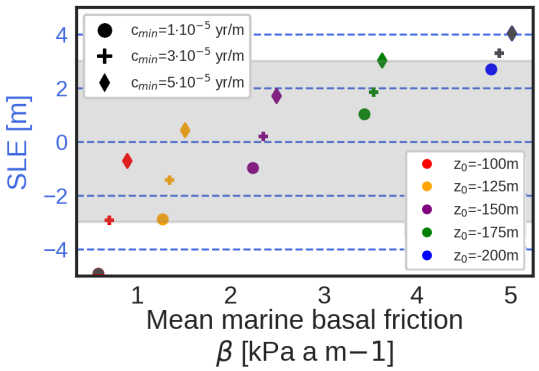

Fig. 4.2: PD AIS ice volume above flotation and sea level equivalent (SLE) simulated for the explored values of friction parameters. To simulate the LGM AIS only those that fall inside the grey band, for which the simulated PD AIS SLE deviates within less than ±3 m from PD observations, are selected (Schaffer et al., 2016).

First, the uncertainty of the impact of the basal friction in marine zones is investigated through the minimum friction allowed ($c_{\min}$) and the e-folding depth (z_0) in Eq. 4.3 taking as the LGM reference state the mean of the PMIP3 ensemble (Fig. 4.1). For this, a sensitivity study is performed to study the phase space of values which simulate realistic PD AIS simulations. Values of $c_{\min}$= $1{\cdot}10^{-5}$, $3{\cdot}10^{-5}$ and $5{\cdot}10^{-5}$ yr m^{-1} and of z_0= -100, -125, -150, -175 and -200 m with a maximum value of $c_{\max}$= $200{\cdot}10^{-5}$ yr m^{-1} are found to simulate the PD AIS in good agreement with observations in terms of grounded ice volume and grounding-line advance (Fig. 4.2, 4.3).

The second part of the sensitivity study investigates the impact of different climatic boundary conditions on an AIS LGM state. For this, a reference friction value is set (z_0= -175 m and $c_{\min}$ = $1{\cdot}10^{-5}$ yr m^{-1}) and each of the 11 models participating in the PMIP3 ensemble is simulated. Because the basal conditions

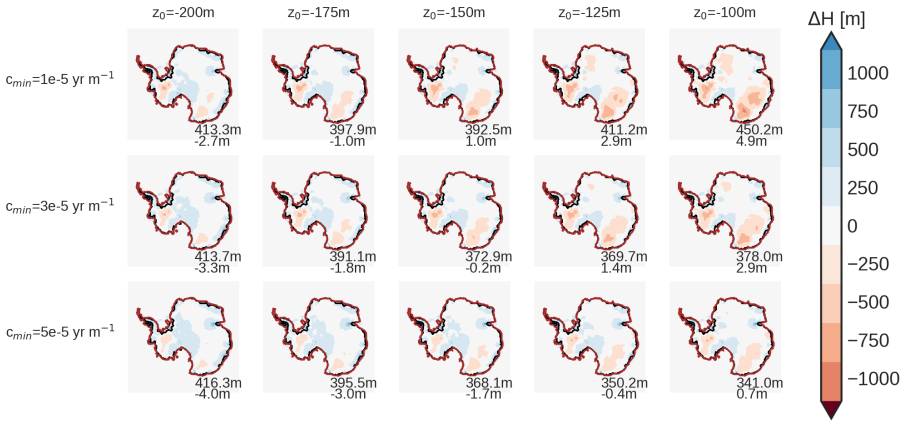

Fig. 4.3: Difference in ice thickness between the simulated and the observed by Schaffer et al. (2016) PD AIS states (simulated minus observed). Black line represents the actual grounding line position, brown line the simulated grounding line position. The upper number in each panel shows the root mean square error (RMSE) of the grounded-ice thickness for the corresponding set of parameters; the lower number represents the SLE anomaly with respect to PD. Ice volume is converted into a sea-level contribution by subtracting the floating portion and taking isostatic depression of the bedrock into account, as suggested by Goelzer et al. (2019).

are the same, changes in the extension and ice volume can only be explained by changes in climatologies. Changes with respect to PD are computed with the simulated PD ice sheets (Fig. 4.2).

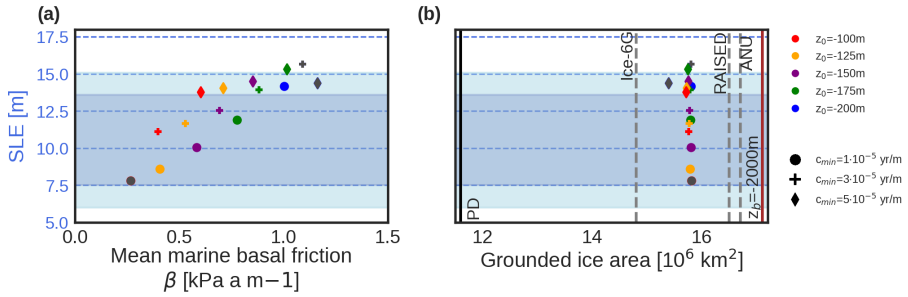

Fig. 4.4: Scatter plot of the simulated LGM ice-volume anomaly (in msle, positive means ice-volume increase at the LGM) with respect to **(a)** the mean basal-drag coefficient and **(b)** the simulated grounded ice area, for the LGM simulations corresponding to different friction parameters. The dark blue horizontal area represents the SLE LGM estimates summarized by Simms et al. (2019) since 2010. The light blue area includes the uncertainties of the two extreme cases. The grey shaded vertical lines in **(b)** show the ice extension estimates from ICE-6G, The RAISED Consortium and the ANU reconstruction at the spatial resolution of the simulations (see main text). The black vertical line is the PD extension and the brown vertical line represents the computed ice area within the continental-shelf break defined as z_b >-2000 m. Grey-colour symbols represent simulations that did not produce a realistic PD state.

4.3 Results

4.3.1 Impact of basal friction

The simulated AIS LGM volumes (in SLE) are summarized in Figure 4.4 with respect to the mean basal-drag coefficient β (Fig. 4.4a) and the grounded ice extension (Fig. 4.4b) for $c_{\min}$= $1{\cdot}10^{-5}$ yr m^{-1} (circles), $3{\cdot}10^{-5}$ yr m^{-1} (crosses) and $5{\cdot}10^{-5}$ yr m^{-1} (diamonds). The computed ice volumes are computed by subtracting the floating portion and taking isostatic depression into account (Goelzer et al., 2019). Simulations which did not fit a realistic PD state are shown in grey

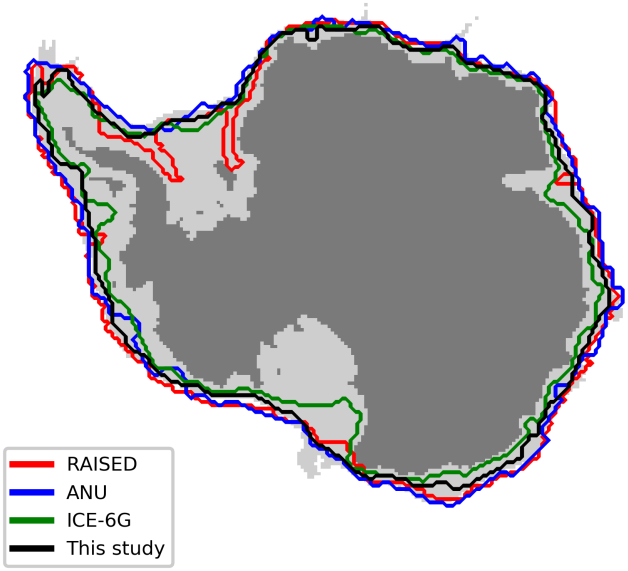

Fig. 4.5: Grounded ice extensions reconstructions from RAISED Consortium in red; ANU in blue and ICE-6G in green. In black, the simulated ice extension in this study for z_0=-175 m and $c_{\min}$= $1{\cdot}10^{-5}$ yr m^{-1}. The grey dark area shows the PD grounded ice. The area between the PD grounded area and the continental-shelf break (z_b¡-2000 m) is shown in light grey.

colors in Figure 4.4. A larger marine friction (associated to lower z_0 values) concludes into larger ice volumes. This occurs because a higher friction slows the ice velocity and less ice is advected, concluding into a thicker ice column. The sea-level difference between a pronounced reduction (e.g. z_0 =-100 m; red color) and a smoother decrease (e.g. z_0 =-200 m; blue color) are found to be around 7 msle. In addition, faster sliding, and thus lower $c_{\min}$ values, also reduces the ice volume because of the same reasoning. Sea-level differences between the explored extreme values can reach up to 5 msle. Independent of the exerted basal friction,

the simulated grounded ice extends similar in all the cases, between 15.6 and 15.8 million km^2. Its not possible to identify a relation between the range of studied friction values and the grounding-line position (Fig. 4.4b). In terms of simulated SLE, simulations fit well within the range of previous studies (Simms et al. 2019 and references therein). Also in comparison with the ice extension, results also show agreement with ICE-6G (Argus et al., 2014a; Peltier et al., 2015, 2018), The RAISED Consortium (2014) and the ANU reconstruction (Lambeck and Johnston, 1998; Lambeck and Chappell, 2001; Lambeck et al., 2002, 2003) (the extension is computed in Yelmo's resolution to avoid biases due to coarse resolution). The simulated ice extension supports almost a fully extended ice sheet towards the continental-shelf break (Fig. 4.5; here with $c_{\min} = 1{\cdot}10^{-5}$ yr m^{-1} and z_0 =-175 m). The simulated grounded area (thick black line) covers 15.8 million km^2 of the 17 million km^2 of the continental-shelf break (i.e. defined by the contour z_b =-2000 m; grey shaded area). This simulated extension stands between the ICE-6G model (green line in Fig. 4.5) and the RAISED Consortium (red line) and the ANU (blue line) model. The largest discrepancies between models occur on the Ross shelf. Whereas ANU and RAISED estimate an advance close to the continental-shelf break, ICE-6G is more retreated.

The employed friction parameterisation enhances ice flow in topographic lows. Thus, regions as the Amery, Wilkes and Victorias land show fast ice streams of more than 50 m yr^{-1} (Fig. 4.6a,b). Naturally, due to the marine character of the WAIS, this sector has also very rapid ice streams. The origin of the volume differences between a larger friction (z_0 =-200 m) and a lower friction (z_0 =-150 m) comes primarily from the WAIS and coastal regions of the EAIS as a consequence of a higher basal velocity (Fig. 4.6). In summary, the simulated ice sheets show a consistent form with lower inland velocities inland and increasing values towards the margins, with clearly marked ice streams as a consequence of the bedrock shape.

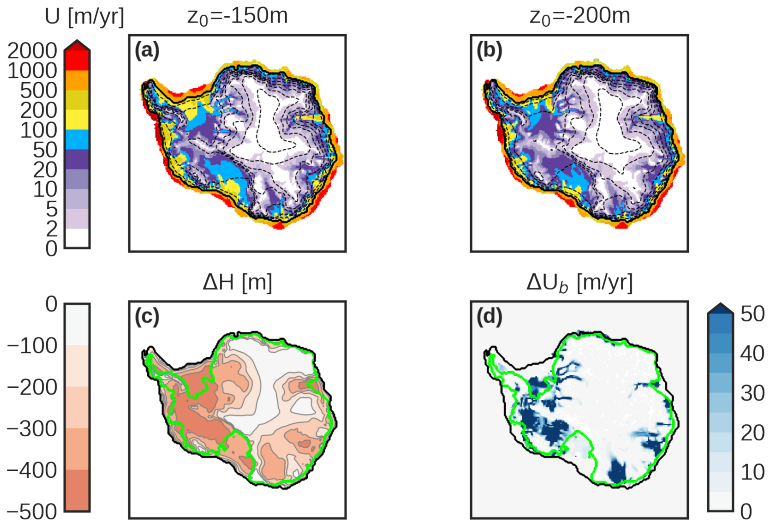

Fig. 4.6: Simulated LGM surface elevation and velocity for $c_{\min}$=1·10^{-5} yr m^{-1} for **(a)** z_0=-150 m and **(b)** z_0=-200 m; brown contours show surface elevation in 500 m intervals up to 3500 m above sea level. Difference in **(c)** ice thickness and **(d)** basal velocity between **(a)** and **(b)** (a minus b); the thick black line shows the grounding-line position of z_0=-200 m and the green line the PD grounding-line position.

4.3.2 Impact of climate forcing

Figure 4.7 shows the simulated LGM AIS state of each individual PMIP3 model for the reference state friction, z_0 =-175 m and $c-$ min =1·10^{-5} yr m^{-1}. The simulated SLE anomaly ranges from 9.7 msle to 13.1 msle and the ice extension from 14.8 million km^2 to 15.9 million km^2 (Fig. 4.8). Thus, a difference of 3.4 msle in ice volume and of 1.1 million km^2 in extension. There is an outsider model which simulates a lower sea-level contribution than PD, -4.3 msle. This case will be discussed later. Compared to the friction sensitivity study, the uncertainty of the ice volume anomalies are found to lie in a slightly smaller range. Grounding-

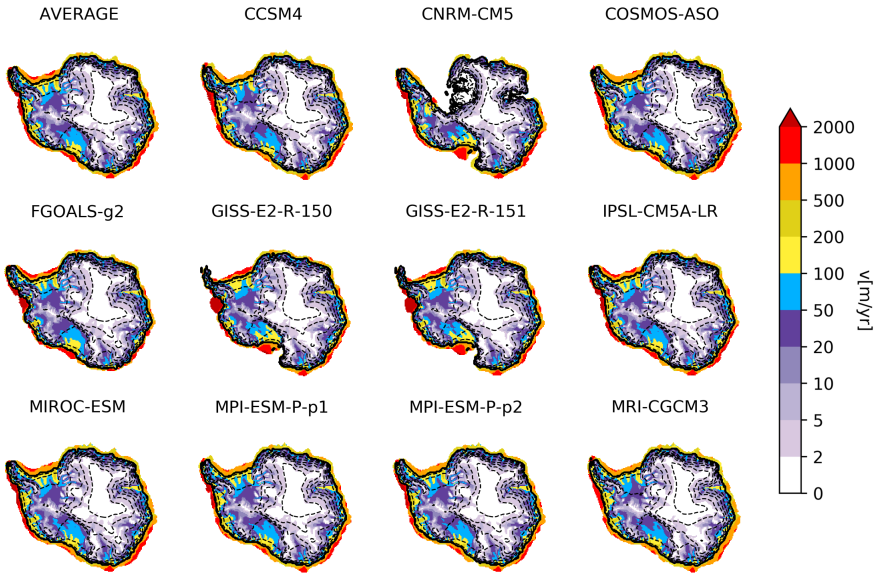

Fig. 4.7: LGM AIS ice elevation (brown contours) and velocity (shaded) simulated using the LGM minus PD anomalies of each of the PMIP3 ensemble-members as forcing (see main text). The thick black line shows the grounding-line position. The brown contours show surface elevation in 500 m intervals up to 3500 m above sea level.

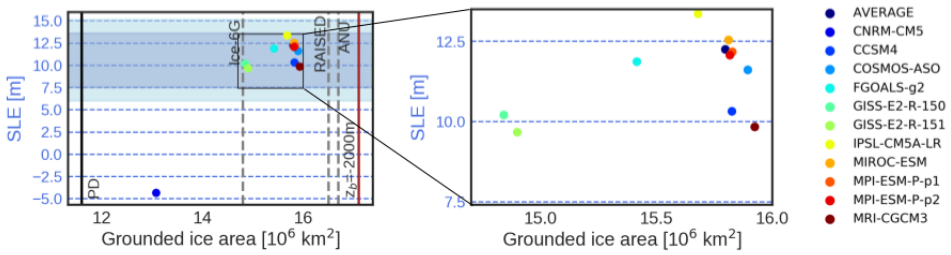

Fig. 4.8: Scatter plot, as in Fig. 4.4, of the simulated LGM ice volume anomaly (SLE) against the grounded ice area for the PMIP3 ensemble and reference values of z_0=-175 m and $c_{\min}$= $1{\cdot}10^{-5}$ yr m^{-1}.

line advances on the other hand are found to be more sensitive to climatic field changes than for the investigated friction phase space.

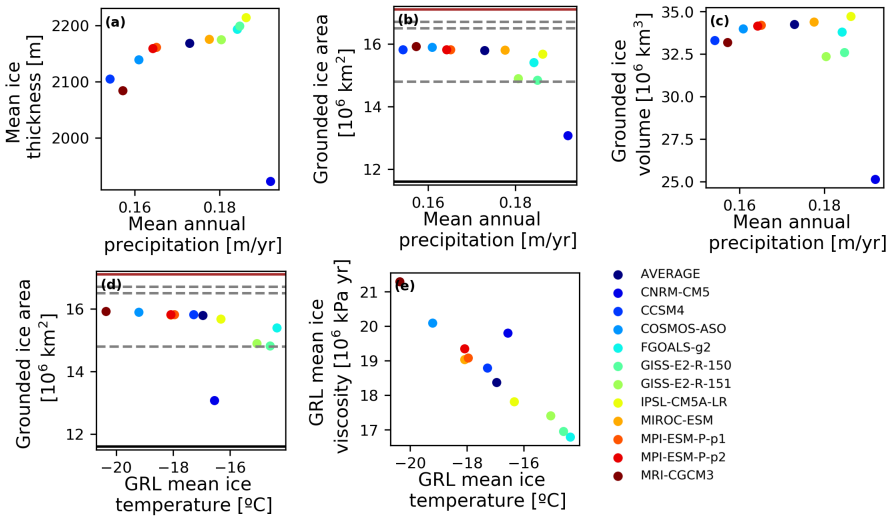

Fig. 4.9: Scatter plots of **(a)** the mean ice thickness vs. the mean annual precipitation of the grounded grid points; **(b)** the grounded ice area vs. the mean annual precipitation of the grounded grid points; **(c)** the grounded ice volume vs. the mean annual precipitation of the grounded grid points; **(d)** the grounded ice area vs. the mean ice temperature at the grounding line; **(e)** the mean ice viscosity at the grounding line vs. the mean ice temperature at the grounding line. The horizontal lines in **(b)** and **(d)** represent the ice extensions described in Fig. 4.4

These simulated changes in ice volume and extension can only be explained through changes in climatic fields as the underlying ice dynamics are the same for all cases. For this purpose, the sensitivity of the ice thickness, volume and extension is investigated towards the climatic fields used to force the ice-sheet model (Fig. 4.9). A higher accumulation results into a thicker ice sheet (Fig. 4.9a). The ice extension on the other hand remains rather unchanged to precipi-

tation changes (Fig. 4.9b). Equally advanced ice sheets, up to the continental-shelf break (an extension of about 15.5 million km^2; Fig. 4.9d), have larger AIS volumes for those with increasing accumulation (Fig. 4.9c). Inside the eleven model realizations however, there are three climate models (CNRM-CM5, GISS-E2-R-150, GISS-E2-R-151) which do not extend as much as the other models (below 15 million km^2) though the accumulation is on average larger than the ensemble mean. These simulations show a smaller AIS volume as a consequence of a less advanced ice sheet, despite the relatively high accumulation rates.

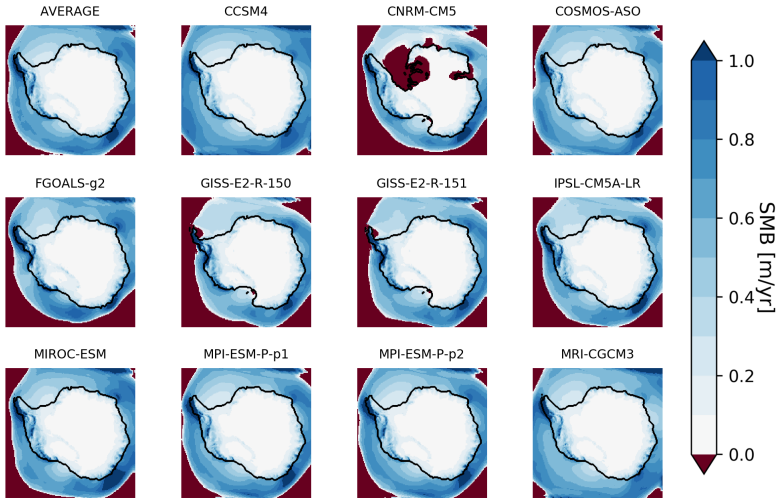

Fig. 4.10: LGM AIS ice elevation (brown contours) and velocity (colors) simulated using the LGM minus PD anomalies of each of the PMIP3 ensemble-members as forcing (see main text). The thick black line shows the grounding-line position. The brown contours show surface elevation in 500 m intervals up to 3500 m above sea level.

A more detailed inspection of the effect of climatic variables at the grounding line allows to identify the atmospheric temperature as a critical factor in determining how far the AIS can advance (Fig. 4.9d). Lower temperatures present more extended ice sheets towards the continental-shelf break. Warmer temperatures

simulate less advanced ice sheets. Ablation in the Antarctic domain, specially at the LGM, can be discarded as the reason for a discrete ice advance (however there is an exception that will be discussed below, Fig. 4.10). Temperatures do also affect ice dynamics through viscosity. The surface temperatures are used as a boundary condition to compute the ice viscosity. Hence warmer ice sheets flow faster, due to low viscosity, than colder ice sheets, due to high viscosity (Fig. 4.9e). However, a necessary condition for marine-based ice sheets to advance is that the ice thickness at the grounding line overcomes the flotation criterion, meaning that the ocean depth (z_b) is shallower than $\sim$90% of the ice thickness. The ice thickness is sustained through ice accumulation and inland ice flow. If ice flows too fast, as a consequence of low viscosity, then the grounding line cannot thick enough to advance towards more depressed bedrock zones. Hence, simulations with low viscosity (GISS-E2-R-150, GISS-E2-R-151 and partly FGOALS-g2) do not fully advance in the Ross shelf or Pine Island region (Fig. 4.7, 4.8).

The CNRM-CM5 model does not follow any of the proposed hypothesis as viscosity does not fall with the ice temperature as seen in the other models (Fig. 4.9e). The LGM configuration of this model shows a partially extended ice sheet in the Ross shelf but a collapsed ice sheet in the Ronne shelf and Amery basin which results into a more extended AIS than PD but lower ice volume. Contrary to other models, the reason for this abnormal behaviour is because ablation is happening in these regions (Fig. 4.10). The anomalous behaviour in ice viscosity is a consequence of two competing effects. On one hand the fully advanced regions, as the Ross basin or the Amery shelf contribute to a rather low ice temperature and high viscosity. On the other hand, the ablation regions, the Ronne and Amery basin, have rather warmer ice temperatures and a lower ice viscosity. This produces on average a warm ice column with a high viscosity as measured in Figure 4.9e. A similar reasoning can be applied to explain the anomalous low viscosity for this model in Figure 4.9a.

Thus, the choice of atmospheric climatologies has a strong impact on the ice-sheet size and extent. Because of the marine character of the AIS it is necessary that enough incoming ice is provided to conquer more depressed bedrock zones. If the ice viscosity is too low, due to high atmospheric temperatures, then ice flows

too fast preventing the ice margins to thicken and advance. For similar extended ice sheets, the precipitation rate determines the total amount of ice volume. For almost fully extended ice sheets a sea-level difference of about 3.5 msle is found only because of precipitation changes (IPSL-CM5A-LR and MRI-CGCM3).

In summary, the choice of the LGM boundary conditions is as crucial as the friction choice for the simulated LGM state. Warmer/colder temperatures enhance/impede ice flow as a consequence of low/high viscosity. Enhanced ice flow thins ice and hampers its advance towards more depressed marine-bedrock zones. For equally extended ice sheets, up to the continental-shelf break, the accumulation pattern determines the total amount of ice volume. Higher accumulation fields (IPSL-CM5A-LR) simulates about 3 msle more than lower accumulation field (MRI-CGCM3).

Spatially homogeneous approach

Other studies use rather a spatially homogeneous temperature and accumulation drop over the whole Antarctic domain based on proxy records (Huybrechts, 2002; Golledge et al., 2012; Whitehouse et al., 2012a; Gomez et al., 2013; Quiquet et al., 2018). Of course at first order this is a valid approach as colder and drier climatic conditions are expected during the LGM. For consistency, also a spatially homogeneous method was tested in this work for the same set of friction parameters. The atmospheric temperature anomaly was set to -10 K and a precipitation drop of 40% with respect to PD as suggested by proxy records (Jouzel et al., 2007; Frieler et al., 2015; Fudge et al., 2016). Differences with respect to the average field of the PMIP3 ensemble show that a spatially homogeneous method simulates systematically a lower ice volume and less extended ice sheet (Fig. 4.11). Nonetheless the simulated ice sheets are consistent with other studies and reconstructions. Of course, dynamics are the same, hence the differences can only be explained by climatologies. The ice thickness anomaly (Fig. 4.12c) between the Average of the PMIP3 ensemble (Fig. 4.12a) and a spatial homogeneous method (Fig. 4.12b) shows that the main source comes primary from the WAIS sector

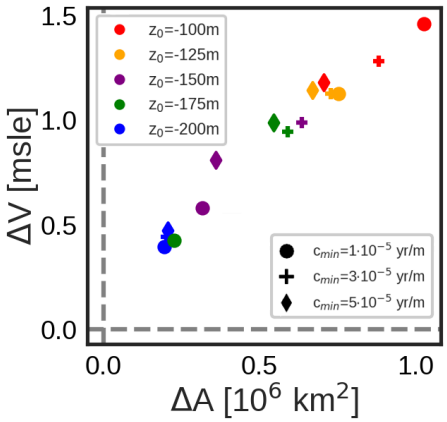

Fig. 4.11: Difference in ice volume in terms of msle against grounded ice area between the PMIP ensemble mean and a spatially homogeneous anomaly (PMIP ensemble mean minus spatially homogeneous) for all permutations of basal friction parameters.

and coastal regions. Only inland of the EAIS simulates a slightly thicker ice for a spatial homogeneous decay in localized regions. This anomaly pattern is explained by the differences in the accumulation fields (Fig. 4.12d). Whereas a the average of the PMIP3 ensemble produces systematically more accumulation at the borders and specially at the Ross, Pine Island and Antarctic Peninsula, the homogeneous decay accumulates more ice inland. This additional accumulation in the Antarctic Peninsula enhances probably its advance. Ice cores are drilled from dome regions with colder and dryer conditions. Thus, it is somehow expected that estimates in the coastal regions are underestimated from a spatially constant change.

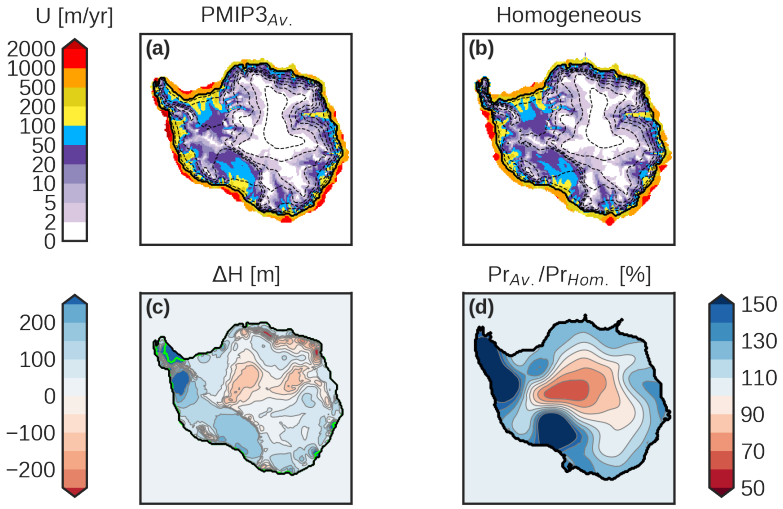

Fig. 4.12: Simulated AIS LGM surface elevation and velocity when forcing with **(a)** the spatially homogeneous method and **(b)** the PMIP3 average snapshot with z_0=-175 m and $c_{\min}$=1·10^{-5} yr m^{-1}. The thick black line shows the grounding-line position. The brown contours show surface elevation in 500 m intervals up to 3500 m above sea level. Panel **(c)** shows the ice thickness difference **(a)** minus **(b)**, where the thick green and black lines show the grounding-line position from the simulation with homogeneous and PMIP3 climatic forcing, respectively. Panel **(d)** shows the ratio of precipitation in the PMIP3 forced simulation to that of the homogeneous simulation and the grey line the continental-shelf break (z_b=-2000 m).

4.4 Discussion

Basal dragging law

At the bedrock interface several important processes occur that are crucial in the evolution of ice sheets. The presence of water and the exerted basal friction determines the dynamics of ice sheets. Nonetheless, even at PD it is difficult to

estimate basal conditions, thus estimating bed properties at the LGM adds a degree of difficulty. To account only for the effect of basal friction, steady state simulations were performed to ignore the drift caused by transient simulations. Based on parameters which simulated realistic PD states (Fig. 4.2, 4.3) LGM sea-level contributions were simulated between 15 and 8 msle, hence a sea-level difference of about 7 msle for the extreme cases (Fig. 4.4). Due to the employed parameterisation, different bedrock frictions had an impact on the ice-stream activity in the marine-based regions. Because all simulations advanced up to the continental-shelf break a more dynamically active AIS had a lower volume than a less dynamically active.

This work only focused on a linear friction law, as used in other studies (Morlighem et al., 2013; Quiquet et al., 2018; Alvarez-Solas et al., 2019). Of course, the choice of a unique friction law for the whole Antarctic domain is arguable and models differ greatly between them (Nowicki et al., 2013; Joughin et al., 2019; Seroussi et al., 2019). The aim here was to investigate the role of more or less dynamically active ice sheets on the simulation of an AIS LGM state. The role of different friction laws is specially relevant for transient simulations involving potential instabilities of the AIS. Because this was out of scope, there is no need to investigate the phase space of friction parameters of other laws. Considering further formulations could increase the uncertainty.

Sea-level and ice extent uncertainty

The simulated sea-level contributions of the participating PMIP3 groups ranged from 9.7 msle (GISS-E2-R-151) to 13.1 msle (IPSL-CM5A-LR) for the used reference friction parameters. Hence, a sea-level difference between models of 3.4 msle, slightly smaller compared to the friction uncertainty. Because all these contributions fall inside the range of other studies there is no apparent reason for ruling out any of these models outputs. The model CNRM-CM5 is an exception to this. With its output a smaller ice sheet than PD is simulated. Given that the

LGM is a colder period than nowadays and that ablation in the PD is almost negligible, the outcome from the CNRM-CM5 models is highly unrealistic.

Surprisingly, atmospheric temperature fields have a more determinant role than it could have been previously thought. The ice extension of the LGM state is highly dependent on the viscosity. Warmer temperatures enhance ice flow by lowering the viscosity, whereas colder temperatures slow the ice flow as a consequence of high viscosity. If the grounding-line tends to advance towards deeper bedrock zones a necessary condition is that the supplied ice is large enough to support the ice flotation limit. Thus, a lower viscosity enhances ice flow leading to thin ice in regions where the bedrock is too deep, which prevents from a complete advance towards the continental-shelf break. The model outputs from GISS-E2-R-150 and GISS-E2-R-151 prevent from a full advance in the Ross shelf as in the ICE-6G reconstruction (Fig. 4.5). FGOALS-g2 impedes for the same reasons a fully advanced Pine Island region (Fig. 4.7). Colder climatologies support a full extended ice sheet as in the ANU reconstruction (Fig. 4.5). The RAISED Consortium simulates an advanced Ross shelf except in the borders. This configuration was not reproducible in Yelmo. In summary, despite of the importance of the precipitation field, as it allows for larger/lower ice volumes, temperature fields are crucial as they drive the ice sheet extension through viscosity changes.

In addition to climatologies and basal friction components, there are other sources which add more uncertainty into LGM volume estimates of large continental ice sheets. Changes in the Earth bedrock have a decisive contribution in assessing the total sea-level budget through local changes. But, in addition to this, a shallower (or deeper) bedrock facilitates (or impedes) an ice advance affecting the total ice volume (Philippon et al., 2006). As commented in Chapter 2, although Yelmo offers the possibility to couple to a GIA model, here a rather simple parameterisation is used (Le Meur and Huybrechts, 1996). Nonetheless, the Antarctic bedrock is a complex component with different rheological properties which is not captures with this parameterisation. The WAIS for instance is a low-viscosity region with different bedrock responses than the EAIS (Whitehouse, 2018; Whitehouse et al., 2019). Although this is out of scope of this work,

it should be taken into account that this is another source of uncertainty which could have an impact on constraining the phase space of friction parameters.

Forcing methods

This work shows that a spatially homogeneous anomaly based on ice core records simulates a lower ice volume due to lower accumulation near the ice sheet margins (Fig. 4.12). This implies that based on other LGM simulations performed with a homogeneous method, the AIS could have stored more ice than previously estimated. Because GCM outputs are based on model simulations local atmospheric effect, such as atmospheric circulation changes or localized precipitation structures, should be captured. The latest ice-sheet models use nowadays more detailed climatic fields (Briggs et al., 2013; Maris et al., 2014; Sutter et al., 2019). However, the simulated ice volume and ice extension uncertainties are even larger than those of basal friction. Because PMIP3 climatologies are built from prescribed ice extension and surface elevation, one should expect a natural tendency to drive to these particular configurations (Abe-Ouchi et al., 2015). Nonetheless, the exposed results show that these models greatly differ among others producing even ablation. A potential way to test the realism of model outputs is to compare with temperature and precipitation reconstructions of ice cores. Future outputs with PMIP4 results should reduce this uncertainty and provide more accurate fields (Kageyama et al., 2019).

4.5 Conclusions

The imposed boundary climatologies, as well as the ice dynamics, are two essential building blocks for simulating an Antarctic LGM state. This work aimed to investigate more profoundly the uncertainty that these two boundary conditions can produce on the total ice volume and extension. For this, a sensitivity study of different representations of basal friction as well as atmospheric forcing was per-

formed. The first part of this work focused on a range of potential basal friction configurations in the marine zones for a simple linear law. Lower/higher friction values enhance/diminish the ice dynamics of the marine regions and result in lower/higher ice volume content. Simulated sea-level estimates ranged from 9.1 msle to 15.5 msle with respect to present volume. Nonetheless, ice sheets were found to extent similar despite of the applied marine friction, up to the continental-shelf break, almost 16 million km^2. Then, for a reference friction value, all the LGM climatologies from the PMIP3 ensemble were investigated. The simulated ice volume anomalies ranged from 9.7 msle to 13.1 msle, with the exception of the CNRM-CM5 model. The extension of the ice sheets showed even a larger spread, ranging from 14.8 to 15.9 million km^2. In comparison with a spatially homogeneous anomaly based on ice cores, GCM model outputs simulate more accumulation along the Antarctic coast and lead to larger ice volumes. Finally, the LGM temperatures were found to have a decisive role for the extension of an ice sheet. Lower/higher temperatures slow/enhance ice flow through increased/reduced viscosity. Because of the marine character of the AIS, high temperatures can prevent to expand further into more depressed bedrocks. This work points to the fact, that climatologies can add an uncertainty comparable to basal friction and that improving the understanding of boundary conditions is crucial to asses the sea-level budget of the LGM and potentially other time periods.

Chapter 5
The Antarctic sea-level contribution since the LGM to the future for different basal-dragging laws*

The AIS, as set in the fifth IPCC report, is the largest source of uncertainty in future sea-level rise projections (Collins et al., 2013). As already mentioned in Chapter 1, the main reason for this is that the marine parts of the WAIS could collapse through the Marine Ice Sheet Instability (MISI), as hypothesized by Weertman (1974). However, how far MISI is from being triggered or whether such a mechanism is already underway remains an open question. Satellite data measurements show that the grounding line is retreating in the Amundsen region, mainly for the Thwaites and Pine Island Glacier (Favier et al., 2014; Rignot et al., 2014), which may hint at an early signal of a MISI. If such an instability is triggered, sea level could rise by 3 meters without accounting for accelerated inland ice (Bamber et al., 2009). Determining when a WAIS collapse can take place is crucial as it is considered one of the nearest potential tipping points in nature and threats to humankind (Lenton et al., 2008; Pattyn et al., 2018).

Confined shrinking ice shelves accelerate inland ice which can induce the grounding line to retreat. The reduction of ice shelves can occur either due to atmospheric processes, such as hydrofracturing, or oceanic processes, as basal melting. Sub-shelf melt represents around 50% of the mass loss of Antarctica (Rignot et al., 2013). If greenhouse gas emission are not reduced, then grounding-line retreat at the WAIS will most probably accelerate in the future due to enhanced penetration of deep warm water onto the continental-shelf (Holland et al., 2019).

* This work has been submitted to Communications Earth & Environment

However, elucidating the future evolution of the AIS is challenging as it depends on several factors. On one hand, projections of atmospheric and oceanic temperatures are uncertain. More concretely, the Southern Ocean (SO) is a complex system that interacts with ice, atmosphere and other greater oceanic basins and predicting its evolution is challenging (Holland et al., 2020). Translating these oceanic changes into basal-melting rates varies for every ice-sheet model. But, in addition to this, ice dynamics, and more specifically basal friction, are treated differently in ice-sheet models. Whereas some models use more conservative approaches, meaning a higher resistance and, hence, slower ice dynamics as a consequence of ice flowing over a hard bedrock, others promote basal sliding in soft bedrock areas. All in all, this results in a wide spread in outcomes.

This work studies the role of ice dynamics in the future evolution of the AIS. The chapter is structured as follows: first a review of previous studies is done and the choice of different basal friction laws is introduced (Section 5.1); then Section 5.2 describes the experimental setup and the forcing methods; Section 5.3 the future Antarctic sea-level contribution is shown for different basal dragging laws. Then these results are discussed (Section 5.4) and the main conclusions are summarized (Section 5.5).

5.1 The AIS response to future warming: previous modelling work

Assessing the AIS response to future anthropogenic warming has not been possible until recently. In order to reproduce a MISI mechanism it was necessary to include other approximations than the SIA solution, mainly the SSA solution, and a high spatial grounding-line resolution or, alternatively, very accurate parameterisations (Pattyn et al., 2012; Pattyn, 2018; Pattyn and Morlighem, 2020). This, together with a successful coupling of floating ice with inland ice, accounting for the buttressing effect that ice shelves exert, improved computational resources and new satellite data, has enabled ice-sheet models to evaluate the future response of the AIS.

Golledge et al. (2015) studied the response of the AIS to four representative concentration pathways (RCPs) scenarios under a spatially constant atmospheric and oceanic warming. They estimated for their worst case scenario (RCP8.5) a SLR of between 1.5 and 3 m by year 2300. Based on the principle that it takes long timescales to reabsorb the emitted CO_2, they concluded that a warming of 2 degrees above PD has already committed us to a SLR of 2 to 4 msle by year 5000. Ritz et al. (2015) performed a probabilistic study of thousands of simulations varying several parameters to assess the most likely future SLR scenario. They concluded that it is unlikely that the AIS contributes more than 1 msle by the year 2200. Feldmann and Levermann (2015) investigated, in a high-resolution model, how long the Amundsen region could remain intact with the actual observed melting rates. Their results indicated that if actual melting rates hold for 60 years, then the WAIS would be committed to an irreversible collapse for the following centuries to millennia, accompanied by a sea-level rise of about 3 msle. DeConto and Pollard (2016) additionally included in their simulations the marine-cliff instability, which boosts afterwards the occurrence of the MISI, and simulated a potential SLR of 1 msle by year 2100 and up to 15 msle by year 2500 for RCP8.5. However, this mechanism is still controversial and it could overestimate mass loss (Clerc et al., 2019; Edwards et al., 2019). Pattyn et al. (2018) studied the response of the GrIS and AIS following a similar approach as Golledge et al. (2015). They investigated the AIS stability for different temperature anomalies focusing on the 1.5-2.0 Paris agreement and concluded that due to the long resilience of carbon in the atmosphere, the threshold of the WAIS collapse is close to the imposed Paris agreement. All these studies agree that a WAIS collapse would be irreversible. However, the timing and the triggering of such a collapse, as well as the expected total ice discharge, remains elusive.

The reason for ambiguity in results is due to several factors. On one hand, some of the studies account for different mechanisms, such as the marine-cliff instability, or different calving laws for instance. In addition, future evolution experiments are highly dependent on oceanic temperature variations, and whereas some models use linear approaches to convert oceanic temperatures into basal melting rates, other models use higher order approximations. Nonetheless, ice-

sheet models do not share the same basal friction laws, which in turn affect the ice dynamics. There is broad consensus that due to the loss of buttressing effect, inland ice will accelerate and discharge ice into the ocean (Fürst et al., 2016), but how far this propagation can go and how much it can accelerate is poorly constrained. Ritz et al. (2015) showed that the Amundsen sea region for instance did not retreat the same way for different basal dragging laws. In a quantification study, Bulthuis et al. (2019) showed that the basal sliding law is one of the main sources of the uncertainty of sea-level rise projections. Furthermore, as concluded by Brondex et al. (2017), different friction laws show different steady state conditions at downward slopes. This represents a handicap in assessing a MISI induced WAIS collapse, as it shows a dependence on the employed friction law, adding more uncertainty into future projections.

Another potential caveat from the mentioned studies, is that they use an initialization spin up that aims to match an almost perfect PD ice sheet through satellite data assimilation. Although this method simulates an almost perfect ice sheet consistent in terms of topography and surface velocity, such a method does not take into account the thermal memory of the ice sheet, which can lead to inconsistencies in ice flow. Considering a transient spin up that contains the past evolution of the ice sheet will simulate a more realistic evolution of the ice sheet.

This work aims to investigate the role of different basal friction laws for future Antarctic sea-level projections. For a more accurate assessment, the employed methodology here includes a deglaciation spin up that accounts for thermal memory of the AIS.

5.2 Experimental design

To investigate the evolution of the AIS for different warming scenarios, the ice-sheet model Yelmo is used as in Chapter 4 (detailed description in Chapter 2; Robinson et al. 2020). Ice deformation of grounded ice is solved by adding the SIA and SSA solution. The SIA solution is non-sliding, thus all sliding occurs within the SSA solution, balancing basal dragging. Ice shelves are solved via the

SSA solution without any basal drag. The spatial resolution is set to 32 x 32 km with 21 vertical adaptive layers. Initial topographic conditions (ice thickness, bedrock depth and surface elevation) are provided from the RTopo-2 dataset (Schaffer et al., 2016). For this work, enhancement factors are set as proposed by Ma et al. (2010) for different flow regimes, namely E_{shear} =3, E_{stream} = 1 and E_{floating} =0.7. The internal temperature of every ice layer is computed through the advection-diffusion energy conservation equation. The adopted surface mass balance scheme is computed through the PDD scheme (Reeh 1989; more information in Chapter 2). Calving at the ice front occurs when the ice front thickness reduces to below a threshold and the incoming ice flux is not sufficient to maintain the ice thickness (Peyaud et al., 2007). For this study a calvingthickness threshold of 175 meters simulates realistic LGM as well as PD states.

The strategy employed for this study consists of two parts, first a spin up from the LGM to PD is performed to determine the most realistic PD cases. Then, those simulations that produce realistic LGM and PD conditions are forced for different RCP scenarios.

Deglaciation spin-up

As in Chapter 4, the model is forced towards an equilibrated LGM state by imposing background LGM conditions for 80 kyr. The LGM climatologies are obtained from the PMIP3 repository (Taylor et al., 2012) and averaged from all the participating groups (the CNRM-CM5 model is excluded due to unrealistic ablation rates). Then, the simulated LGM state is forced transiently until the PD through an index method described by the following equations:

$$T^{\text{atm}}(t) = T_0^{\text{atm}} + \alpha(t)\,\Delta T^{\text{atm}}_{\text{LGM-PD}} + \lambda \Delta z_s \tag{5.1}$$

$$P(t) = P_0\,(1-\alpha(t))\,\delta P_{\text{LGM/PD}} \exp\left(f_p \lambda \Delta z_s\right) \tag{5.2}$$

where T_0^{atm} and P_0 are the monthly PD temperature and precipitation field respectively from Van Wessem et al. (2014). $T^{\text{atm}}_{\text{LGM-PD}}$ and $\delta P_{\text{LGM/PD}}$ are the

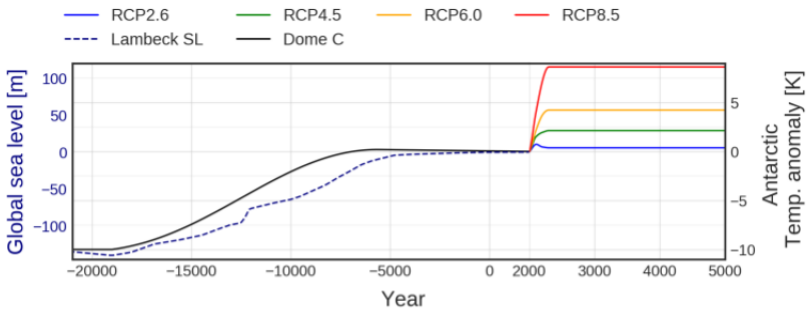

Fig. 5.1: The applied forcing in this study. The black line represents the deglaciation signal from LGM to PD, obtained from Dome C ice core. The dashed dark-blue line shows the applied sea-level forcing from Lambeck et al. (2014). Colored continuous curves represent different RCP scenarios for Antarctica based on CMIP5 data (Taylor et al., 2012; Golledge et al., 2015).

temperature and relative precipitation anomaly fields between the LGM and PD state. $\alpha\,(t)$ is the climatic index, where α =0 represents PD conditions and α =1 LGM conditions. In addition, temperature as well as precipitation are corrected with a lapse rate (λ) that accounts for changes in surface elevation (z_s). In this work λ is set to 0.08/0.065 K m^{-1} for annual/summer fields. The scaling coefficient f_p in Eq. (5.2) takes into account the Clausius-Clapeyron-relationship, by which a warmer atmosphere enhances atmospheric moisture transport and hence more accumulation occurs. For this study the value is set to f_p = 0.5 % K^{-1} suggested by Frieler et al. (2015). For the deglaciation spin up, α follows the orbital-filtered curve from the Dome C ice core (dashed black curve in Fig. 5.1a). Also sea-level is set to -120 m at the LGM and evolves to PD levels following Lambeck et al. (2014) (dark blue curve in Fig. 5.1).

Future warming

Future temperature and precipitation projections in the Antarctic domain are highly uncertain. To have more realistic estimates, it would be desirable to have projected warming in localized regions. Instead, a simpler approach is just applying a spatially homogeneous change over the whole domain, with precipitation changes proportional to the temperature described by the following equations:

$$T^{\mathrm{atm}}(t) = T_0^{\mathrm{atm}} + \Delta T^{\mathrm{atm}}(t) + \lambda \Delta z_s \tag{5.3}$$

$$P(t) = P_0 \exp\left(f_p\left(\Delta T^{\mathrm{atm}}(t) + \lambda \Delta z_s\right)\right) \tag{5.4}$$

Again, T_0^{atm} and P_0 are the monthly PD temperature and precipitation fields. $\Delta T^{\mathrm{atm}}(t)$ represents the spatially homogeneous anomaly temperature field applied in the Antarctic domain (coloured curves in Fig. 5.1a). Precipitation is scaled through the Clausius-Clapeyron-relationship but here with the spatial temperature anomaly. The values of the lapse rate (λ), accounting for elevation changes, as well as the precipitation scaling coefficient (f_p) are the same as in the deglaciation spin up.

Sub-shelf melting

As described in Chapter 2, and used in the work of Chapter 3, basal melting is parameterised through a linear equation that evolves based on oceanic temperature anomalies with respect to PD

$$B(t) = B_0 + \kappa \Delta T^{\mathrm{ocn}}(t) \tag{5.5}$$

Here, B_0 represents PD basal-melting rates obtained from Rignot et al. (2013) and smoothed and extrapolated for the Antarctic domain (Fig. 2.7). ΔT^{ocn} is the oceanic temperature anomaly with respect to PD. Following results from CMIP5 (Taylor et al., 2012), and as in Golledge et al. (2015), the ocean warms (and cools) with a ratio of one-fourth of the atmospheric anomaly (valid for

the spin up and future warming). Negative melt rates (ie, basal freezing) is not permitted. The heat flux coefficient κ is set to 10 K m^{-1} yr^{-1} as suggested by Rignot and Jacobs (2002), meaning that per every degree that the ocean warms, melting rates increase by ten. No basal-melting is applied to partially grounded grounding-line points to avoid overestimation in the sea-level projections (Seroussi and Morlighem, 2018).

Basal-dragging law

In this work, the basal hydrology does not play a direct role in the ice dynamics. Instead, different flowing regimes are parametrised through different basal friction laws as described in Chapter 2. Basal drag is computed as

$$\tau_{\mathbf{b}} = -c_b f(\mathbf{u_b})\mathbf{u_b} \tag{5.6}$$

Here c_b is the bedrock friction coefficient with units of [Pa], which is intended to describe only bedrock characteristics, such as effective pressure, temperature at the base or bedrock depth. $f(\mathbf{u_b})$, with units of [yr m^{-1}], determines the employed friction law,and hence the flow regime. This work investigates four friction laws. Three of them (linear, power and plastic) are described through the following equation:

$$f(\mathbf{u_b}) = \left(\frac{|\mathbf{u_b}|}{u_0}\right)^q \frac{1}{|\mathbf{u_b}|}, \tag{5.7}$$

and the regularized-power law is represented through:

$$f(\mathbf{u_b}) = \left(\frac{|\mathbf{u_b}|}{u_0 + |\mathbf{u_b}|}\right)^q \frac{1}{|\mathbf{u_b}|}. \tag{5.8}$$

Here setting $q = 1$ or $q = 0$ in Eq. 5.7 leads to a linear viscous or plastic flow law, respectively.Meanwhile, $q = \frac{1}{3}$ represents a power law (Eq. 5.7) and the regularized-power law (Eq. 5.8), following others (e.g. Pattyn et al. 2012).

The bedrock friction coefficient is described following the same approach as in Chapter 4. It is split up into a unitless friction coefficient c_f, the effective pressure N_{eff} and a scaling factor λ which is depth dependent, but with no lower limit, thus:

$$c_b = c_f \lambda_b N_{\text{eff}} \tag{5.9}$$

$$\lambda_b = \begin{cases} 1 & \text{if } z_b \geq z_1 \\ \exp\left(\frac{z_b - z_1}{z_1 - z_0}\right) & \text{if } z_b < z_1 \end{cases} \tag{5.10}$$

This parameterisation intends to capture the fact that sliding is more likely in topographic lows, especially in the marine based zones, where the bed will be softer, due to sediment deposition and the likely presence of water.

Experimental setup

The first part of this work consists of a deglaciation spin-up. The model is forced towards an equilibrated LGM state with constant boundary conditions, as in Chapter 4, and then forced towards PD conditions following the Dome C temperature curve (dashed black curve in Fig. 5.1). Precipitation, atmospheric temperatures and basal-melting rates evolve in phase with this curve. Sea-level variations are prescribed from Lambeck et al. (2014) (dark blue curve Fig. 5.1). This spin-up is run for several friction parameters through a large ensemble analysis (summary in Table 5.1). Only those that match a realistic PD and LGM state are considered for future RCP scenarios (colored curves Fig. 5.1).

As seen in Chapter 4, the configuration of the AIS LGM ice distribution is still poorly known. Thus, only the grounded-ice extent was considered as a metric. A simulation is considered a good match if the LGM extension is above 14.5 million km^2. This value is based on the results from the ICE-6G model, which represents a grounded, but not fully advanced Ross shelf. A PD AIS is considered as realistic if the simulated PD ice volume difference does not differ more than 3 msle and

Parameter	Units	Value(s)
Calving limit H_{calv}	m	175
Enhancement factor shear regime	-	3.0
Enhancement factor stretching regime	-	1.0
Enhancement factor shelf regime	-	0.7
Heat flux coefficient κ	m yr^{-1} K^{-1}	10
Threshold velocity u_0	m yr^{-1}	10,50,100,200,300,400,500
Upper bedrock depth-limit z_1	m	0,100,200,300,400,500,600
e-folding depth z_0	m	-600,-500,-400,-300,-200,-100,-50
Bedrock friction coef. c_f	-	0.1

Table 5.1: Summary of parameter values.

the WAIS extension lies between 2 to 2.5 million km^2. Larger extensions imply a too advanced Ronne shelf, and lower extension for a too retreated Ross shelf.

5.3 Results

Deglaciation spin up

A total of 1048 simulations were performed. Only 152 simulations matched a realistic PD state as described above. Applying the additional LGM constraints, the number of realistic simulations were reduced to 137. From these 137 simulations 31 cases were for a linear friction law (green; Fig. 5.2), 56 for the power law (orange), 43 for a regularized-power law (purple) and 7 for a purely plastic friction law (pink).

LGM AIS

The simulated LGM ice volumes ranges from 13.0 to 16.0 msle above PD, with an ice extension ranging from 14.5 to 15.1 million km^2. The Ronne shelf, or the Amundsen sea have fully extended grounding lines, up to the continental-shelf

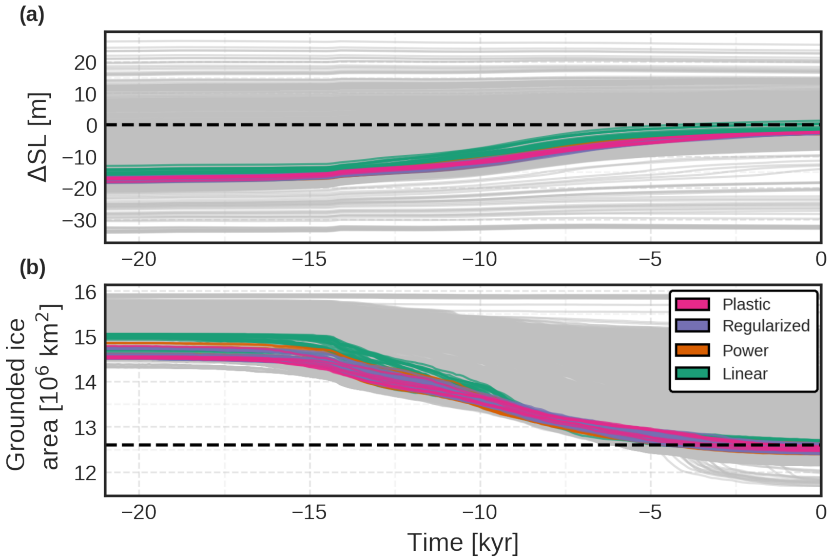

Fig. 5.2: The simulated deglaciation of the **(a)** ice volume in msle; **(b)** grounded ice area in million km^2 for the large ensemble. Grey colors represent simulations that are not consistent with the PD and LGM constraints. In colors, simulations that are consistent with constraints.

break. On the other hand, the lowest ice extensions correspond to a grounded, but not fully advanced Ross shelf (green lines Fig. 5.3). Larger values represents a more advanced Ross shelf (black lines Fig. 5.3). Overall, these results are in agreement with previous reconstructions and model results (Simms et al. 2019 and references therein).

PD AIS

The simulated PD AIS volume ranges from 2.9 msle (larger ice sheet) to -1.3 msle (smaller ice sheet). On average, all friction laws simulate a larger ice volume than observations. A linear friction law simulates the lowest ice volumes with a mean value of 1.4 msle (ranging from -1.3 to 2.8 msle). The remaining friction laws have

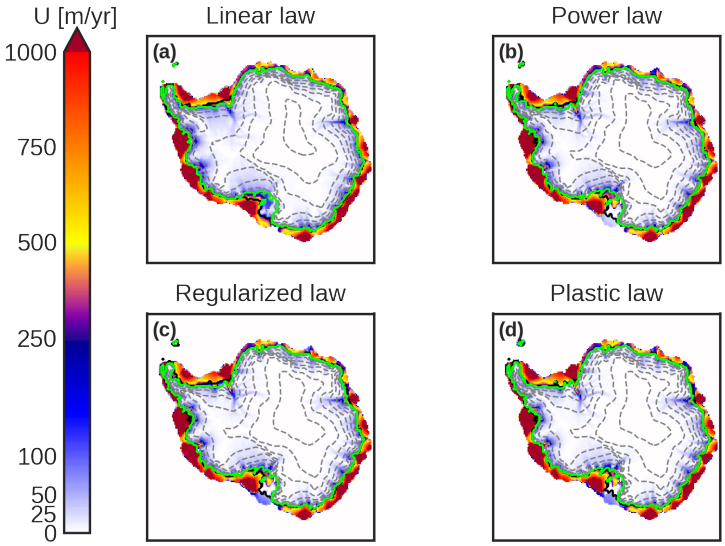

Fig. 5.3: The mean simulated LGM velocity pattern for a **(a)** linear friction law; **(b)** power friction law; **(c)** regularized-power friction law; **(d)** plastic friction law. The black contour line represents the most advanced grounding-line position, the green line the less advanced grounding-line position. Discontinuous contour lines represent surface elevation every 500 meters up to 3500 meters.

a similar contribution, with a mean value of 2.6 msle (2.5 to 2.9 msle) for the power friction law, 2.6 msle (2.2 to 2.9 msle) for a regularized-power law and 2.3 msle (2.2 to 2.6 msle) for a plastic friction law. As seen in Figure 5.2, differences in ice extension to PD conditions do not differ by more than 0.2 million km^2. All PD simulations have on average a slightly more retreated grounding-line position in the Ross shelf, and a more advanced grounding line Ronne shelf (black lines vs. green lines in Fig. 5.4). Ice shelves are also more advanced than observations. The size of ice shelves is highly dependent on the calving limit, $H_{calv} = 175$ m. Larger values are found to simulate too small ice shelves, whereas larger values too large ice shelves.

The computed root-mean square errors (RMSE) of the four friction laws fall inside the range of initMIP and ISMIP6 experiments (Seroussi et al., 2019, 2020).

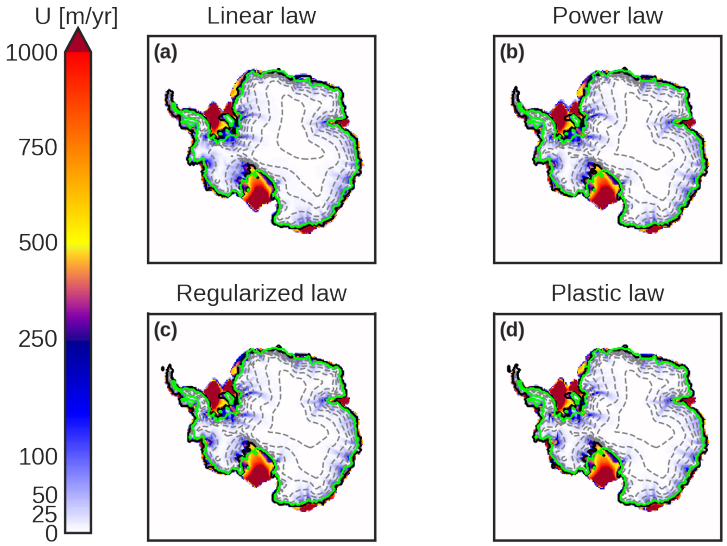

Fig. 5.4: The mean simulated present-day velocity pattern for a **(a)** linear friction law; **(b)** power friction law; **(c)** regularized-power friction law; **(d)** plastic friction law. The black contour line represents the simulated present-day, grounding-line position. The green line represents the actual measured grounding-line position. Discontinuous contour lines represent surface elevation every 500 meters up to 3500 meters.

Small differences are found for all the simulations. The RMSE in ice thickness lies slightly above 300 meters, with more variability for the linear law (upper panels Fig. 5.5a). This is due to the major dispersion in ice volume found in the linear law. The RMSE of surface ice velocities are around 300 m yr^{-1} (upper panels Fig. 5.5b). The large variability is due to the size of the ice shelves. Larger ice shelves will simulate a larger error. Finally, the RMSE of the logarithm of the surface ice velocity, which highlights the error of the slower inland ice, are found to be less variable (upper panels Fig. 5.5c).

Looking at the spatial pattern of the ice thickness anomaly (middle panel Fig. 5.5) and surface ice velocity anomaly (lower panel Fig. 5.5) allows identification of the sources of the computed RMSE. A linear friction law has a lower ice extension

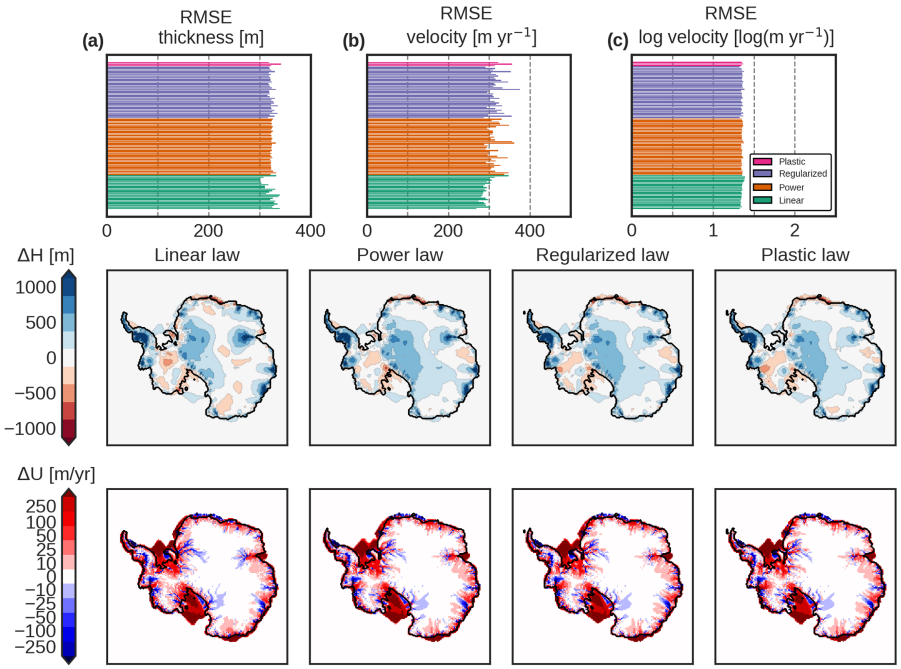

Fig. 5.5: Upper row: Root mean square error (RMSE) of the simulated PD conditions compared to observations of Fretwell et al. (2013) and Rignot et al. (2011) for **(a)** ice thickness, **(b)** surface velocity and **(c)** the logarithm of the ice surface velocity, which highlights the error on the slower parts. Middle row: ice thickness anomaly (mean simulated PD minus observed PD) for every friction law. Lower row: surface velocity anomaly (mean simulated PD minus observed PD) for every friction law.

in the middle of the WAIS an parts of the EAIS. On the other hand the Amery, and the EAIS close to the Ronne shelf have thicker ice. The other friction laws simulate a similar pattern, with a larger positive anomaly in the EAIS and a lower ice thickness in the Amundsen region. All cases simulate systematically a larger ice thickness in the Antarctic Peninsula, probably due to the coarse resolution which does not capture precisely the mountainous region there. The ice velocity anomaly is very similar for all four laws and shows on average a faster ice sheet with a large positive anomaly in the ice shelves.

Future scenarios

Sea-level rise

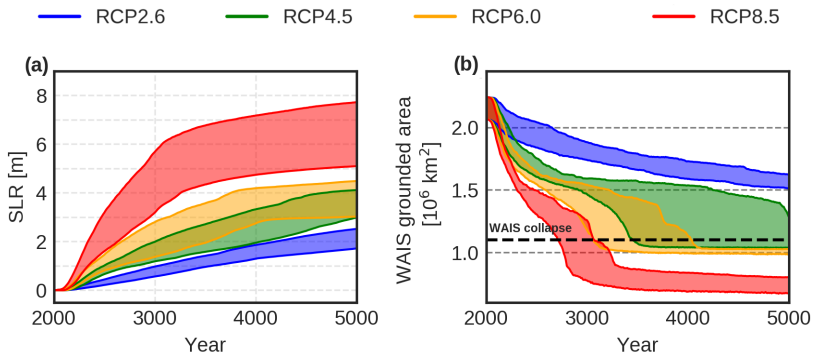

Fig. 5.6: Simulated range of **(a)** sea-level rise and **(b)** grounded WAIS extension for every RCP scenario. Black discontinuous line represents a complete WAIS collapse.

The main driver of the future Antarctic contribution to sea-level rise is the RCP scenario (Fig. 5.6a). Overall, the largest contribution at year 5000 is 8.4 msle, and the lowest contributions 1.7 msle, hence a range of 6.7 msle. RCP2.6 is representative for a scenario where the Paris agreement is accomplished and the mean temperatures do not exceed two degrees above pre-industrial level. For this scenario the simulated sea-level contribution of the AIS ranges from 1.6 to 2.7 msle (blue curves in Fig. 5.6a). On the other hand for the highest emission scenario, RCP8.5, the simulated sea-level contribution goes from to 5.1 to 8.4 msle (red curves). The simulated uncertainty range for the highest scenario is three times larger than for the lowest emission scenario. The uncertainty range for intermediate scenario, namely RCP4.5 (green line; 3.0-4.5 msle) and RCP6.0 (yellow line; 3.0-5.1 msle) substantially overlap.

At shorter timescales (next 100-300 years) projections of sea-level contribution are strongly dependent on the friction law (Fig. 5.7a,b). This difference is more

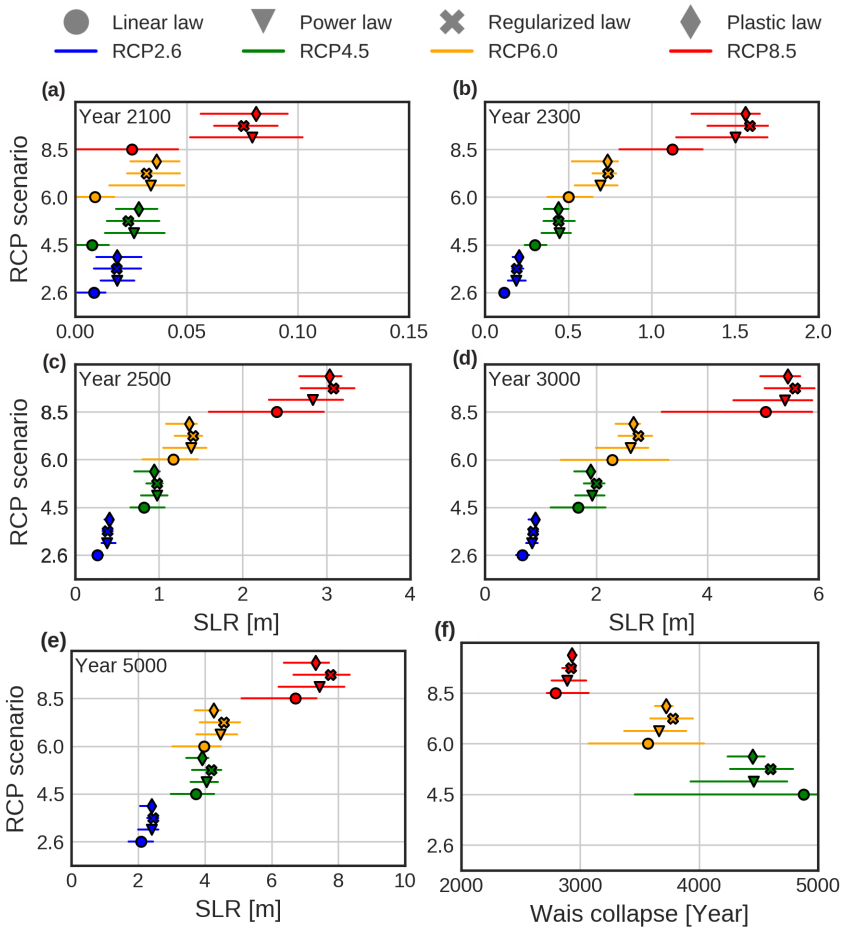

Fig. 5.7: Mean simulated sea-level contribution for a linear (circles), power (triangles), regularized-power (crosses) and plastic (diamonds) friction law for year **(a)** 2100; **(b)** 2300; **(c)** 2500; **(d)** 3000; **(e)** 5000. Panel **(f)** shows when the model simulates a complete WAIS collapse. Colorbars represent the simulated range for every RCP scenario and friction law.

noticeable for higher RCP scenarios. For RCP8.5 (red), sea-level projections by year 2100 stay within a similar range for the power (triangles), regularized-power (crosses) and plastic (diamonds) friction laws, mainly 5-10 cm and by 2300 1.1-1.7 m. On the other hand, a linear friction law (circles) simulates a lower contribution, 2.5 cm by year 2100 and 1.1 m by year 2300, but spanning a wider range of uncertainty (0-5 cm for year 2100 and 0.7-1.4 m by year 2300). At longer timescales, year 5000, when the climate stands constant, the response for all friction laws tend to converge. As seen in Figure 5.7e the distance between a linear law and the others is substantially reduced by year 5000, although the former law preserves a wider spread in the projections.

WAIS collapse

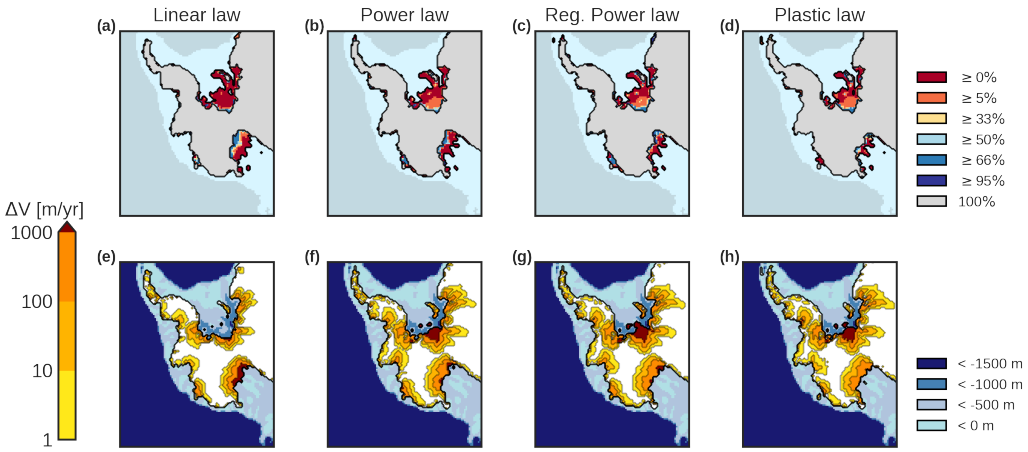

Fig. 5.8: Lower probability bounds of finding grounded ice for RCP4.5 scenario by the year 2300 for **(a)** linear friction law; **(b)** power friction law; **(c)** regularized-power friction law; **(d)** plastic friction law. Ice velocity difference between year 2300 and PD for the same friction laws (**efgh**). Black line represents the grounding line position for the most advanced simulated ice sheet.

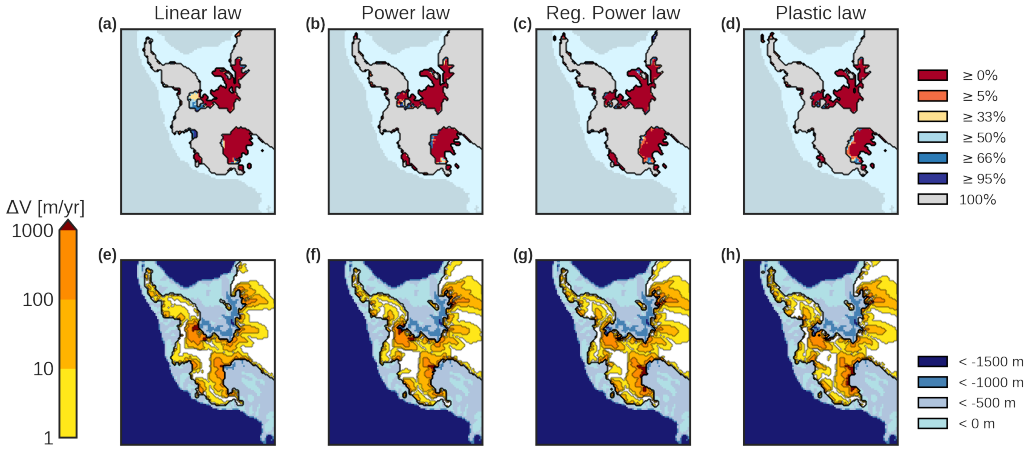

Fig. 5.9: Same as Figure 5.8 but for year 3000.

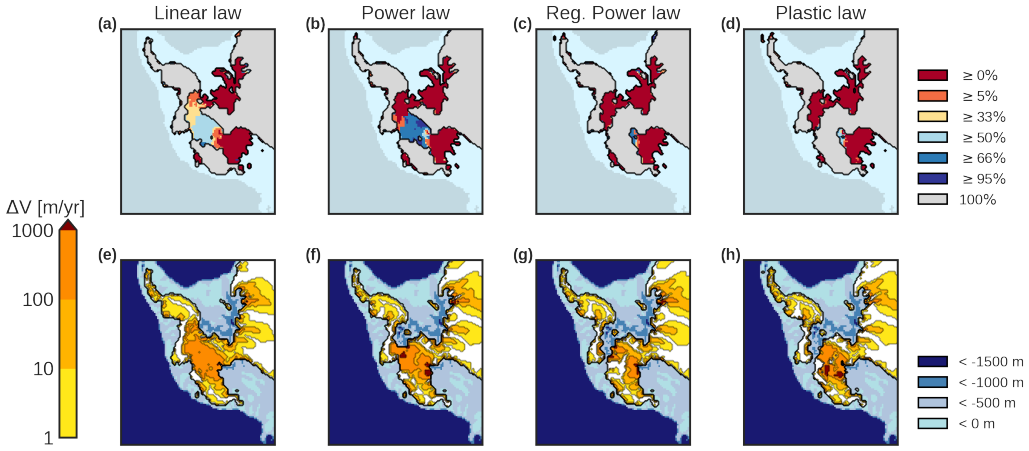

Fig. 5.10: Same as Figure 5.8 but for year 4000.

WAIS extensions below 1.1 million km^2 are found to be representative of a fully retreated grounding line in the marine sectors. As shown in Figure 5.6b, the probability of a WAIS collapse increases with RCP scenario. Whereas the lowest emission scenario, RCP2.6, does not collapse for any of the friction laws, higher emission scenarios simulate a fully collapsed WAIS by year 5000 (with some exceptions for the linear case in RCP4.5). Simulations under RCP4.5 range from a collapsed WAIS from year 3460 to no collapse. The collapse-timing band, dependent on the friction law, ranges from year 3460 to no collapse for RCP4.5, year 3070-4040 for RCP6.0 and from year 2720-3070 for RCP8.5 (Fig. 5.6b). Hence, higher emission scenarios do not only accelerate a MISI mechanism, but narrow the timing band, meaning that it increases the likelihood to occur. Further inspection allows analysis of the uncertainty band for every friction law and RCP scenario (Fig. 5.7f). Results show that a linear friction law can collapse earlier than other laws but still contribute less to sea-level rise overall. This points to a different dynamic response of inland ice.

Although floating ice does not directly contribute to sea-level rise, ice shelves exert a backward force to the interior of the ice sheet, reducing ice velocities (Fürst et al., 2016). An increase in oceanic temperatures shrinks the size of these ice shelves, reducing the buttressing effect, which enhances inland ice discharge into the ocean, causing sea-level rise. How much ice streams accelerate after an ice shelf collapse is determined by the basal conditions and ultimately through the basal friction law (Joughin et al., 2019). RCP4.5 scenario represents a good situations for visualizing this phenomenon as ice shelves collapse early but the WAIS remains grounded until year 4000. By year 2300 the WAIS still remains grounded (Fig. 5.8) with a slightly more retreated grounding-line in the Ronne sector for all cases. Looking at the velocity anomaly it is possible to analyze how much inland ice has accelerated. Ice streams such as the Recovery or the Support Force accelerate for all the laws, nonetheless the velocity anomaly for the power, the regularized-power and the plastic friction law penetrate deeper inland than for a linear law. Also close to the Amundsen Sea, at the Thwaites and Pine Island glacier, ice accelerates less for a linear law. For year 3000 (Fig. 5.9) the WAIS is still grounded, but the MISI mechanism is started to be triggered in the western

part of the Ronne shelf (with some exceptions for the linear case, where it still remains grounded). The velocity anomaly has increased in comparison with the year 2300, and penetrated deeper inland. Nonetheless, the linear case is still less accelerated, leading to a lower sea-level rise.

Finally, at year 4000 simulations using a linear friction law range from a fully grounded to a fully collapsed WAIS (around 50%; Fig 5.10). A power law has also some cases with a fully collapsed WAIS but less probable (around one third). On the other hand, a plastic and a regularized-power friction law do not fully collapse, but the MISI mechanism has already started through the Ronne shelf. Now, for this committed scenario, velocity anomalies have a similar pattern for all cases, and thus sea-level rise is similar for all the laws. This shows, that at short timescales, a linear friction law contributes less to sea-level rise because more resistance occurs at the ice base, which slows ice velocity, and inland ice accelerates less. So, despite a potential earlier collapse, less ice is discharged into the ocean. Its not until later, with a committed scenario, when sea-level contributions reach similar values.

5.4 Discussion

Comparison with previous studies

At short timescales, year 2100, Golledge et al. (2015) simulated for RCP8.5 (RCP2.6) scenario a sea-level contribution from 0.10 to 0.39 (-0.01 to 0.1) msle. Their upper bound limit resulted from adding subgrided basal-melting rates at the grounding line. Similar to this result, Ritz et al. (2015) obtained through a probabilistic study a sea-level rise up to 0.3 msle. These results are in agreement with this work, where a sea-level rise of 0.0 to 0.1 msle is computed for RCP8.5 and 0.0 to 0.03 for RCP2.6. On the other hand, DeConto and Pollard (2016) obtained for RCP8.5 (RCP2.6) scenario a larger contribution of 0.64 to 1.01 (0.02 to 0.11) msle. They based their results on the calibration of model parameters to match different warm periods as the LIG and the Pliocene (the upper bound

was caused by a larger Pliocene target) together with the inclusion of the MICI mechanism.

At longer timescales, no other study computes more than 1 msle for RCP2.6 scenario. This work points to a contributions above 1 msle for year 3000 and above 2 msle for year 5000. his sea-level rise can partially be due to the Antarctic drift, which is discussed below, up to 0.6 msle. The rest can be explained due to a potential overestimated oceanic warming. Nonetheless, for the rest of the RCP scenarios, DeConto and Pollard (2016) simulate the largest contributions, more than 10 msle, partly due to the MICI mechanism. Meanwhile, the results of Golledge et al. (2015) and Bulthuis et al. (2019) at long timescales are in agreement with this work.

Furthermore, Bulthuis et al. (2019) investigated different sources of uncertainty for future AIS projections. Among other variables, they tested different friction law exponents for optimized bedrock friction coefficients following Pollard and DeConto (2012b) for the Weertman sliding law. Similar to this work, they found that friction laws close to a plastic friction law simulated a faster response at shorter time scales. Sea-level differences of 0.04 (0.01) msle by year 2100 and 0.47 (0.07) msle by year 2300 were obtained for the scenario RCP8.5 (RCP2.6). This work supports a larger difference between a linear friction law and a power friction law. Nonetheless, for longer, committed scenarios, by year 3000, the results of Bulthuis et al. (2019) for laws close to the purely plastic flow are close, but differences of almost 3 msle are simulated between a linear law and a power law. This work does not support such large differences at longer timescales, where sea-level contributions for all exponents tend to converge.

WAIS collapse

Satellite data observations show that the Amundsen sea region has elevated mass loss and basal-melting rates (Rignot et al., 2013, 2014; Favier et al., 2014). This regions represents a threat as a MISI mechanism could be triggered there. Therefore, the latest studies have paid special attention to this zone (Cornford et al.,

2015; Ritz et al., 2015; Alevropoulos-Borrill et al., 2020). Feldmann and Levermann (2015) for instance showed that under PD conditions the Pine Island and Thwaites glaciers are close to collapse. This work, however, does not support such an initial triggering through the Amundsen region, but rather through the western part of the Ronne shelf (and some exceptions for the linear friction law, through the Siple Coast in the Ross shelf). Ice-sheet models have been shown to simulate grounding-line retreat for different sensitivity calibrations through different zones (Schlegel et al., 2018). Bulthuis et al. (2019) simulated a MISI driven WAIS collapse via the Siple Coast. They attributed this larger sensitivity there to an oversimplification of the oceanic forcing. However, there are more sources which could affect this, like the grounding line subgrid treatment, for instance. In contrast to these future experiments, LIG experiments, which are often run from idealized PD initial conditions, support a collapse driven through the Ronne shelf as in this work (Sutter et al., 2016; Turney et al., 2020). All in all, the model initialisation, the calibration of the oceanic sensitivity or the employed resolution are potential factors in determining the location where a WAIS collapse is likely to occur.

Oceanic warming

Future evolution studies of the AIS focus mainly on the crucial role of the ocean. A warmer ocean has the potential to shrink the size of ice shelves, which in turn affect inland ice dynamics, and enhances the likelihood of occurrence of a WAIS collapse. Nonetheless, the evolution of the SO is difficult to assess, not only for the future, but also for past periods due to the complexity of the system (Alevropoulos-Borrill et al., 2020). Basal melt occurs due to enhanced warm penetrating circumpolar deep waters onto the continental shelf. Model results show that the penetration of these dense waters is directly connected to wind shifts at the continental-shelf edge as a consequence of changes in the tropics (Thoma et al., 2008; Paolo et al., 2018). Moreover, this wind pattern change could be directly connected to anthropogenic forcing, suggesting that more warm waters

will penetrate on the the ice shelf cavities, enhancing subshelf melting (Holland et al., 2019). Thus, to asses the response of the AIS to oceanic warming it is necessary to have a more profound understanding of the dynamics of the SO and ACC, eddy activity and ice-ocean interaction (Sallée, 2018; Holland et al., 2020).

This work does not take into account all of these issues and considers a simplified scenario with a spatial homogeneous warming in phase with the ocean, similar to other studies (Golledge et al., 2015; Ritz et al., 2015; DeConto and Pollard, 2016; Pattyn et al., 2018; Bulthuis et al., 2019). A potential caveat of the employed basal-melting strategy is that it does not include localized warming (or cooling) nor changes in ocean depth or salinity. In a region with more depressed bedrock for instance, more warm waters could penetrate, enhancing melting. These processes cannot be taken into account with a constant heat-flux coefficient.

In addition, the collapse of large ice shelves as the Ronne or the Ross, is strongly dependent on this heat flux coefficient. Only RCP2.6 scenario is able to sustain ice shelves in the Ross and a smaller and retreated Ronne shelf until year 3000 and 4000, respectively (Fig. 5.11). The rest of the scenarios have a faster collapse. It is clear that a larger (smaller) value would have enhanced (reduced) basal-melting, affecting the results. However, because the future evolution of the ocean is so uncertain, so is the future configuration of ice shelves. Also, ice shelves are found to be very sensitive to the employed parameterisations of calving processes at the ice-shelf front (Yu et al., 2019). Whereas Golledge et al. (2015) were able to maintain larger ice shelves than in this work, DeConto and Pollard (2016) had rather a low capability to sustain large ice shelves partly due to the inclusion of MICI mechanism. LIG experiments that start with PD-like configurations have collapsed ice shelves even for low oceanic anomalies, as in this work (Sutter et al., 2016; Turney et al., 2020). A sensitivity study of the AIS to oceanic warming was out of the scope of this work and there are large uncertainties associated to the response of ice sheets to oceanic warmings. Thus a constant value of 10 m yr^{-1} K^{-1} was chosen in agreement with observations (Rignot and Jacobs, 2002) and other studies (Levermann et al., 2020). To avoid potential overestimation in sea-level rise due to the simplified basal-melting pa-

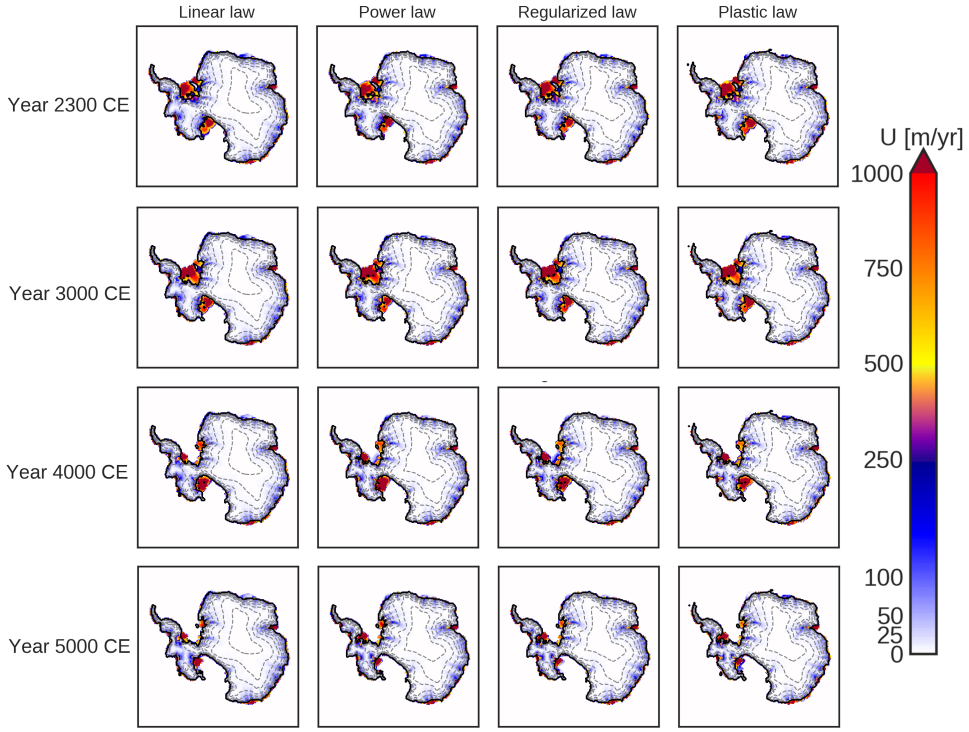

Fig. 5.11: Mean simulated velocity for RCP2.6 scenario for all the friction laws by year 2300, 3000, 4000 and 5000. The black thick line represents the simulated grounding-line position. Controu lines are drawn every 500 meters up to 3500 meters. RCP2.6 is the only scenario capable of sustain large ice shelves.

rameterisation, no basal melting was allowed at the grounding line itself, or larger basal-melting rates in floating grid points close to the grounding line (Gladstone et al., 2017; Seroussi and Morlighem, 2018).

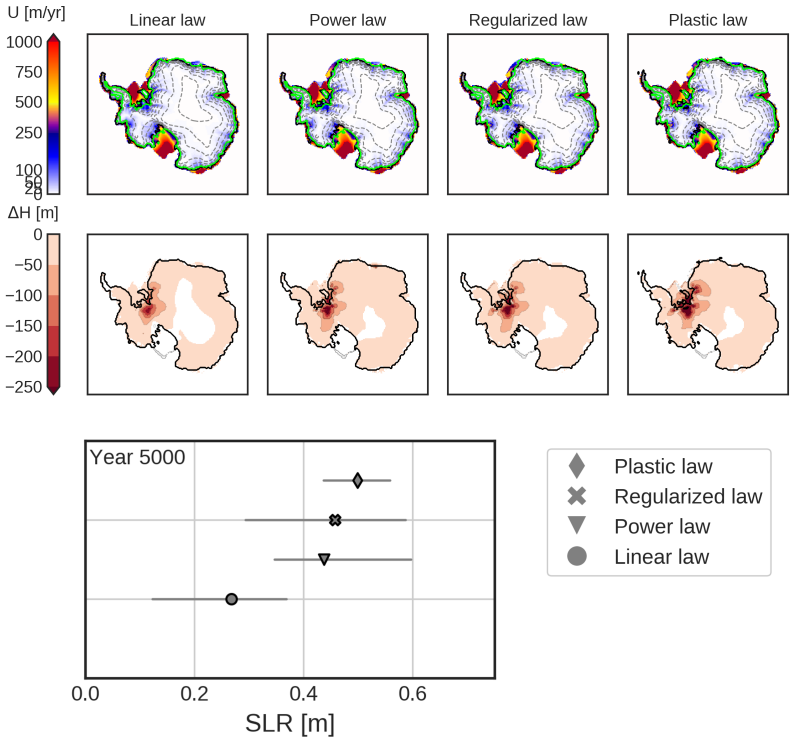

Fig. 5.12: Upper panel: Simulated AIS velocity pattern with present-day (PD) conditions for year 5000. Black contour line represents the simulated grounding-line position and green line the PD grounding-line position. Discontinuous contour lines represent surface elevation every 500 meters up to 3500 meters. Middle panel: Ice thickness anomaly between the simulated AIS for year 5000 under PD conditions and the simulated PD AIS. Lower panel: Simulated sea-level rise for every friction law for year 5000.

Antarctic drift

Future warming studies often use inversion methods for optimizing bedrock conditions, intending to capture idealized stable present-day AIS configurations (Pollard and DeConto, 2012a; Morlighem et al., 2013; Bulthuis et al., 2019). These

inversion methods optimize bedrock coefficients either by tracking the surface elevation or the surface ice velocity. The first method ensures continuity of the ice sheet geometry but a less precise representation of ice flow, the second ensures a realistic ice flow connectivity but poor ice sheet geometry. However, these methods may not be realistic, but represent compensated model errors with badly represented physical processes and unrealistic bed properties, yielding to an accurate PD state for the wrong reasons. In this work a different approach was employed. Instead of optimizing the bedrock parameters, a large ensemble (1048 simulations) was launched that ran from the LGM to PD. By doing so, the aim was to find model versions that simulated realistic LGM and PD configurations and took into account the thermal memory of the ice sheet. However, due to the large ensemble analysis, in order to perform 1048 simulations, a coarse resolution had to be set which can affect grounding-line migration (Pattyn et al., 2012; Pattyn and Durand, 2013).

To analyze the potential drift caused by the deglaciation spin up, constant PD background conditions are applied till year 5000 (Fig. 5.12). The measured sea-level rise is small, between 0.1 and 0.6 msle, being lower for the linear case again. The anomalies of the ice thickness show that the origin of this sea-level rise is the ice streams close to the Ronne shelf, similar to the perturbed experiments. All friction laws show stable ice shelves. This was rather expected, as the used basal melting rate from Rignot et al. (2013) is consistent with the large ice shelves today. However, in order to fully analyze the implications of the spin up procedure, it would be necessary to run the same ensemble under constant PD conditions and then force it with the RCP scenarios.

Role of the initial state

As seen in the Results section, a linear law simulates on average a lower ice volume than the other friction laws, thus it is necessary to confirm that the lower response of a linear law is a consequence of ice velocities and not a systematic bias. To do so, the resulting sea-level contribution for year 2300 and 5000 for RCP8.5 scenario

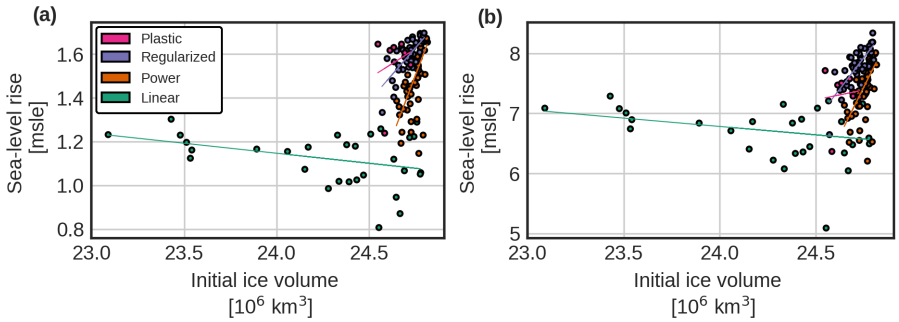

Fig. 5.13: Simulated sea-level rise for year **(a)** 2300; **(b)** 5000 for scenario RCP8.5 against the initial ice volume. Table 5.2 shows the computed exponent of the linear regression.

Year	Linear	Power	Regular	Plastic
2300	-0.1	2.2	1.0	0.5
5000	-0.3	6.4	4.2	0.7

Table 5.2: Exponents of the linear regression of Figure 5.13.

is plotted against the initial ice volume for all simulations (Fig. 5.13). As already mentioned, the power law (purple), the regularized-power (orange) and the plastic law (green) simulate a lower range than the linear law (pink). Within this range, the former laws discharge more ice for larger a PD ice volumes. The computed coefficients of the linear regression (Table 5.2) show an abrupt fall, which is the probable cause why these friction laws cannot simulate lower ice volumes. On the other hand, for a linear friction law, sea-level discharge decreases for larger ice volumes. This points to the probable cause that a lower volume occurs due to faster ice streams. Thus it can enhance ice flow after the loss of buttressing effect. Simulations that fall inside a similar ice volume range show that a linear law causes less ice discharge, hence the initial hypothesis, that a linear law impedes inland ice to accelerate more compared to the rest of laws is valid.

5.5 Conclusions

Basal friction is an essential, and yet unknown, characteristic of the AIS, as it balances the ice dynamics of the AIS. This work aimed to investigate the future projection of the AIS for four different basal dragging laws, which mimic four different flowing regimes. In order to ensure, that the AIS maintained thermal memory, and the choice of friction coefficients was not only realistic for PD periods, but also to past periods, the model was spun up from an equilibrated LGM state to PD. Through a large ensemble analysis of the depth-dependent friction coefficient the phase space of possible friction configurations that matched realistic LGM and PD conditions was covered. From there, realistic configurations were forced for four different RCP scenarios. As expected, the future evolution is mainly driven by the RCP scenarios. Whereas the lowest emission scenario (RCP2.6) contributes to a sea-level rise of 1.6-2.7 msle for year 5000, the highest emission scenario (RCP8.5) contributes to a sea-level rise of 5.1-8.4 msle. Also the occurrence of a WAIS collapse increases with RCP scenario. Whereas no collapse is found for RCP2.6 and around year 4500 for RCP4.5, the WAIS collapses at around year 3000 for RCP8.5. Nonetheless, the choice of friction law is crucial at short timescales. The linear friction law, intended to reflect ice flowing over hard bedrock, accelerates less inland ice. On the other hand, for soft beds, represented by the plastic and power-regularized law, inland ice accelerates more, producing more ice discharge into the ocean. In summary, this work shows that invariably a warmer climate-change scenario will produce higher sea-level rise, but at short timescales, due to the loss of buttressing effect, the choice of friction law is crucial in accelerating inland ice and provoking ice discharges. Thus it is necessary to include the friction law as a fundamental source of structural uncertainty in future work.

Chapter 6
Discussion

This thesis investigated the Antarctic sea-level contribution since the LGP and into the future using a three-dimensional hybrid ice-sheet-shelf model. Ice dynamics, as well as climatic boundary conditions, are two essential building blocks that drive the evolution of the AIS. However, due to the scarcity of available data, especially for past periods, basal conditions as well as past climatologies are highly uncertain. Understanding their impact on past periods is highly relevant for future predictions. Following a chronological order, first paleo runs were performed to investigate the sensitivity of the AIS to unconstrained parameters regarding ice-ocean interactions, as well as ice dynamics. From there, this was extended to estimate future sea-level contributions. The results described within this thesis address the three main questions presented in Section 1.4.

Does the AIS respond to glacial millennial-scale climate variability?

To answer this question, the ice-sheet-shelf GRISLI-UCM model was used and forced with millennial-scale climate variability. Because these variations occur under glacial conditions, first a spin-up of an AIS LGM state in equilibrium was simulated. Then, the model was transiently forced with millennial variations, obtained from the temperature signal of the Dome C ice core. Atmospheric

temperature and precipitation fields for the glacial and AIM state are obtained from the climatic model of intermediate complexity Climber-3α (Montoya and Levermann, 2008). Oceanic temperatures were set spatially constant and converted into basal-melting rates through a heat-flux coefficient. Here, two major issues appeared. On one hand, oceanic temperatures in the past are difficult to estimate, as there is not much data providing such information. Thus, for this purpose a simple approach was adopted. Also, simulating ice-ocean interactions, even at PD, is highly challenging. The ocean is a complex system that involves oceanic currents, stratification and upwelling, all of which is not currently feasible to simulate with confidence. Therefore, because the response of the AIS to a warming ocean is unclear, several oceanic sensitivities were tested through the heat-exchange coefficient. Accounting for this ice-ocean interaction resulted in a pronounced response of the AIS in terms of SLR and grounding-line migration. This highlights two issues: first, atmospheric millennial-scale variability by itself is not enough to produce a response of the AIS, which was expected given its cold polar climate. Even at PD, variations in the atmospheric temperatures are rather unimportant, thus a warming of 2 K over a colder climate (around 10 K colder) had a negligible impact. Second, when the ocean was considered, the AIS did respond to glacial millennial timescales variations. This points to an important role of the ocean, not only during warm interglacial stages, but also during colder interstadial stages.

Paleo-simulations of the AIS have mainly focused on glacial-interglacial cycles. These studies highlight the importance of the ocean during warm stages, such as the Holocene, the LIG or the Pliocene (Pollard and DeConto, 2009; De Boer et al., 2014; Sutter et al., 2016, 2019). However, the impact of oceanic temperature changes during cold periods of the AIS has not been assessed. Forcing an ice-sheet model through Earth's orbital changes, neglects natural internal climatic variability. Antarctic ice cores show episodes of smooth warming events at millennial timescales during glacial stages. These warming events are hypothesized to occur as a consequence of an inherent instability of the AMOC. A weak AMOC transports less heat into higher, Northern latitudes through the bipolar seesaw mechanism and leads to more heat accumulation in the South (Crowley,

1992; Stocker, 1998). Stocker and Johnsen (2003) argue that this heat can be transferred into the SO, which acts as a heat reservoir. If oceanic temperatures are only forced through orbital changes, then these millennial variations are neglected. An approach such as that proposed by Banderas et al. (2018) would be an appropriate one to capture this phenomenon. Thus, the importance of the ocean during cold periods cannot be excluded. In addition, the response of the AIS to rapid oceanic warming is of tremendous value because it allows us to gain insight into abrupt climate changes. As highlighted by Sutter et al. (2016), the future evolution of the AIS depends not only on the amplitude of the warming subsurface, but also on the rate of warming, as corroborated by the results presented here.

However, the existence of a unique heat reservoir is still an open question. Pedro et al. (2018) argue that rather than the SO alone, the global ocean acts as a heat reservoir. They explain that the intrusion of warm waters is hampered by the presence of the strong ACC. Only in localized regions warm waters penetrate in the form of eddy heat fluxes that trigger sea-ice melt. This sea-ice melt is further amplified by the sea-ice albedo feedback. The rest of heat remaining in the Atlantic is transferred into the atmosphere and Pacific Ocean rather than the SO. Nonetheless, Kusahara et al. (2015) show in their model results, that the basal melting rates of the Antarctic ice shelves close to the continental-shelf break are higher than PD values as a consequence of warmer CDW due to strong stratification. Hence, an increase in strength of the SO westerly winds as shown by Banderas et al. (2015) could enhance the penetration of the warmer CDW onto the continental-shelf, as hypothesized by Thoma et al. (2008), provoking a potential response of the marine sectors of the AIS (Lachlan-Cope and Connolley, 2006; Steig et al., 2012). The heat-flux coefficient κ can thus also be reinterpreted as a weighting parameter of the amount of heat that has entered into the SO.

However, it is important to mention that in this experimental setup, melting at the grounding line was allowed. It is a common approach in coarse resolution models to apply a scaled basal melt in grounding-line-adjacent grid points, weighted by the floating ice fraction (Golledge et al., 2015; Ritz et al., 2015). As our understanding of ice-sheet models has improved over time, it has become

clear that this approach, rather than resulting in more realistic sea-level estimates, may overestimate the response of idealized marine ice sheets to oceanic warmings (Seroussi and Morlighem, 2018). Nonetheless, the main goal of this study was to show that the AIS responded to glacial millennial-scale variability and these results should be reasonable for a first-order response to oceanic temperature anomalies. The results of this work show that for a certain threshold value (κ <10 m yr^{-1} K^{-1}) the AIS is able to regrow to its glacial state on millennial timescales. As recorded by sea-level records during MIS-3, large continental ice sheets discharged large amounts of ice, around 20 msle, but also recovered to their glacial states on the involved timescales (Siddall et al., 2008; Rohling et al., 2009; Grant et al., 2012). Therefore an Antarctic SLR of about 6 m falls inside the range of possible contributions as it recovers to its glacial state. This confirms that the primary contributor to millennial sea-level fluctuations are NH paleo ice sheets but with a non-negligible contribution from the AIS.

In this work melting at the grounding-line points (the last floating points before the grounding line) was set ten times larger than at the rest of the floating points as suggested by observations (Rignot and Jacobs, 2002). This is intended to capture the phenomenon by which basal melting rates are larger close to the grounding line and diminish towards the ice shelf front. This is a consequence of the high density of the warm CDW, together with plume formation (e.g., Jacobs et al. 2011; Jenkins 2011; Pritchard et al. 2012). Still, as pointed out by Gladstone et al. (2017), in coarse resolution models the melt parameterisation should reduce in abruptness towards the grounding line rather than applying high melt in order to avoid overestimation of SLR. From observations, the expected theoretical value for the heat-exchange value is κ=10 m yr^{-1} K^{-1} (Rignot and Jacobs, 2002), however as seen in this work, this value is not sufficient for regrowing to its glacial state. Taking into account that these results may be overestimated as a consequence of large imposed melting rates close to the grounding line, as well as applying melt inside the grounding-line grid point, a heat exchange values of κ=10 m yr^{-1} K^{-1} cannot be excluded with a more sophisticated experimental setup.

Finally, in this work a simple oceanic warming scheme was adopted to depict the bipolar seesaw mechanism. Assuming a constant warming and freezing over the whole SO is rather a simplification of reality and potentially overestimates/underestimates Antarctic responses in different regions (Martin et al., 2013, 2014). Marine proxies of the SO which could provide information of past temperature are scarce and cover roughly the involved timescale. The evidence of large ice sheets responding to climatic changes could be inferred by sporadic IRD deposition as for the NH (Alvarez-Solas et al., 2013; Bassis et al., 2017). However, the evidence of deposition of IRD in the SH are minimal (Weber et al., 2012, 2014; Kim et al., 2018). A more robust signal of a periodic deposition of land sediments eroded by icebergs could prove a potential response of the AIS to oceanic changes and strengthen the understanding of the bipolar seesaw mechanism. In the future, more data will be available from marine proxies to shed light on this issue. These data will provide sufficient information for a more realistic assessment of the Antarctic response to oceanic warmings.

To what extent do different boundary conditions affect the simulated LGM AIS?

This question has been addressed by forcing the ice-sheet-shelf Yelmo model by different LGM atmospheric boundary conditions with varying basal conditions. The basal friction parameterisation used here, which is based on other studies (e.g., Winkelmann et al. 2011; Martin et al. 2011; Albrecht et al. 2019), enhances sliding for the marine parts of the ice sheet and assumes a hard bedrock character for bedrock elevations above sea-level. This parameterisation assumes that ice flow is promoted in the topographic lows and that marine parts will most likely have a lower friction due to loose sediment material and higher probability of the presence of basal water. The LGM climatology, such as annual and summer temperatures as well as precipitation fields, was obtained from the PMIP3 repository. Glacial basal-melt rates of ice shelves were set to zero to allow for maximum ice extension. This is a vast simplification, however, there is no inter-comparison

group of Antarctic basal melt rates at the LGM and converting oceanic temperatures from PMIP3 into basal-melting rates requires a sensitivity study of ice-ocean interactions. Given the lack of constraints, this was out of the scope for this work and so, for simplicity, no basal melt was allowed. The main results show that the uncertainty in ice volume as well as extension are large and of a similar magnitude for friction parameters and for climatic boundary conditions.

Simms et al. (2019) reviewed the total sea-level budget of the LGM. They showed that the sum of all the large continental ice sheets as well as smaller ice caps did not match the total inferred sea-level budget by about 15 msle. This missing ice can only be explained either by a larger contribution of continental ice sheets or by a larger contribution of smaller glaciers and ice caps. Simms et al. (2019) even hypothesize that an unknown missing ice sheet has to be found. This works highlights the fact that an additional 6 m of sea-level difference can be obtained from the AIS, which is due to the uncertainty in basal friction and the AIS glacial climate. If this relation holds for other ice sheets such as the LIS, GrIS or EIS, then it may be that the missing 15 msle of ice can be reconciled by the large ice sheets.

One key issue for reducing this uncertainty is the need for improved climatic boundary conditions. More than the half of the PMIP3 LGM model outputs underestimate/overestimate the reconstructions of the accumulation–temperature relationships in localized regions (Cauquoin et al., 2015). In fact, the existence of ablation near the Ronne shelf in one of the output models makes it highly unlikely. This points to the necessity of improved LGM climatologies as expected for the PMIP4 results. Also, to infer the past basal friction conditions is difficult as data are unavailable. Satellite observations allow through inversion methods to estimate PD friction conditions, but this represents a particular configuration which does not necessarily hold for other time periods.

However, it should be noted that there are other sources of uncertainty that can explain this difference in sea-level without necessarily invoking the missing ice sheets and ice caps, for instance, the bedrock depth. It is clear that a deeper bedrock has the capability to store more ice than a shallower bedrock. However, the bedrock configuration at the LGM remains unconstrained. As described in

Chapter 2, Yelmo uses a simple approach to account for bedrock changes, namely the ELRA method (Le Meur and Huybrechts, 1996). This method assumes homogeneous viscosity and rheology properties of the bedrock. However, it is well established, that the WAIS sector has different rheological properties than the EAIS (Whitehouse et al., 2019). Thus, a different and more realistic GIA model could have an impact on the exposed results.

In addition, there are model and technical issues that need to be addressed. For instance, it is important to mention that PD as well as LGM simulations were run under steady state conditions. Of course, this is a simplification compared to its transient evolution in reality. Nonetheless, the late LGP was a cold and sufficiently long period in the Antarctic domain, and thus, constant LGM conditions could be enough to potentially stabilize the ice sheet near its real LGM state. However, the purpose of this work was to capture the ice differences produced only by friction and climatic boundary conditions. Such a simple design allows to compare the impact of purely boundary conditions. Thus, only steady-state simulations were considered. In a transient simulation, the results would additionally include a potential internal drift. Chapter 5 includes LGM steady-state simulations and transient PD states for four different friction laws. For these experiments LGM volumes ranged between 12.9 to 15.6 msle. In comparison with steady-state simulations, transient experiments simulated on average larger volumes. However, these experiments were run with another calving limit value. Transient experiments show a strong sensitivity to the calving limit parameter (H_{calv}). Although PD calving loss in Antarctica is almost as large as basal melting, ice models use simple and potentially inadequate expressions for other time periods and further inspection is needed (Yu et al., 2019).

This work only included uncertainties associated with a Weertman-type linear friction law. Of course there are other types of laws which could have been included, such as a pseudo-plastic power law or a regularized Coulomb law (Aschwanden et al., 2013; Joughin et al., 2019). The obtained results of the transient simulations in Chapter 5 showed similar ice volumes but less extended ice sheets for a power, a regularized-power and a plastic law, particularly in the Ross basin as for the ICE-6G reconstruction. However, rather than investigating the uncer-

tainty associated with different basal friction laws, the work of Chapter 4 was focused on the uncertainty related to bedrock characteristics and more specifically the marine sectors. Of course another friction law would have required a new calibration of tuning parameters. However, for a steady LGM state, changing friction coefficients would have simulated more/less active ice streams. The inclusion of different friction laws is particularly relevant for transient simulations, which may lead to faster retreat due to saturated tills, but this was out of the scope of this study. Only the friction coefficients of the linear law, which were assumed to reflect properties of the bedrock, were investigated.

How does the AIS respond to anthropogenic warming for different friction laws?

This question has been addressed in Chapter 5 by investigating the response of the ice sheet using four friction laws, mainly a linear, a power, a regularized-power and a plastic law, to different RCP scenarios. Simulations were forced towards an equilibrated LGM state and then spun up through a transient deglaciation to PD conditions. An ensemble of several friction parameters were tested and only those that produced realistic PD and LGM states were chosen for future warming scenarios. Through a large ensemble analysis it was possible to investigate the mean response of different friction laws. Results showed that the main driver of future sea-level rise is the RCP warming scenario. This was expected: a warmer climate will enhance basal melting at the base of ice shelves reducing the buttressing effect. Furthermore, as seen in Chapter 4, a warmer climate, through viscosity changes, promotes more ice flow into the ocean, increasing sea-level rise. Of course, more precipitation is also likely occur in a warmer climate, but not enough to maintain the AIS in its present configuration. A linear friction law was shown to simulate less sea-level rise than the other friction laws, because under a loss of the buttressing effect, the inland ice accelerated less. On the other hand, a power friction law, a regularized-power friction law, and a plastic friction law simulated responses in a similar range.

A necessary condition for future-warming-scenario experiments is to have an AIS as close as possible to PD conditions. Ice-sheet models use two types of approach to achieve a realistic PD ice sheet. The first method consists on a spin-up based on its paleo evolution. In this case, the model is forced from an equilibrated LGM state towards the PD through a deglaciation spin up. This approach ensures thermal memory of the ice sheet but generally fails in simulating an accurate geometry and velocity pattern. Of course it would be more accurate to go one step further and force though glacial-interglacial periods. However, as the spin-up time becomes longer, so does the necessary computational time. Consequently, in order to perform an ensemble analysis through a deglaciation spin-up without excessive computational time, a coarse resolution of 32 x 32 km was used. The other method consists on the simulation of an equilibrated PD through the assimilation of satellite data. This approach matches an accurate PD in terms of geometry and velocity but does not preserve the thermal memory, and hence properties of the ice flow. One advantage of this method, in addition to its accurate PD representation, is that it allows for high resolution, which is crucial for a realistic assessment of grounding-line migrations. Future warming scenarios have used this approach due to its simplicity and realistic PD configuration (DeConto and Pollard, 2016; Pattyn et al., 2018; Bulthuis et al., 2019). However, one issue with this tactic is that it requires precise tuning of model variables, such a basal friction coefficients or melting parameterisations, for instance. This optimization represents a particular configuration of the PD AIS which does not necessarily conserve the transient character of the ice sheet. Thus, although it is a valid strategy to simulate a precise PD state, it is arguable whether it is realistic to force this ice sheet under future warming scenarios. All in all this represents a handicap on reliable future Antarctic sea-level contributions (Pattyn and Morlighem, 2020).

A common approach to simulate realistic stable PD states is to infer basal friction coefficients. Basal friction coefficients are deduced through inversion methods by two approaches, either matching precise surface velocities (e.g. Morlighem et al. 2013) or surface elevations (e.g. Pollard and DeConto 2012a). Both strategies have been shown to be applicable to different friction laws accounting even

for the basal temperatures (DeConto and Pollard, 2016; Bulthuis et al., 2019). Whereas the first method ensures continuity on the ice flow but a less precise ice sheet geometry, the second ensures a realistic geometry but potentially poor ice flow connectivity. Nonetheless, this validation is limited for a purely plastic friction law, as a saturated till is independent of the basal velocity. However, as analyzed in Chapter 5, one particular configuration is not enough for a complete analysis considering the uncertainties associated with basal conditions. Furthermore, as pointed out by Pollard and DeConto (2012a), these methods may not be realistic, but represent compensated model errors with badly represented physical processes and unrealistic bed properties. This could yield to accurate PD states for the wrong reasons. Performing a large ensemble analysis over friction coefficients since the LGM to PD conditions ensures that the phase space of realistic configurations is covered and permits analyzing the extreme cases.

Nonetheless, a potential caveat in the results of Chapter 5 is the variation of effective pressure with bed elevation (Leguy et al., 2014). This was done to ensure continuity of basal drag at the grounding line. However, this should apply rather to regions near the coast (e.g. grounding line), where the influence of the ocean is effective, rather than at the interior of the ice sheet, where sea water has no (or less) impact (Tsai et al., 2015). A more sophisticated approach would be to take into account changes due to subglacial hydrology. The presence of basal water has profound implications on the ice flow. Water saturated tills have a lower shear strength and hence ice slides faster. There is ample evidence of the existence of broad areas with basal water present (Wright and Siegert, 2012). Water forms at the base of ice sheets as a consequence of melting from geothermal heat flux, the pressure from the ice column and basal frictional heating. This basal water reduces the effective pressure at the ice bed as it exerts a force at the ice base. Thus, precise models should account for this process. However it is not an easy task to trace this Antarctic drainage system. One necessary condition is to have an accurate map of PD melting rates. Nonetheless, there are few datasets of the geothermal heat-flux maps that encompass the whole AIS. In addition, differences between these maps are large, adding more uncertainty to the potential predictability of subglacial water (Martos et al., 2017). All in all,

subglacial drainage models are beginning to emerge now but their coupling to large continental ice sheets is challenging and precise model calibration is needed (Flowers, 2015).

Due to the lack of a robust hydrology model, different friction laws were employed to simulate different flowing regimes. A linear law represents a friction that scales linearly with basal velocity. Thus, larger velocities also generate more friction. This is representative of ice flowing over a rigid/solid bedrock. A power law is also representative of ice flowing over hard bedrock as basal shear stress increases with basal velocity (Fig. 2.4). However, for high velocity regimes, the exerted basal friction is lower than for a linear case. This intends to capture the effect by which more frictional heat enhances water production at the ice base. In contrast, a plastic law represents a water saturated till. The exerted basal friction is independent of the basal velocity as water lubricates the ice motion. Finally a regularized-power law represents a mixture between a power law and a plastic law. For low velocity regimes it behaves close to a power law but at large regimes, friction saturates due to heat release.

Recently, new satellite data together with laboratory experiments have further elucidated the nature of basal friction of ice sheets. Gillet-Chaulet et al. (2016) inferred through inverse modeling studies the exponent of a Coulomb power friction law. They estimated that this exponent had to be closer to a plastic regime. Similar results were obtained by Zoet and Iverson (2020). Through laboratory experiments they estimated for a regularized-power law that the sliding exponent had to be also close to a plastic regime, as in Gillet-Chaulet et al. (2016). This indicates potentially that a linear friction law may be the least adequate friction law for simulating the AIS, at least on short timescales.

The results of Chapter 5 show that a linear law simulates on average a lower sea-level rise than the rest of the friction laws, despite a WAIS collapse that can occur even earlier. This occurs because velocity perturbations do not penetrate inland as far as for other friction laws. In addition, a linear friction law showed the most uncertain response to future warming scenarios. On the other hand, the rest of the friction laws showed a more constrained response and a similar uncertainty range between them. Also the velocity distribution and inland propagation of the

velocity perturbation was similar but also a wide spread was found in the results. These results show the necessity of including the friction law as a fundamental source of structural uncertainty and that a particular, idealized configuration may be not sufficient to adequately represent the future AIS response to global warming.

Common model limitations

The three studies presented here share some model limitations that should be acknowledged. First, the Yelmo model (as well as GRISLI-UCM) computes the motion of ice by adding the SIA solution (shearing regime) to the fast SSA solution (stretching regime). In order to ensure continuity at the grounding line it is necessary to consider the SSA solution, as the SIA solution does not take into account membrane stresses. The accurate representation of the grounding-line position is a necessary condition for the evolution of marine ice sheets and is especially relevant for simulating its reversibility (e.g. Pattyn et al. 2012; Pattyn and Durand 2013). At the marine boundaries, high spatial resolution is required for representing precise grounding-line motions (below 1 km resolution). Because such a resolution for the whole Antarctic domain is computationally prohibitive, the most sophisticated models use sub-gridding methods (Gladstone et al., 2010). In addition, even with a sub-grid parameterisation, coarse resolution models do not fully capture grounding-line migrations correctly (Seroussi et al., 2014; Gladstone et al., 2017). The most accurate ice-sheet models at continental-scale that have studied future scenarios at a spatial resolution of around 10 km. However, high-resolution simulations also require high-resolution fields, such as bedrock characteristics. Nonetheless, even the most modern maps have low resolution in certain zones (Morlighem et al., 2020). The results in this thesis have rather a low resolution, 40 by 40 km in Chapter 3 and 32 by 32 km in Chapters 4 and 5. For Chapter 4 this is not a major concern as steady state simulations were studied and the transient character of the AIS was neglected. However, the capability of the grounding-line to advance and retreat is relevant for Chapters 3 and 5. To

ensure that the AIS is able to migrate correctly, basal friction is reduced in the grounding-line points to 10% of its default value. With this simple parameterisation, realistic advances and retreats are simulated given the boundary forcing that is applied. In addition, performing a large ensemble analysis that covers the whole phase space of potential friction configurations ensures that results will be more robust and fall inside the range of realness. Thus, while a higher resolution could lead to some differences in local retreat patterns, the main conclusions of these works would remain unchanged.

As described in Chapter 2, surface melt applied to Yelmo is calculated using the PDD model (Reeh, 1989). This method calculates the number of days that temperatures are sufficiently high to melt ice from a normal statistical distribution around a mean. This method is commonly used in ice models in the Antarctic domain, because ablation at these latitudes is almost negligible (Winkelmann et al., 2011; Pollard and DeConto, 2012b; Pattyn, 2017). For regions where surface melt has a major influence, such as Greenland, there are more sophisticated methods, as the ITM (Robinson et al., 2011). However, surface melt has a strong influence on driving ice-shelf collapse, as evidenced by the Larsen B and C collapses. Surface melt over ice shelves enhances the hydrofracturing of crevasses (Scambos et al., 2000; MacAYEAL et al., 2003; van den Broeke, 2005; McGrath et al., 2012; Bevan et al., 2017) and also induces "hydrostatic rebound" when meltwater lakes drain (MacAyeal and Sergienko, 2013). This can ultimately lead to the MICI mechanism, where grounded ice cliffs may rapidly collapse after ice shelf breakup (DeConto and Pollard, 2016). However, how such processes are implemented in ice-sheet models, through calving laws and supralakes formation, remains one of the biggest challenges in the glaciological community (Yu et al., 2019; Pattyn and Morlighem, 2020). As shown in Sun et al. (2020), the removal of ice shelves has a strong influence on the AIS, and assessing the ice shelf stability is crucial for future predictions.

An LGM state was simulated in all three studies. To do so no basal melting is applied, allowing for a maximum ice extension as suggested by geological constraints (Briggs et al., 2014). This assumption is a vast simplification of reality. As shown by Kusahara et al. (2015) ice shelves that crossed, or are close to the

continental-shelf break, were most likely exposed to more basal melt at the LGM than nowadays. This high melt rates were caused due to oceanic stratification. The high salinity content of the LGM enhances the production of warmer CDW, which in turn could be transported into the ice shelf cavities. However, because the AIS is fully advanced, these warm waters apply to overhung ice shelves at the continental-shelf break and would not necessarily produce the same melting for constrained ice shelves inside the continental shelf. In addition, as the salinity changes, so does the heat-flux coefficient. Thus, in order to apply realistic LGM melting rates it is necessary to account for a more accurate basal-melting parameterisation. As this was out of the scope of this work, no melting was allowed at the LGM.

For a precise evaluation of past and future sea-level contributions of ice sheets, correct assessment of ice-ocean interactions is needed. However, the ocean is a complex system composed mainly of dense shelf waters, warm circumpolar deep waters and colder Antarctic surface waters together with its natural currents (Dinniman et al. 2016; Holland et al. 2020 and references therein). Also, when the ice melts, turbulent buoyant plumes are formed at the ice-ocean interface which are propagated from the grounding line towards the ice front (Jenkins, 2011). Because accounting for all these processes is a complicated task for ice-sheet models, the choice of basal-melting law is somewhat arbitrary. Several laws have been proposed and all succeed in simulating a realistic PD state with accurate parameter tuning (Seroussi et al., 2019, 2020).

A linear law is a common approach in ice models (Philippon et al., 2006; Martin et al., 2011; Alvarez-Solas et al., 2013; Golledge et al., 2015; Levermann et al., 2020), however other studies use a quadratic approach (Holland et al., 2008; Pattyn, 2017; Pollard and DeConto, 2012b). Pollard and DeConto (2012b) went a step forward and included a scaling factor to account for changes in the oceanic currents depending on the embayment shape. Nowadays even more sophisticated models are available which include box models of the ocean and/or a buoyant plume melt rate parameterisation (Lazeroms et al., 2018; Reese et al., 2018; Pelle et al., 2019). Because the past oceanic temperature and salinity is not clearly defined, it is convenient to use a parameterisation more suitable for paleo

studies. The employed melting parameterisation in this thesis allows for a rapid and easy way to investigate the impact of oceanic temperature changes and a first-order study of future contributions.

Chapter 7
Conclusions

In this thesis the sensitivity and uncertainty of the AIS to climatologies and basal friction was investigated from a modelling point of view using simulations of the past and future. These represent two main building blocks of ice models, namely boundary conditions and ice dynamics. Little is known about past and future oceanic conditions due to the lack of marine data in the SO. In addition, the representation of accurate ice dynamics through basal conditions represents a major challenge as it is difficult to infer from satellite data, and likely transient in nature. This thesis represents an important step towards deeper understanding of these topics. The work presented here is divided into three different sensitivity studies seeking for realism.

In the first study, described in Chapter 3, the sensitivity of the AIS to rapid climatic millennial variability during the LGP was investigated. More concretely, this work highlighted the potential leading role of the SO during glacial periods. Through the bipolar seesaw mechanism it is suggested that the SO acted as a heat reservoir during slow AMOCs (i.e. glacial periods) by warming up, as recorded by Antarctic ice core records. During cold epochs, the AIS is in its major part marine based as it advanced up to the continental-shelf edge. Thus, a warmer ocean has the potential to drive a response of the AIS. The obtained results showed that if no ice-ocean interaction were taken into account, hence only atmospheric millennial variability, then no substantial ice discharges nor grounding-line retreat

occurred. This was expected and in agreement with the general assumption that the AIS does not respond to glacial millennial scale variability. However, once the ocean was taken into account, ice-volume changes as well as grounding-line migrations occurred. The response of the AIS to oceanic warming increased with increasing oceanic sensitivity. Moreover, this study highlights that the AIS has the potential to contribute up to 6 m of SLR during MIS-3 which is equivalent to 25% of the measured millennial sea-level fluctuation for the involved time period. The measured grounding-line migrations have a significant role as the AIS has been classically considered a slow-reacting ice sheet that responds to orbital timescales rather than abrupt climate changes. In addition, the simulated grounding-line migrations open a path for a potential mechanism that triggers stadial/glacial to interstadial/interglacial transitions through the stratification of deep ocean waters due to brine rejection. This work is the first that studied the response of the AIS to glacial millennial-scale variability and its potential implications for the climate system.

The second work of this thesis, described in Chapter 4, aimed to investigate the impact of the boundary conditions on the simulation of the AIS during the LGM. More specifically, the uncertainty of bedrock friction and climatologies were assessed. First, a set of potential basal friction values of marine zones were tested which simulated realistic LGM states. Larger friction values simulated less dynamically active ice sheets, i.e. slower ice streams, and hence larger ice volumes. On the other hand, faster ice sheets resulted in lower ice volumes. Nonetheless, almost fully extended ice sheets were simulated in all cases. In brief, the simulated sea-level ranged from 9.1-15.5 msle and the ice extension almost 16 million km^2. Hence, the friction choice implied a difference of about 6 msle. Then, to investigate the effect of the climate boundary conditions, the individual sea-level contribution of the eleven PMIP3 participating groups for a particular friction reference state was tested. The simulated ice volumes ranged from 9.1-13.1 msle and an extension of 14.8-15.9 million km^2. The anomaly between the atmospheric models was of the same magnitude as to the friction coefficients. The LGM extension showed strong dependency on the atmospheric temperatures. Higher tem-

peratures allowed the ice sheet to flow faster, as a consequence of a lower viscosity (a larger fluidity), and thin the ice. This prevented the ice sheet from advancing because of the marine character of the AIS and the warm temperatures near the coast, especially during the LGM. For equally advanced ice sheets, up to the continental-shelf break, sea-level content of about 3 msle could be accounted for by accumulation differences among models. If the model was forced through a spatially homogeneous method, systematically lower extensions and ice volumes were simulated as a consequence of less accumulation in coastal regions. This work is the first that studied the AIS contribution with a model forced by the PMIP3 ensemble. It demonstrated that the choice of climatologies are as important as the choice of basal conditions and further constraining is needed to reduce uncertainty in the AIS volume estimates for the LGM.

The third work, described in Chapter 5 investigated the role of different friction laws in the past and future evolution of the AIS. Through a sensitivity study, from a large ensemble analysis, different friction configurations were tested over the LGM to future RCP scenarios. First, a transient spin-up from glacial LGM to PD conditions with different friction parameters was performed. This spin-up procedure intended to improve the methodology used by other studies, based on steady PD states. Then, only those that matched realistic LGM and PD conditions were chosen for future warming scenarios. The main conclusion was that future Antarctic projections are primarily driven by the RCP scenario. Higher emission scenarios increase the total sea-level rise and accelerate a WAIS collapse through the MISI mechanism. This was expected, as a warmer ocean leads to smaller ice shelves and, consequently, inland ice accelerates due to the loss of the buttressing effect. Nonetheless, the choice of friction law plays an important role in determining how much inland ice accelerates. Ice streams were found to accelerate less if a linear friction law was chosen. On the other hand, a power, a regularized-power, and a plastic friction law, showed larger ice velocity anomalies which penetrated deeper inland, provoking major ice discharges. This was found to be more clearly visible on shorter timescales (i.e. hundreds of years). On longer timescales (i.e. thousands of years), with a committed warming, the AIS config-

urations tended to converge. These results highlight the need for replacing single friction-law estimates by ensembles including the friction law as a fundamental source of structural uncertainty.

To conclude, basal friction and basal melting parameterisations are some of the most important, and yet unknown, building blocks in defining the evolution of the AIS. Although in the last years there has been great progress, through new assimilation of satellite data (Depoorter et al., 2013; Liu et al., 2015; Morlighem et al., 2020), the understanding and parameterisation of physical processes (Reese et al., 2018; Zoet and Iverson, 2020) and formation of large inter-comparison groups (Pattyn et al., 2012; Seroussi et al., 2019, 2020; Levermann et al., 2020), there are still open questions that need to be addressed. This occurs partly because these processes require high resolution, expensive computational cost, and are compounded into complex physical systems. Models will always be simplifications of reality and are not perfect representations. Nonetheless, they help to understand physical mechanisms that occur in nature. This thesis has shed light on the role of basal friction, boundary conditions and ice-ocean interactions in the past, present and future evolution of the AIS.

List of publications and conference contributions related to this thesis

Scientific publications as first author

- Blasco, J., Tabone, I., Alvarez-Solas, J., Robinson, A., and Montoya, M., 2019: The Antarctic Ice Sheet response to glacial millennial scale variability. *Climate of the Past*, **15**, 121-133. DOI 10.5194/cp-15-121-2019.

- Blasco, J., Alvarez-Solas, J., Robinson, A., and Montoya, M., 2019: Exploring the impact of atmospheric forcing and basal boundary conditions on the simulation of the Antarctic ice sheet at the Last Glacial Maximum. *The Cryosphere Discussion*. DOI 10.5194/tc-2020-28.

- Blasco, J., Robinson, A., Alvarez-Solas, J., Tabone, I., and Montoya, M., 2020: The Antarctic sea-level contribution from the LGM to the future for different basal-dragging laws. *Communications Earth & Environment*. Submitted.

Contribution in other scientific publications

- Tabone, I., Blasco, J., Robinson, A., Alvarez-Solas, J. and Montoya, M., 2018: The sensitivity of the Greenland Ice Sheet to glacial-interglacial oceanic forcing. *Climate of the Past*, **14**, 455-472. DOI 10.5194/cp-14-455-2018.

Oral contributions - Conferences

- Blasco, J., Alvarez-Solas, J., Robinson, A. and Montoya, M., 2016: Ocean sensitivity of the Antarctic Ice Sheet. XI congress TOPCART 2016, Toledo (Spain), 27 september 2016. This contribution has been published in: Especial TOPCART 2016, XI Congreso de Geomática y Ciencias de la Tierra - Criosfera y Cambio Climático, Vol. XXXII, num. 170, 2016, ISSN: 1212-9280.

- Blasco, J., Alvarez-Solas, J., Robinson, A. and Montoya, M., 2017: Modelling the Antarctic Ice Sheet for the last 420kyr. *Geophysical Research Abstracts*, **19**, EGU2017-822, 2017. Contribution presented at EGU General Assembly, Vienna (Austria), 23-28 April 2017.

- Blasco, J., Alvarez-Solas, J., Robinson, A. and Montoya, M., 2017: Antarctic Ice Sheet sensitivity to oceanic temperature changes., *PAGES Abstract Book*, 2017. Contribution presented at PAGES - 5^{th} Open Science Meeting on Global Challenges for our Common Future: a paleoscience perspective, Zaragoza (Spain), 9-13 May 2017.

- Blasco, J., Tabone, I., Alvarez-Solas, J., Robinson, A. and Montoya, M., 2018: The effect of millennial scale glacial climate variability on the Antarctic Ice Sheet. *Geophysical Research Abstracts*, **20**, EGU2018-16562, 2018. Contribution presented at EGU General Assembly, Vienna (Austria), 8-13 April 2018.

- Blasco, J., Tabone, I., Moreno, D., Alvarez-Solas, J., Robinson, A. and Montoya, M., 2020: The uncertainty in Antarctic sea-level rise projections due to ice dynamics. *Geophysical Research Abstracts*, EGU2020-14352, 2020. Contribution presented at EGU General Assembly, Vienna (Austria), 4-8 May 2020.

Poster contributions - Conferences and Schools

- Blasco, J., Tabone, I., Alvarez-Solas, J., Robinson, A. and Montoya, M., 2018: The response of the Antarctic Ice Sheet to millennial-scale glacial variability, presented at the 17^{th} International Swiss Climate Summer School - Earth system variability through time, Grindelwald (Switzerland), 26-31 August 2018.

- Blasco, J., Tabone, I., Alvarez-Solas, J., Robinson, A. and Montoya, M., 2019: Exploring the impact of uncertainty in ice dynamics and climatic forcing on the simulation of Antarctica during the Last Glacial Period. *Geophysical Research Abstracts*, **21**, EGU2019-12359, 2019. Contribution presented at EGU General Assembly, Vienna (Austria), 7-12 April 2019.

Other oral and poster contributions

- Blasco, J., Tabone, I., Alvarez-Solas, J., Robinson, A. and Montoya, M., 2017: Modeling the past and future evolution of the Antarctic Ice Sheet. *Poster contribution*, PhDay Físicas 2017, Madrid (Spain), 15-20 December 2017.

- Blasco, J., 2018: The evolution of the Antarctic Ice Sheet during abrupt glacial climate changes. *Oral contribution*, I Jornada Jóvenes Investigadores en Ciencias de la Tierra, IGEO, Madrid (Spain), 10 May 2018.

- Blasco, J., 2018: The evolution of the Antarctic Ice Sheet during abrupt glacial climate changes. *Oral contribution*, Jornadas de doctorandos de la UCM, Madrid (Spain), 13-16 March 2018.

References

Abe-Ouchi, A., F. Saito, M. Kageyama, P. Braconnot, S. P. Harrison, K. Lambeck, B. L. Otto-Bliesner, W. Peltier, L. Tarasov, J.-Y. Peterschmitt, and K. Takahashi, 2015: Ice-sheet configuration in the cmip5/pmip3 last glacial maximum experiments. *GMD*, **8**, 3621–3637, doi:10.5194/gmd-8-3621-2015.

Albrecht, T., R. Winkelmann, and A. Levermann, 2019: Glacial cycles simulation of the Antarctic Ice Sheet with PISM – Part 1: Boundary conditions and climatic forcing (in review). *The Cryosphere Discussion*, doi:10.5194/tc-2019-71.

Alevropoulos-Borrill, A. V., I. J. Nias, A. J. Payne, N. R. Golledge, and R. J. Bingham, 2020: Ocean-forced evolution of the Amundsen Sea catchment, West Antarctica, by 2100. *The Cryosphere*, **14**, 1245–1258, doi:10.5194/tc-14-1245-2020.

Allen, J. R., U. Brandt, A. Brauer, H.-W. Hubberten, B. Huntley, J. Keller, M. Kraml, A. Mackensen, J. Mingram, J. F. Negendank, et al., 1999: Rapid environmental changes in southern europe during the last glacial period. *Nature*, **400**, 740, doi:10.1038/23432.

Alley, R. B., S. Anandakrishnan, and a. P. Jung, 2001: Stochastic resonance in the north atlantic. *Paleoceanography*, **16**, 190–198, doi:10.1029/2000PA000518.

Alvarez-Solas, J., R. Banderas, A. Robinson, and M. Montoya, 2019: Ocean-driven millennial-scale variability of the eurasian ice sheet during the last glacial period simulated with a hybrid ice-sheet-shelf model. *Climate of the Past*, **15**, 957–979, doi:10.5194/cp-15-957-2019.

Alvarez-Solas, J., A. Robinson, M. Montoya, and C. Ritz, 2013: Iceberg discharges of the last glacial period driven by oceanic circulation changes. *Proceedings of the National Academy of Sciences*, **110**, 16350–16354, doi:10.1073/pnas.1306622110.

Anderson, J. B., H. Conway, P. J. Bart, A. E. Witus, S. L. Greenwood, R. M. McKay, B. L. Hall, R. P. Ackert, K. Licht, M. Jakobsson, and J. Stone, 2014: Ross Sea paleo-ice sheet drainage and deglacial history during and since the LGM. *Quaternary Science Reviews*, **100**, 31–54, doi:10.1016/j.quascirev.2013.08.020.

Anderson, J. B., S. S. Shipp, A. L. Lowe, J. S. Wellner, and A. B. Mosola, 2002: The Antarctic Ice Sheet during the Last Glacial Maximum and its subsequent retreat history: a review. *Quaternary Science Reviews*, **21**, 49–70, doi:10.1016/S0277-3791(01)00083-X.

Andrews, J. T. and A. H. Voelker, 2018: "heinrich events"(& sediments): A history of terminology and recommendations for future usage. *Quaternary Science Reviews*, **187**, 31–40, doi:10.1016/j.quascirev.2018.03.017.

Argus, D., W. Peltier, R. Drummond, and A. Moore, 2014a: The Antarctica component of postglacial rebound model ICE-6G_C (VM5a) based on GPS positioning, exposure age dating of ice thicknesses, and relative sea level histories. *Geophys. J. Int.*, **198**, 537–563, doi:10.1093/gji/ggu140.

Argus, D. F., W. Peltier, R. Drummond, and A. W. Moore, 2014b: The Antarctica component of postglacial rebound model ICE-6G_C (VM5a) based on GPS positioning, exposure age dating of ice thicknesses, and relative sea level histories. *Geophysical Journal International*, **198**, 537–563, doi:10.1093/gji/ggu140.

Arz, H. W., F. Lamy, A. Ganopolski, N. Nowaczyk, and J. Pätzold, 2007: Dominant northern hemisphere climate control over millennial-scale glacial sea-level variability. *Quaternary Science Reviews*, **26**, 312–321, doi:10.1016/j.quascirev.2006.07.016.

Aschwanden, A., G. Adalgeirsdóttir, and C. Khroulev, 2013: Hindcasting to measure ice sheet model sensitivity to initial states. *The Cryosphere*, **7**, doi:10.5194/tc-7-1083-2013.

Asmerom, Y., V. J. Polyak, and S. J. Burns, 2010: Variable winter moisture in the southwestern united states linked to rapid glacial climate shifts. *Nature Geoscience*, **3**, 114, doi:10.1038/ngeo754.

Austermann, J., J. X. Mitrovica, K. Latychev, and G. A. Milne, 2013: Barbados-based estimate of ice volume at last glacial maximum affected by subducted plate. *Nature Geoscience*, **6**, 553, doi:10.1038/ngeo1859.

Bakker, A. M., D. Louchard, and K. Keller, 2017a: Sources and implications of deep uncertainties surrounding sea-level projections. *Climatic change*, **140**, 339–347, doi:10.1007/s10584-016-1864-1.

Bakker, A. M., T. E. Wong, K. L. Ruckert, and K. Keller, 2017b: Sea-level projections representing the deeply uncertain contribution of the West Antarctic ice sheet. *Scientific reports*, **7**, 3880, doi:10.1038/s41598-017-04134-5.

Bakker, P., V. Masson-Delmotte, B. Martrat, S. Charbit, H. Renssen, M. Gröger, U. Krebs-Kanzow, G. Lohmann, D. J. Lunt, M. Pfeiffer, et al., 2014: Temperature trends during the Present and Last Interglacial periods–a multi-model-data comparison. *Quaternary Science Reviews*, **99**, 224–243, doi:10.1016/j.quascirev.2014.06.031.

Bamber, J. L., R. E. Riva, B. L. Vermeersen, and A. M. LeBrocq, 2009: Reassessment of the potential sea-level rise from a collapse of the west antarctic ice sheet. *Science*, **324**, 901–903, doi:10.1126/science.1169335.

Banderas, R., J. Alvarez-Solas, and M. Montoya, 2012: Role of co 2 and southern ocean winds in glacial abrupt climate change. *Climate of the Past*, **8**, 1011–1021, doi:10.5194/cp-8-1011-2012.

Banderas, R., J. Alvarez-Solas, A. Robinson, and M. Montoya, 2015: An interhemispheric mechanism for glacial abrupt climate change. *Climate Dynamics*, **44**, 2897–2908, doi:10.1007/s00382-014-2211-8.

— 2018: A new approach for simulating the paleo-evolution of the Northern Hemisphere ice sheets. *Geoscientific Model Development*, **11**, 2299–2314, doi:10.5194/gmd-11-2299-2018.

Barker, P. and J. Burrell, 1977: The opening of drake passage. *Marine geology*, **25**, 15–34, doi:10.1016/0025-3227(77)90045-7.

Barker, S., J. Chen, X. Gong, L. Jonkers, G. Knorr, and D. Thornalley, 2015: Icebergs not the trigger for north atlantic cold events. *Nature*, **520**, 333, doi:10.1038/nature14330.

Bassett, S., G. Milne, M. Bentley, and P. Huybrechts, 2007: Modelling Antarctic sea-level data to explore the possibility of a dominant Antarctic contribution to meltwater pulse IA. *Quaternary Science Reviews*, **26**, 2113–2127, doi:10.1016/j.quascirev.2007.06.011.

Bassis, J. N., S. V. Petersen, and L. Mac Cathles, 2017: Heinrich events triggered by ocean forcing and modulated by isostatic adjustment. *Nature*, **542**, 332–334, doi:10.1038/nature21069.

Beckmann, A. and H. Goosse, 2003: A parameterization of ice shelf–ocean interaction for climate models. *Ocean modelling*, **5**, 157–170, doi:10.1016/S1463-5003(02)00019-7.

Benson, L. V., J. W. Burdett, M. Kashgarian, S. P. Lund, F. M. Phillips, and R. O. Rye, 1996: Climatic and hydrologic oscillations in the owens lake basin and adjacent sierra nevada, california. *Science*, **274**, 746–749, doi:10.1126/science.274.5288.746.

Bevan, S., A. Luckman, B. Hubbard, B. Kulessa, D. Ashmore, P. Kuipers Munneke, M. O'Leary, A. Booth, H. Sevestre, and D. McGrath, 2017: Centuries of intense melt on Larsen C Ice Shelf. *The Cryosphere*, **11**, 2743–2753, doi:10.5194/tc-11-2743-2017.

Bindoff, N., P. Stott, K. AchutaRao, M. Allen, N. Gillett, D. Gutzler, K. Hansingo, G. Hegerl, Y. Hu, S. Jain, I. Mokhov, J. Overland, J. Perlwitz, R. Sebbari, and X. Zhang, 2013: Detection and Attribution of Climate Change: from Global to Regional. In: Climate Change 2013: The Physical Science Basis. Contribution of Working Group I to the Fifth Assessment Report of the Intergovernmental Panel on Climate Change [Stocker, T.F., D. Qin, G.-K. Plattner, M. Tignor, S.K. Allen, J. Boschung, A. Nauels, Y. Xia, V. Bex and P.M. Midgley (eds.)]. *Cambridge University Press, Cambridge, United Kingdom and New York, NY, USA*.

Blunier, T. and E. J. Brook, 2001: Timing of millennial-scale climate change in antarctica and greenland during the last glacial period. *Science*, **291**, 109–112,

doi:10.1126/science.291.5501.109.

Boers, N., M. Ghil, and D.-D. Rousseau, 2018: Ocean circulation, ice shelf, and sea ice interactions explain Dansgaard-Oeschger cycles. *Proceedings of the National Academy of Sciences*, **115**, E11005–E11014, doi:10.1073/pnas.1802573115.

Böhm, E., J. Lippold, M. Gutjahr, M. Frank, P. Blaser, B. Antz, J. Fohlmeister, N. Frank, M. Andersen, and M. Deininger, 2015: Strong and deep atlantic meridional overturning circulation during the last glacial cycle. *Nature*, **517**, 73, doi:10.1038/nature14059.

Bond, G., W. Broecker, S. Johnsen, J. McManus, L. Labeyrie, J. Jouzel, and G. Bonani, 1993: Correlations between climate records from north atlantic sediments and greenland ice. *Nature*, **365**, 143, doi:10.1038/365143a0.

Bond, G., H. Heinrich, W. Broecker, L. Labeyrie, J. McManus, J. Andrews, S. Huon, R. Jantschik, S. Clasen, C. Simet, et al., 1992: Evidence for massive discharges of icebergs into the north atlantic ocean during the last glacial period. *Nature*, **360**, 245, doi:10.1038/360245a0.

Bradley, R., 1985: *Quaternary paleoclimatology*. Allen & Unwin Boston.

Braun, H., M. Christl, S. Rahmstorf, A. Ganopolski, A. Mangini, C. Kubatzki, K. Roth, and B. Kromer, 2005: Possible solar origin of the 1,470-year glacial climate cycle demonstrated in a coupled model. *Nature*, **438**, 208, doi:10.1038/nature04121.

Briggs, R., D. Pollard, and L. Tarasov, 2013: A glacial systems model configured for large ensemble analysis of Antarctic deglaciation. *The Cryosphere*, **7**, 1949–1970, doi:10.5194/tc-7-1949-2013.

Briggs, R. D., D. Pollard, and L. Tarasov, 2014: A data-constrained large ensemble analysis of Antarctic evolution since the Eemian. *Quaternary Science Reviews*, **103**, 91–115, doi:10.1016/j.quascirev.2014.09.003.

Broecker, W. S., D. M. Peteet, and D. Rind, 1985: Does the ocean-atmosphere system have more than one stable mode of operation? *Nature*, **315**, 21, doi:10.1038/315021a0.

Brondex, J., O. Gagliardini, F. Gillet-Chaulet, and G. Durand, 2017: Sensitivity of grounding line dynamics to the choice of the friction law. *Journal of Glaciology*, **63**, 854–866, doi:10.1017/jog.2017.51.

Budd, W., D. Jenssen, and I. Smith, 1984: A three-dimensional time-dependent model of the west antarctic ice sheet. *Annals of Glaciology*, **5**, 29–36, doi:10.3189/1984AoG5-1-29-36.

Budd, W. and I. Smith, 1982: Large-scale numerical modelling of the antarctic ice sheet. *Annals of Glaciology*, **3**, 42–49, doi:10.3189/S0260305500002500.

Bulthuis, K., M. Arnst, S. Sun, and F. Pattyn, 2019: Uncertainty quantification of the multi-centennial response of the Antarctic ice sheet to climate change. *The Cryosphere*, **13**, 1349–1380, doi:10.5194/tc-13-1349-2019.

Cacho, I., J. O. Grimalt, C. Pelejero, M. Canals, F. J. Sierro, J. A. Flores, and N. Shackleton, 1999: Dansgaard-oeschger and heinrich event imprints in alboran sea paleotemperatures. *Paleoceanography*, **14**, 698–705, doi:10.1029/1999PA900044.

Capron, E., A. Govin, E. J. Stone, V. Masson-Delmotte, S. Mulitza, B. Otto-Bliesner, T. L. Rasmussen, L. C. Sime, C. Waelbroeck, and E. W. Wolff, 2014: Temporal and spatial structure of multi-millennial temperature changes at high latitudes during the last interglacial. *Quaternary Science Reviews*, **103**, 116–133, doi:10.1016/j.quascirev.2014.08.018.

Cauquoin, A., A. Landais, G. Raisbeck, J. Jouzel, L. Bazin, M. Kageyama, J.-Y. Peterschmitt, M. Werner, E. Bard, and ASTER Team, 2015: Comparing past accumulation rate reconstructions in East Antarctic ice cores using 10Be, water isotopes and CMIP5-PMIP3 models. *Climate of the Past*, **11**, 355–367, doi:10.5194/cp-11-355-2015.

Clark, P. U., D. Archer, D. Pollard, J. D. Blum, J. A. Rial, V. Brovkin, A. C. Mix, N. G. Pisias, and M. Roy, 2006: The middle pleistocene transition: characteristics, mechanisms, and implications for long-term changes in atmospheric pco2. *Quaternary Science Reviews*, **25**, 3150–3184, doi:10.1016/j.quascirev.2006.07.008.

Clark, P. U., A. M. McCabe, A. C. Mix, and A. J. Weaver, 2004: Rapid rise of sea level 19,000 years ago and its global implications. *Science*, **304**, 1141–1144, doi:10.1126/science.1094449.

Clark, P. U. and A. C. Mix, 2002: Ice sheets and sea level of the last glacial maximum. *Quaternary Science Reviews*, **21**, 1–7, doi:10.1016/S0277-3791(01)00118-

4.

Clark, P. U., N. G. Pisias, T. F. Stocker, and A. J. Weaver, 2002: The role of the thermohaline circulation in abrupt climate change. *Nature*, **415**, 863, doi:10.1038/415863a.

Clark, P. U. and L. Tarasov, 2014: Closing the sea level budget at the last glacial maximum. *Proceedings of the National Academy of Sciences*, **111**, 15861–15862, doi:10.1073/pnas.1418970111.

Clerc, F., B. M. Minchew, and M. D. Behn, 2019: Marine Ice Cliff Instability Mitigated by Slow Removal of Ice Shelves. *Geophysical Research Letters*, doi:10.1029/2019GL084183.

Collins, M., R. Knutti, J. M. Arblaster, J. L. Dufresne, T. Fichefet, P. Friedlingstein, X. Gao, W. J. Gutowski, T. Johns, G. Krinner, M. Shongwe, C. Tebaldi, A. J. Weaver, and M. Wehner, 2013: Climate Change 2013: The Physical Science Basis. Contribution of Working Group I to the Fifth Assessment Report of the Intergovernmental Panel on Climate Change (eds Stocker, T., Qin, D., Plattner, G., Tignor, M. M. B., Allen, S. K., Boschung, J., Nauels, A., Xia, Y., Bex, V., Midgley, P. M.). *Cambridge Univ. Press*, 1029–1136.

Cornford, S. L., D. F. Martin, D. T. Graves, D. F. Ranken, A. M. Le Brocq, R. M. Gladstone, A. J. Payne, E. G. Ng, and W. H. Lipscomb, 2013: Adaptive mesh, finite volume modeling of marine ice sheets. *Journal of Computational Physics*, **232**, 529–549, doi:10.1016/j.jcp.2012.08.037.

Cornford, S. L., D. F. Martin, A. J. Payne, E. G. Ng, A. M. Le Brocq, R. M. Gladstone, T. L. Edwards, S. R. Shannon, C. Agosta, M. R. van den Broeke, H. H. Hellmer, G. Krinner, S. R. M. Ligtenberg, R. Timmermann, and D. G. Vaughan, 2015: Century-scale simulations of the response of the West Antarctic Ice Sheet to a warming climate. *The Cryosphere*, **9**, 1579–1600, doi:10.5194/tc-9-1579-2015.

Coxall, H. K., P. A. Wilson, H. Pälike, C. H. Lear, and J. Backman, 2005: Rapid stepwise onset of antarctic glaciation and deeper calcite compensation in the pacific ocean. *Nature*, **433**, 53, doi:10.1038/nature03135.

Crowley, T. and G. North, 1991: Paleoclimatology.

Crowley, T. J., 1992: North Atlantic deep water cools the Southern Hemisphere. *Paleoceanography*, **7**, 489–497, doi:10.1029/92PA01058.

Cuffey, K. M. and W. Paterson, 2010: *The physics of glaciers*. Academic Press.

Dansgaard, W. and S. Johnsen, 1969: A flow model and a time scale for the ice core from Camp Century, Greenland. *Journal of Glaciology*, **8**, 215–223, doi:10.3189/S0022143000031208.

Dansgaard, W., S. Johnsen, H. Clausen, D. Dahl-Jensen, N. Gundestrup, C. Hammer, and H. Oeschger, 1984: North Atlantic climatic oscillations revealed by deep Greenland ice cores. *Climate processes and climate sensitivity*, **29**, 288–298, doi:10.1029/GM029p0288.

De Boer, B., L. J. Lourens, and R. S. Van De Wal, 2014: Persistent 400,000-year variability of Antarctic ice volume and the carbon cycle is revealed throughout the Plio-Pleistocene. *Nature Communications*, **5**, 2999, doi:10.1038/ncomms3999.

DeConto, R. M. and D. Pollard, 2003: Rapid Cenozoic glaciation of Antarctica induced by declining atmospheric CO 2. *Nature*, **421**, 245, doi:10.1038/nature01290.

— 2016: Contribution of Antarctica to past and future sea-level rise. *Nature*, **531**, 591, doi:10.1038/nature17145.

Dee, D. P., S. M. Uppala, A. J. Simmons, P. Berrisford, P. Poli, S. Kobayashi, U. Andrae, M. A. Balmaseda, G. Balsamo, P. Bauer, P. Bechtold, A. C. M. Beljaars, L. van de Berg, J. Bidlot, N. Bormann, C. Delsol, R. Dragani, M. Fuentes, A. J. Geer, L. Haimberger, S. B. Healy, H. Hersbach, E. V. Hólm, L. Isaksen, P. Kållberg, M. Köhler, M. Matricardi, A. P. McNally, B. M. Monge-Sanz, J.-J. Morcrette, B.-K. Park, C. Peubey, P. de Rosnay, C. Tavolato, J.-N. Thépaut, and F. Vitart, 2011: The ERA-Interim reanalysis: Configuration and performance of the data assimilation system. *Quarterly Journal of the royal meteorological society*, **137**, 553–597, doi:10.1002/qj.828.

Defrance, D., G. Ramstein, S. Charbit, M. Vrac, A. M. Famien, B. Sultan, D. Swingedouw, C. Dumas, F. Gemenne, J. Alvarez-Solas, and J.-P. Vanderlinden, 2017: Consequences of rapid ice sheet melting on the Sahelian population vulnerability. *Proceedings of the National Academy of Sciences*, **114**, 6533–

6538, doi:10.1073/pnas.1619358114.

Denton, G. H. and T. J. Hughes, 2002: Reconstructing the Antarctic ice sheet at the Last Glacial Maximum. *Quaternary Science Reviews*, **21**, 193–202, doi:10.1016/S0277-3791(01)00090-7.

Depoorter, M. A., J. Bamber, J. Griggs, J. T. Lenaerts, S. R. Ligtenberg, M. R. van den Broeke, and G. Moholdt, 2013: Calving fluxes and basal melt rates of Antarctic ice shelves. *Nature*, **502**, 89, doi:10.1038/nature12567.

Dinniman, M. S., X. S. Asay-Davis, B. K. Galton-Fenzi, P. R. Holland, A. Jenkins, and R. Timmermann, 2016: Modeling ice shelf/ocean interaction in Antarctica: A review. *Oceanography*, **29**, 144–153, doi:10.5670/oceanog.2016.106.

Dokken, T. M., K. H. Nisancioglu, C. Li, D. S. Battisti, and C. Kissel, 2013: Dansgaard-oeschger cycles: Interactions between ocean and sea ice intrinsic to the nordic seas. *Paleoceanography*, **28**, 491–502, doi:10.1002/palo.20042.

Dutrieux, P., D. G. Vaughan, H. F. Corr, A. Jenkins, P. R. Holland, I. Joughin, and A. Fleming, 2013: Pine Island glacier ice shelf melt distributed at kilometre scales. *The Cryosphere*, **7**, 1543–1555, doi:10.5194/tc-7-1543-2013.

Dutton, A., A. Carlson, A. Long, G. Milne, P. Clark, R. DeConto, B. Horton, S. Rahmstorf, and M. Raymo, 2015: Sea-level rise due to polar ice-sheet mass loss during past warm periods. *Science*, **349**, aaa4019, doi:10.1126/science.aaa4019.

Dutton, A. and K. Lambeck, 2012: Ice volume and sea level during the last interglacial. *Science*, **337**, 216–219, doi:10.1126/science.1205749.

Edwards, T. L., M. A. Brandon, G. Durand, N. R. Edwards, N. R. Golledge, P. B. Holden, I. J. Nias, A. J. Payne, C. Ritz, and A. Wernecke, 2019: Revisiting Antarctic ice loss due to marine ice-cliff instability. *Nature*, **566**, 58, doi:10.1038/s41586-019-0901-4.

EPICA Community Members, 2004: Eight glacial cycles from an antarctic ice core. *Nature*, **429**, 623–628, doi:10.1038/nature02599.

EPICA, Community Members, 2006: One-to-one coupling of glacial climate variability in greenland and antarctica. *Nature*, **444**, 195, doi:10.1038/nature05301.

Erhardt, T., E. Capron, S. O. Rasmussen, S. Schupach, M. Bigler, F. Adolphi, and H. Fischer, 2019: Decadal-scale progression of dansgaard-oeschger warming

events. *Climate of the Past*, **15**, 811–825, doi:10.5194/cp-15-811-2019.

Fairbanks, R. G., 1989: A 17,000-year glacio-eustatic sea level record: influence of glacial melting rates on the younger dryas event and deep-ocean circulation. *Nature*, **342**, 637.

Favier, L., G. Durand, S. L. Cornford, G. H. Gudmundsson, O. Gagliardini, F. Gillet-Chaulet, T. Zwinger, A. Payne, and A. M. Le Brocq, 2014: Retreat of Pine Island Glacier controlled by marine ice-sheet instability. *Nature Climate Change*, **4**, 117, doi:10.1038/nclimate2094.

Feldmann, J. and A. Levermann, 2015: Collapse of the West Antarctic Ice Sheet after local destabilization of the Amundsen Basin. *Proceedings of the National Academy of Sciences*, **112**, 14191–14196, doi:10.1073/pnas.1512482112.

Feldmann, J., A. Levermann, and M. Mengel, 2019: Stabilizing the West Antarctic Ice Sheet by surface mass deposition. *Science advances*, **5**, eaaw4132, doi:10.1126/sciadv.aaw4132.

Flowers, G. E., 2015: Modelling water flow under glaciers and ice sheets. *Proceedings of the Royal Society A: Mathematical, Physical and Engineering Sciences*, **471**, 20140907, doi:10.1098/rspa.2014.0907.

Fretwell, P., H. D. Pritchard, D. G. Vaughan, J. L. Bamber, N. Barrand, R. Bell, C. Bianchi, R. Bingham, D. D. Blankenship, G. Casassa, et al., 2013: Bedmap2: improved ice bed, surface and thickness datasets for antarctica. *The Cryosphere*, **7**, 375–393, doi:10.5194/tc-7-375-2013.

Frieler, K., P. U. Clark, F. He, C. Buizert, R. Reese, S. R. Ligtenberg, M. R. Van Den Broeke, R. Winkelmann, and A. Levermann, 2015: Consistent evidence of increasing Antarctic accumulation with warming. *Nature Climate Change*, **5**, 348, doi:10.1038/nclimate2574.

Frigola, J., M. Canals, I. Cacho, A. Moreno, F. J. Sierro, J. A. Flores, S. Berné, G. Jouet, B. Dennielou, G. Herrera, et al., 2012: A 500 kyr record of global sea-level oscillations in the gulf of lion, mediterranean sea: new insights into mis 3 sea-level variability. *Climate of the Past*, **8**, 1067–1077, doi:10.5194/cp-8-1067-2012.

Fudge, T., B. R. Markle, K. M. Cuffey, C. Buizert, K. C. Taylor, E. J. Steig, E. D. Waddington, H. Conway, and M. Koutnik, 2016: Variable relationship between

accumulation and temperature in West Antarctica for the past 31,000 years. *Geophysical Research Letters*, **43**, 3795–3803, doi:10.1002/2016GL068356.

Fürst, J. J., G. Durand, F. Gillet-Chaulet, L. Tavard, M. Rankl, M. Braun, and O. Gagliardini, 2016: The safety band of antarctic ice shelves. *Nature Climate Change*, **6**, 479, doi:10.1038/NCLIMATE2912.

Gagliardini, O. and T. Zwinger, 2008: The ISMIP-HOM benchmark experiments performed using the Finite-Element code Elmer. *The Cryosphere*, **2**, 67–76, doi:10.5194/tc-2-67-2008.

Galbraith, E. D., S. L. Jaccard, T. F. Pedersen, D. M. Sigman, G. H. Haug, M. Cook, J. R. Southon, and R. Francois, 2007: Carbon dioxide release from the north pacific abyss during the last deglaciation. *Nature*, **449**, 890, doi:10.1038/nature06227.

Galeotti, S., R. DeConto, T. Naish, P. Stocchi, F. Florindo, M. Pagani, P. Barrett, S. M. Bohaty, L. Lanci, D. Pollard, et al., 2016: Antarctic ice sheet variability across the eocene-oligocene boundary climate transition. *Science*, **352**, 76–80, doi:10.1126/science.aab0669.

Ganopolski, A., R. Calov, and M. Claussen, 2010: Simulation of the last glacial cycle with a coupled climate ice-sheet model of intermediate complexity. *Climate of the Past*, **6**, 229–244, doi:10.5194/cp-6-229-2010.

Ganopolski, A. and S. Rahmstorf, 2001: Rapid changes of glacial climate simulated in a coupled climate model. *Nature*, **409**, 153, doi:10.1038/409153A0.

— 2002: Abrupt glacial climate changes due to stochastic resonance. *Physical Review Letters*, **88**, 038501, doi:10.1103/PhysRevLett.88.038501.

Gasson, E., R. DeConto, and D. Pollard, 2015: Antarctic bedrock topography uncertainty and ice sheet stability. *Geophysical Research Letters*, **42**, 5372–5377, doi:10.1002/2015GL064322.

Gildor, H. and E. Tziperman, 2003: Sea-ice switches and abrupt climate change. *Philosophical Transactions of the Royal Society of London. Series A: Mathematical, Physical and Engineering Sciences*, **361**, 1935–1944, doi:10.1098/rsta.2003.1244.

Gillet-Chaulet, F., G. Durand, O. Gagliardini, C. Mosbeux, J. Mouginot, F. Rémy, and C. Ritz, 2016: Assimilation of surface velocities acquired between

1996 and 2010 to constrain the form of the basal friction law under Pine Island Glacier. *Geophysical Research Letters*, **43**, 10–311, doi:10.1002/2016GL069937.

Gladstone, R., V. Lee, A. Vieli, and A. Payne, 2010: Grounding line migration in an adaptive mesh ice sheet model. *Journal of Geophysical Research: Earth Surface*, **115**, doi:10.1029/2009JF001615.

Gladstone, R. M., R. C. Warner, B. K. Galton-Fenzi, O. Gagliardini, T. Zwinger, and R. Greve, 2017: Marine ice sheet model performance depends on basal sliding physics and sub-shelf melting. *The Cryosphere*, **11**, 319–329, doi:10.5194/tc-11-319-2017.

Glen, J. W., 1955: The creep of polycrystalline ice. *Proceedings of the Royal Society of London. Series A. Mathematical and Physical Sciences*, **228**, 519–538.

Goelzer, H., V. Coulon, F. Pattyn, B. de Boer, and R. S. Van De Wal, 2019: Brief communication: On calculating the sea-level contribution in marine ice-sheet models. *The Cryosphere Discussions*, doi:10.5194/tc-2019-185.

Goelzer, H., A. Robinson, H. Seroussi, and R. S. Van De Wal, 2017: Recent progress in Greenland ice sheet modelling. *Current climate change reports*, **3**, 291–302, doi:10.1007/s40641-017-0073-y.

Golledge, N., L. Menviel, L. Carter, C. Fogwill, M. England, G. Cortese, and R. Levy, 2014: Antarctic contribution to meltwater pulse 1A from reduced Southern Ocean overturning. *Nature Communications*, **5**, 5107, doi:10.1038/ncomms6107.

Golledge, N. R., C. J. Fogwill, A. N. Mackintosh, and K. M. Buckley, 2012: Dynamics of the last glacial maximum Antarctic ice-sheet and its response to ocean forcing. *Proceedings of the National Academy of Sciences*, **109**, 16052–16056, doi:10.1073/pnas.1205385109.

Golledge, N. R., E. D. Keller, N. Gomez, K. A. Naughten, J. Bernales, L. D. Trusel, and T. L. Edwards, 2019: Global environmental consequences of twenty-first-century ice-sheet melt. *Nature*, **566**, 65, doi:10.1038/s41586-019-0889-9.

Golledge, N. R., D. E. Kowalewski, T. R. Naish, R. H. Levy, C. J. Fogwill, and E. G. Gasson, 2015: The multi-millennial antarctic commitment to future sea-level rise. *Nature*, **526**, 421, doi:10.1038/nature15706.

Gomez, N., D. Pollard, and J. X. Mitrovica, 2013: A 3-D coupled ice sheet–sea level model applied to Antarctica through the last 40 ky. *Earth and Planetary Science Letters*, **384**, 88–99, doi:10.1016/j.epsl.2013.09.042.

Grant, K., E. Rohling, M. Bar-Matthews, A. Ayalon, M. Medina-Elizalde, C. B. Ramsey, C. Satow, and A. Roberts, 2012: Rapid coupling between ice volume and polar temperature over the past 150,000 years. *Nature*, **491**, 744, doi:10.1038/nature11593.

Greve, R., 1997: Application of a polythermal three-dimensional ice sheet model to the greenland ice sheet: response to steady-state and transient climate scenarios. *Journal of Climate*, **10**, 901–918, doi:10.1175/1520-0442.

Greve, R. and H. Blatter, 2009: *Dynamics of ice sheets and glaciers*. Springer Science & Business Media.

Hanebuth, T., K. Stattegger, and P. M. Grootes, 2000: Rapid flooding of the sunda shelf: a late-glacial sea-level record. *Science*, **288**, 1033–1035, doi:10.1126/science.288.5468.1033.

Hays, J. D., J. Imbrie, and N. J. Shackleton, 1976: Variations in the earth's orbit: pacemaker of the ice ages. *Science*, **194**, 1121–1132, doi:10.1126/science.194.4270.1121.

Heinrich, H., 1988: Origin and consequences of cyclic ice rafting in the northeast atlantic ocean during the past 130,000 years. *Quaternary research*, **29**, 142–152, doi:10.1016/0033-5894(88)90057-9.

Hemming, S. R., 2004: Heinrich events: Massive late pleistocene detritus layers of the north atlantic and their global climate imprint. *Reviews of Geophysics*, **42**, doi:10.1029/2003RG000128.

Henry, L., J. F. McManus, W. B. Curry, N. L. Roberts, A. M. Piotrowski, and L. D. Keigwin, 2016: North atlantic ocean circulation and abrupt climate change during the last glaciation. *Science*, **353**, 470–474, doi:10.1126/science.aaf5529.

Hillenbrand, C.-D., M. J. Bentley, T. D. Stolldorf, A. S. Hein, G. Kuhn, A. G. Graham, C. J. Fogwill, Y. Kristoffersen, J. A. Smith, J. B. Anderson, R. D. Larter, M. Melles, D. A. Hodgson, R. Mulvaney, and D. E. Sugden, 2014: Reconstruction of changes in the Weddell Sea sector of the Antarctic Ice Sheet

since the Last Glacial Maximum. *Quaternary Science Reviews*, **100**, 111–136, doi:10.1016/j.quascirev.2013.07.020.

Hillenbrand, C.-D., M. Melles, G. Kuhn, and R. D. Larter, 2012: Marine geological constraints for the grounding-line position of the Antarctic Ice Sheet on the southern Weddell Sea shelf at the Last Glacial Maximum. *Quaternary Science Reviews*, **32**, 25–47, doi:10.1016/j.quascirev.2011.11.017.

Holland, D. M., K. W. Nicholls, and A. Basinski, 2020: The Southern Ocean and its interaction with the Antarctic Ice Sheet. *Science*, **367**, 1326–1330, doi:10.1126/science.aaz5491.

Holland, P. R., T. J. Bracegirdle, P. Dutrieux, A. Jenkins, and E. J. Steig, 2019: West antarctic ice loss influenced by internal climate variability and anthropogenic forcing. *Nature Geoscience*, 1–7, doi:10.1038/s41561-019-0420-9.

Holland, P. R., A. Jenkins, and D. M. Holland, 2008: The response of ice shelf basal melting to variations in ocean temperature. *Journal of Climate*, **21**, 2558–2572, doi:10.1175/2007JCLI1909.1.

Holloway, M. D., L. C. Sime, C. S. Allen, C.-D. Hillenbrand, P. Bunch, E. Wolff, and P. J. Valdes, 2017: The spatial structure of the 128 ka Antarctic sea ice minimum. *Geophysical Research Letters*, **44**, 11–129, doi:10.1002/2017GL074594.

Holloway, M. D., L. C. Sime, J. S. Singarayer, J. C. Tindall, P. Bunch, and P. J. Valdes, 2016: Antarctic last interglacial isotope peak in response to sea ice retreat not ice-sheet collapse. *Nature communications*, **7**, 12293, doi:10.1038/ncomms12293.

Hutter, K., 1983: *Theoretical glaciology: material science of ice and the mechanics of glaciers and ice sheets*, volume 1. Springer.

Huybrechts, P., 1990: A 3-d model for the antarctic ice sheet: a sensitivity study on the glacial-interglacial contrast. *Climate Dynamics*, **5**, 79–92, doi:10.1007/BF00207423.

— 2002: Sea-level changes at the LGM from ice-dynamic reconstructions of the Greenland and Antarctic ice sheets during the glacial cycles. *Quaternary Science Reviews*, **21**, 203–231, doi:10.1016/S0277-3791(01)00082-8.

Huybrechts, P. and J. Oerlemans, 1990: Response of the antarctic ice sheet to future greenhouse warming. *Climate Dynamics*, **5**, 93–102,

doi:10.1007/BF00207424.

Ivins, E. R. and T. S. James, 2005: Antarctic glacial isostatic adjustment: a new assessment. *Antarctic Science*, **17**, 541–553, doi:10.1017/S0954102005002968.

Ivins, E. R., T. S. James, J. Wahr, E. J. O. Schrama, F. W. Landerer, and K. M. Simon, 2013: Antarctic contribution to sea level rise observed by GRACE with improved GIA correction. *Journal of Geophysical Research: Solid Earth*, **118**, 3126–3141, doi:10.1002/jgrb.50208.

Jacobs, S. S., A. Jenkins, C. F. Giulivi, and P. Dutrieux, 2011: Stronger ocean circulation and increased melting under Pine Island Glacier ice shelf. *Nature Geoscience*, **4**, 519, doi:10.1038/ngeo1188.

Jenkins, A., 2011: Convection-driven melting near the grounding lines of ice shelves and tidewater glaciers. *Journal of Physical Oceanography*, **41**, 2279–2294, doi:10.1175/JPO-D-11-03.1.

Jensen, M. F., J. Nilsson, and K. H. Nisancioglu, 2016: The interaction between sea ice and salinity-dominated ocean circulation: implications for halocline stability and rapid changes of sea ice cover. *Climate Dynamics*, **47**, 3301–3317, doi:10.1007/s00382-016-3027-5.

Johnsen, S. J., D. Dahl-Jensen, N. Gundestrup, J. P. Steffensen, H. B. Clausen, H. Miller, V. Masson-Delmotte, A. E. Sveinbjörnsdottir, and J. White, 2001: Oxygen isotope and palaeotemperature records from six Greenland ice-core stations: Camp Century, Dye-3, GRIP, GISP2, Renland and NorthGRIP. *Journal of Quaternary Science: Published for the Quaternary Research Association*, **16**, 299–307, doi:10.1002/jqs.622.

Joughin, I. and R. B. Alley, 2011: Stability of the west antarctic ice sheet in a warming world. *Nature Geoscience*, **4**, 506, doi:10.1038/ngeo1194.

Joughin, I., B. E. Smith, and C. G. Schoof, 2019: Regularized Coulomb friction laws for ice sheet sliding: Application to Pine Island Glacier, Antarctica. *Geophysical Research Letters*, **46**, 4764–4771, doi:10.1029/2019GL082526.

Jouzel, J., C. Lorius, J. Petit, C. Genthon, N. Barkov, V. Kotlyakov, and V. Petrov, 1987: Vostok ice core: a continuous isotope temperature record over the last climatic cycle (160,000 years). *Nature*, **329**, 403, doi:10.1038/329403a0.

Jouzel, J. and V. Masson-Delmotte, 2007: EPICA Dome C Ice Core 800KYr deuterium data and temperature estimates.
URL https://doi.org/10.1594/PANGAEA.683655

Jouzel, J., V. Masson-Delmotte, O. Cattani, G. Dreyfus, S. Falourd, G. Hoffmann, B. Minster, J. Nouet, J.-M. Barnola, J. Chappellaz, et al., 2007: Orbital and millennial Antarctic climate variability over the past 800,000 years. *Science*, **317**, 793–796, doi:10.1126/science.1141038.

Kageyama, M., S. P. Harrison, M.-L. Kapsch, M. Lofverstrom, J. M. Lora, U. Mikolajewicz, S. Sherriff-Tadano, T. Vadsaria, A. Abe-Ouchi, N. Bouttes, D. Chandan, A. N. LeGrande, F. Lhardy, G. Lohmann, P. A. Morozova, R. Ohgaito, W. R. Peltier, A. Quiquet, D. M. Roche, X. Shi, A. Schmittner, J. E. Tierney, and E. Volodin, 2019: The PMIP4-CMIP6 Last Glacial Maximum experiments: preliminary results and comparison with the PMIP3-CMIP5 simulations. *Climate of the Past*, doi:10.5194/cp-2019-169.

Kanner, L. C., S. J. Burns, H. Cheng, and R. L. Edwards, 2012: High-latitude forcing of the south american summer monsoon during the last glacial. *Science*, **335**, 570–573, doi:10.1126/science.1213397.

Kaspi, Y., R. Sayag, and E. Tziperman, 2004: A "triple sea-ice state" mechanism for the abrupt warming and synchronous ice sheet collapses during heinrich events. *Paleoceanography*, **19**, doi:10.1029/2004PA001009.

Kawamura, K., F. Parrenin, L. Lisiecki, R. Uemura, F. Vimeux, J. P. Severinghaus, M. A. Hutterli, T. Nakazawa, S. Aoki, J. Jouzel, et al., 2007: Northern hemisphere forcing of climatic cycles in antarctica over the past 360,000 years. *Nature*, **448**, 912, doi:10.1038/nature06015.

Kim, S., K.-C. Yoo, J. I. Lee, M. K. Lee, K. Kim, H. I. Yoon, and H. S. Moon, 2018: Relationship between magnetic susceptibility and sediment grain size since the last glacial period in the southern ocean off the northern antarctic peninsula-linkages between the cryosphere and atmospheric circulation. *Palaeogeography, Palaeoclimatology, Palaeoecology*, **505**, 359–370, doi:10.1016/j.palaeo.2018.06.016.

Kindler, P., M. Guillevic, M. Baumgartner, J. Schwander, A. Landais, and M. Leuenberger, 2014: Temperature reconstruction from 10 to 120 kyr b2k

from the ngrip ice core. *Climate of the Past*, **10**, 887–902, doi:10.5194/cp-10-887-2014.

King, A. D. and L. J. Harrington, 2018: The inequality of climate change from 1.5 to 2 c of global warming. *Geophysical Research Letters*, **45**, 5030–5033, doi:10.1029/2018GL078430.

Kirchner, N., K. Hutter, M. Jakobsson, and R. Gyllencreutz, 2011: Capabilities and limitations of numerical ice sheet models: a discussion for Earth-scientists and modelers. *Quaternary Science Reviews*, **30**, 3691–3704, doi:10.1016/j.quascirev.2011.09.012.

Kissel, C., C. Laj, L. Labeyrie, T. Dokken, A. Voelker, and D. Blamart, 1999: Rapid climatic variations during marine isotopic stage 3: magnetic analysis of sediments from nordic seas and north atlantic. *Earth and Planetary Science Letters*, **171**, 489–502, doi:10.1016/S0012-821X(99)00162-4.

Kleppin, H., M. Jochum, B. Otto-Bliesner, C. A. Shields, and S. Yeager, 2015: Stochastic atmospheric forcing as a cause of greenland climate transitions. *Journal of Climate*, **28**, 7741–7763, doi:10.1175/JCLI-D-14-00728.1.

Kopp, R. E., F. J. Simons, J. X. Mitrovica, A. C. Maloof, and M. Oppenheimer, 2009: Probabilistic assessment of sea level during the last interglacial stage. *Nature*, **462**, 863, doi:10.1038/nature08686.

Kusahara, K., T. Sato, A. Oka, T. Obase, R. Greve, A. Abe-Ouchi, and H. Hasumi, 2015: Modelling the Antarctic marine cryosphere at the Last Glacial Maximum. *Annals of Glaciology*, **56**, 425–435, doi:10.3189/2015AoG69A792.

Lachlan-Cope, T. and W. Connolley, 2006: Teleconnections between the tropical Pacific and the Amundsen-Bellinghausens Sea: Role of the El Niño/Southern Oscillation. *Journal of Geophysical Research: Atmospheres*, **111**, doi:10.1029/2005JD006386.

Lambeck, K. and J. Chappell, 2001: Sea level change through the last glacial cycle. *Science*, **292**, 679–686, doi:10.1126/science.1059549.

Lambeck, K. and P. Johnston, 1998: The viscosity of the mantle: Evidence from analyses of glacial rebound phenomena. *The Earth's Mantle: Composition, Structure and Evolution*, 461–502, doi:10.1017/CBO9780511573101.013.

Lambeck, K., A. Purcell, P. Johnston, M. Nakada, and Y. Yokoyama, 2003: Water-load definition in the glacio-hydro-isostatic sea-level equation. *Quaternary Science Reviews*, **22**, 309–318, doi:10.1016/S0277-3791(02)00142-7.

Lambeck, K., H. Rouby, A. Purcell, Y. Sun, and M. Sambridge, 2014: Sea level and global ice volumes from the Last Glacial Maximum to the Holocene. *Proceedings of the National Academy of Sciences*, **111**, 15296–15303, doi:10.1073/pnas.1411762111.

Lambeck, K., Y. Yokoyama, and T. Purcell, 2002: Into and out of the Last Glacial Maximum: Sea-level change during Oxygen Isotope Stages 3 and 2. *Quaternary Science Reviews*, **21**, 343–360, doi:10.1016/S0277-3791(01)00071-3.

Landsat Image Mosaic Of Antarctica, 2008: Landsat image mosaic of antarctica. URL https://lima.usgs.gov/

Lazeroms, W. M., A. Jenkins, G. H. Gudmundsson, and R. S. Van De Wal, 2018: Modelling present-day basal melt rates for Antarctic ice shelves using a parametrization of buoyant meltwater plumes. *The Cryosphere*, **12**, 49–70, doi:10.5194/tc-12-49-2018.

Le clec'h, S., A. Quiquet, S. Charbit, C. Dumas, M. Kageyama, and C. Ritz, 2019: A rapidly converging initialisation method to simulate the present-day Greenland ice sheet using the GRISLI ice sheet model (version 1.3). *Geoscientific Model Development*, **12**, 2481–2499, doi:10.5194/gmd-12-2481-2019.

Le Meur, E. and P. Huybrechts, 1996: A comparison of different ways of dealing with isostasy: examples from modelling the Antarctic ice sheet during the last glacial cycle. *Annals of Glaciology*, **23**, 309–317, doi:10.3189/S0260305500013586.

Leduc, G., L. Vidal, K. Tachikawa, F. Rostek, C. Sonzogni, L. Beaufort, and E. Bard, 2007: Moisture transport across central america as a positive feedback on abrupt climatic changes. *Nature*, **445**, 908, doi:10.1038/nature05578.

Leguy, G., X. Asay-Davis, and W. Lipscomb, 2014: Parameterization of basal friction near grounding lines in a one-dimensional ice sheet model. *The Cryosphere*, **8**, 1239–1259, doi:10.5194/tc-8-1239-2014.

Lenton, T. M., H. Held, E. Kriegler, J. W. Hall, W. Lucht, S. Rahmstorf, and H. J. Schellnhuber, 2008: Tipping elements in the Earth's climate sys-

tem. *Proceedings of the national Academy of Sciences*, **105**, 1786–1793, doi:10.1073/pnas.0705414105.

Lenton, T. M., J. Rockström, O. Gaffney, S. Rahmstorf, K. Richardson, W. Steffen, and H. J. Schellnhuber, 2019: Climate tipping points—too risky to bet against.

Levermann, A., R. Winkelmann, T. Albrecht, H. Goelzer, N. R. Golledge, R. Greve, P. Huybrechts, J. Jordan, G. Leguy, D. Martin, M. Morlighem, F. Pattyn, D. Pollard, A. Quiquet, C. Rodehacke, H. Seroussi, J. Sutter, T. Zhang, J. Van Breedam, R. Calov, R. DeConto, C. Dumas, J. Garbe, G. H. Gudmundsson, M. J. Hoffman, A. Humbert, T. Kleiner, W. H. Lipscomb, M. Meinshausen, E. Ng, S. M. J. Nowicki, M. Perego, S. F. Price, F. Saito, N.-J. Schlegel, S. Sun, and R. S. W. van de Wal, 2020: Projecting Antarctica's contribution to future sea level rise from basal ice shelf melt using linear response functions of 16 ice sheet models (LARMIP-2). *Earth System Dynamics*, **11**, 35–76, doi:10.5194/esd-11-35-2020.

Li, C., D. S. Battisti, and C. M. Bitz, 2010: Can north atlantic sea ice anomalies account for dansgaard–oeschger climate signals? *Journal of climate*, **23**, 5457–5475, doi:10.1175/2010JCLI3409.1.

Li, C., D. S. Battisti, D. P. Schrag, and E. Tziperman, 2005: Abrupt climate shifts in greenland due to displacements of the sea ice edge. *Geophysical Research Letters*, **32**, doi:10.1029/2005GL023492.

Li, C. and A. Born, 2019: Coupled atmosphere-ice-ocean dynamics in Dansgaard-Oeschger events. *Quaternary Science Reviews*, **203**, 1–20, doi:10.1016/j.quascirev.2018.10.031.

Lipscomb, W., R. Bindschadler, E. Bueler, D. Holland, J. Johnson, and S. Price, 2009: A community ice sheet model for sea level prediction. *Eos*, **90**, 23, doi:10.1029/2009EO030004.

Lipscomb, W. H., S. F. Price, M. J. Hoffman, G. R. Leguy, A. R. Bennett, S. L. Bradley, K. J. Evans, J. G. Fyke, J. H. Kennedy, M. Perego, D. M. Ranken, W. J. Sacks, A. G. Salinger, L. J. Vargo, and P. H. Worley, 2019: Description and evaluation of the Community Ice Sheet Model (CISM) v2. 1. *Geoscientific Model Development*, **12**, 387–424, doi:10.5194/gmd-12-387-2019.

Liu, J., G. A. Milne, R. E. Kopp, P. U. Clark, and I. Shennan, 2016: Sea-level constraints on the amplitude and source distribution of meltwater pulse 1a. *Nature Geoscience*, **9**, 130, doi:10.1038/ngeo2616.

Liu, Y., J. C. Moore, X. Cheng, R. M. Gladstone, J. N. Bassis, H. Liu, J. Wen, and F. Hui, 2015: Ocean-driven thinning enhances iceberg calving and retreat of Antarctic ice shelves. *Proceedings of the National Academy of Sciences*, **112**, 3263–3268, doi:10.1073/pnas.1415137112.

Lynch-Stieglitz, J., 2017: The atlantic meridional overturning circulation and abrupt climate change. *Annual review of marine science*, **9**, 83–104, doi:10.1146/annurev-marine-010816-060415.

Ma, Y., O. Gagliardini, C. Ritz, F. Gillet-Chaulet, G. Durand, and M. Montagnat, 2010: Enhancement factors for grounded ice and ice shelves inferred from an anisotropic ice-flow model. *Journal of Glaciology*, **56**, 805–812, doi:10.3189/002214310794457209.

MacAyeal, D., 1993: Binge/purge oscillations of the Laurentide ice sheet as a cause of the North Atlantic's Heinrich events. *Paleoceanography*, **8**, 75–784, doi:10.1029/93PA02200.

MacAyeal, D. R., 1989: Large-scale ice flow over a viscous basal sediment: Theory and application to ice stream B, Antarctica. *Journal of Geophysical Research: Solid Earth*, **94**, 4071–4087, doi:10.1029/JB094iB04p04071.

MacAyeal, D. R., R. A. Bindschadler, and T. A. Scambos, 1995: Basal friction of ice stream E, West Antarctica. *Journal of Glaciology*, **41**, 247–262, doi:10.3189/S0022143000016154.

MacAYEAL, D. R., T. A. Scambos, C. L. Hulbe, and M. A. Fahnestock, 2003: Catastrophic ice-shelf break-up by an ice-shelf-fragment-capsize mechanism. *Journal of Glaciology*, **49**, 22–36, doi:10.3189/172756503781830863.

MacAyeal, D. R. and O. V. Sergienko, 2013: The flexural dynamics of melting ice shelves. *Annals of Glaciology*, **54**, 1–10, doi:10.3189/2013AoG63A256.

Mackintosh, A., N. Golledge, E. Domack, R. Dunbar, A. Leventer, D. White, D. Pollard, R. DeConto, D. Fink, D. Zwartz, D. Gore, and C. Lavoie, 2011: Retreat of the East Antarctic ice sheet during the last glacial termination. *Nature Geoscience*, **4**, 195, doi:10.1038/ngeo1061.

Mackintosh, A. N., E. Verleyen, P. E. O'Brien, D. A. White, R. S. Jones, R. McKay, R. Dunbar, D. B. Gore, D. Fink, A. L. Post, et al., 2014: Retreat history of the East Antarctic ice sheet since the last glacial maximum. *Quaternary Science Reviews*, **100**, 10–30, doi:10.1016/j.quascirev.2013.07.024.

Manabe, S. and R. J. Stouffer, 1995: Simulation of abrupt climate change induced by freshwater input to the north atlantic ocean. *Nature*, **378**, 165.

Maris, M., B. De Boer, S. Ligtenberg, M. Crucifix, W. Van De Berg, and J. Oerlemans, 2014: Modelling the evolution of the Antarctic ice sheet since the last interglacial. *The Cryosphere*, **8**, 1347–1360, doi:10.5194/tc-8-1347-2014.

Martin, M. A., R. Winkelmann, M. Haseloff, T. Albrecht, E. Bueler, C. Khroulev, and A. Levermann, 2011: The Potsdam Parallel Ice Sheet Model (PISM-PIK)–Part 2: Dynamic equilibrium simulation of the Antarctic ice sheet. *The Cryosphere*, **5**, 727–740, doi:10.5194/tc-5-727-2011.

Martin, T., W. Park, and M. Latif, 2013: Multi-centennial variability controlled by Southern Ocean convection in the Kiel Climate Model. *Climate dynamics*, **40**, 2005–2022, doi:10.1007/s00382-012-1586-7.

Martin, T., M. Steele, and J. Zhang, 2014: Seasonality and long-term trend of Arctic Ocean surface stress in a model. *Journal of Geophysical Research: Oceans*, **119**, 1723–1738, doi:10.1002/2013JC009425.

Martin-Español, A., J. L. Bamber, and A. Zammit-Mangion, 2017: Constraining the mass balance of east antarctica. *Geophysical Research Letters*, **44**, 4168–4175, doi:10.1002/2017GL072937.

Martin-Español, A., A. Zammit-Mangion, P. J. Clarke, T. Flament, V. Helm, M. A. King, S. B. Luthcke, E. Petrie, F. Rémy, N. Schön, et al., 2016: Spatial and temporal antarctic ice sheet mass trends, glacio-isostatic adjustment, and surface processes from a joint inversion of satellite altimeter, gravity, and gps data. *Journal of Geophysical Research: Earth Surface*, **121**, 182–200, doi:10.1002/2015JF003550.

Martinson, D. G., 2012: Antarctic circumpolar current's role in the antarctic ice system: An overview. *Palaeogeography, Palaeoclimatology, Palaeoecology*, **335**, 71–74, doi:10.1016/j.palaeo.2011.04.007.

Martos, Y. M., M. Catalán, T. A. Jordan, A. Golynsky, D. Golynsky, G. Eagles, and D. G. Vaughan, 2017: Heat flux distribution of Antarctica unveiled. *Geophysical Research Letters*, **44**, 11–417, doi:10.1002/2017GL075609.

Marzeion, B., A. Jarosch, and M. Hofer, 2012: Past and future sea-level change from the surface mass balance of glaciers. *The Cryosphere*, **6**, 1295–1322, doi:10.5194/tc-6-1295-2012.

McGrath, D., K. Steffen, H. Rajaram, T. Scambos, W. Abdalati, and E. Rignot, 2012: Basal crevasses on the Larsen C Ice Shelf, Antarctica: Implications for meltwater ponding and hydrofracture. *Geophysical research letters*, **39**, doi:10.1029/2012GL052413.

McKay, N. P., J. T. Overpeck, and B. L. Otto-Bliesner, 2011: The role of ocean thermal expansion in last interglacial sea level rise. *Geophysical Research Letters*, **38**, doi:10.1029/2011GL048280.

McManus, J. F., R. Francois, J.-M. Gherardi, L. D. Keigwin, and S. Brown-Leger, 2004: Collapse and rapid resumption of atlantic meridional circulation linked to deglacial climate changes. *Nature*, **428**, 834, doi:10.1038/nature02494.

Menviel, L., A. Timmermann, T. Friedrich, and M. England, 2014: Hindcasting the continuum of dansgaard-oeschger variability: mechanisms, patterns and timing. *Climate of the Past*, **10**, 63–77, doi:10.5194/cp-10-63-2014.

Mercer, J. H., 1978: West antarctic ice sheet and co2 greenhouse effect: a threat of disaster. *Nature*, **271**, 321, doi:10.1038/271321a0.

Milankovitch, M. K., 1941: Kanon der erdbestrahlung und seine anwendung auf das eiszeitenproblem. *Royal Serbian Academy Special Publication*, **133**, 1–633.

Montoya, M. and A. Levermann, 2008: Surface wind-stress threshold for glacial Atlantic overturning. *Geophysical Research Letters*, **35**, doi:10.1029/2007GL032560.

Morlighem, M., E. Rignot, T. Binder, D. Blankenship, R. Drews, G. Eagles, O. Eisen, R. Forsberg, P. Fretwell, V. Goel, J. Greenbaum, G. Gudmundsson, J. Guo, V. Helm, C. Hofstede, I. Howat, A. Humbert, W. Jokat, and D. Young, 2020: Deep glacial troughs and stabilizing ridges unveiled beneath the margins of the Antarctic ice sheet. *Nature Geoscience*, **13**, 132–137, doi:10.1038/s41561-019-0510-8.

Morlighem, M., H. Seroussi, E. Larour, and E. Rignot, 2013: Inversion of basal friction in Antarctica using exact and incomplete adjoints of a higher-order model. *Journal of Geophysical Research: Earth Surface*, **118**, 1746–1753, doi:10.1002/jgrf.20125.

Mouginot, J., E. Rignot, A. A. Bjørk, M. van den Broeke, R. Millan, M. Morlighem, B. Noël, B. Scheuchl, and M. Wood, 2019: Forty-six years of greenland ice sheet mass balance from 1972 to 2018. *Proceedings of the National Academy of Sciences*, **116**, 9239–9244, doi:10.1073/pnas.1904242116.

Nakada, M., R. Kimura, J. Okuno, K. Moriwaki, H. Miura, and H. Maemoku, 2000: Late Pleistocene and Holocene melting history of the Antarctic ice sheet derived from sea-level variations. *Marine Geology*, **167**, 85–103, doi:10.1016/S0025-3227(00)00018-9.

Neumann, B., A. T. Vafeidis, J. Zimmermann, and R. J. Nicholls, 2015: Future coastal population growth and exposure to sea-level rise and coastal flooding-a global assessment. *PloS one*, **10**, e0118571, doi:10.1371/journal.pone.0118571.

Nicholls, R. J. and A. Cazenave, 2010: Sea-level rise and its impact on coastal zones. *Science*, **328**, 1517–1520, doi:10.1126/science.1185782.

North Greenland Ice Core Project members, 2004: High-resolution record of Northern Hemisphere climate extending into the last interglacial period. *Nature*, **431**, 147.

Nowicki, S., R. A. Bindschadler, A. Abe-Ouchi, A. Aschwanden, E. Bueler, H. Choi, J. Fastook, G. Granzow, R. Greve, G. Gutowski, U. Herzfeld, C. Jackson, J. Johnson, C. Khroulev, E. Larour, A. Levermann, W. H. Lipscomb, M. A. Martin, M. Morlighem, B. R. Parizek, D. Pollard, S. F. Price, D. Ren, E. Rignot, F. Saito, T. Sato, H. Seddik, H. Seroussi, K. Takahashi, R. Walker, and W. L. Wang, 2013: Insights into spatial sensitivities of ice mass response to environmental change from the SeaRISE ice sheet modeling project I: Antarctica. *Journal of Geophysical Research: Earth Surface*, **118**, 1002–1024, doi:10.1002/jgrf.20081.

Oeschger, H., J. Beer, U. Siegenthaler, B. Stauffer, W. Dansgaard, and C. Langway, 1983: Late-glacial climate history from ice cores. *Palaeoclimatic research and models*, Springer, 95–107.

Otto-Bliesner, B. L., N. Rosenbloom, E. J. Stone, N. P. McKay, D. J. Lunt, E. C. Brady, and J. T. Overpeck, 2013: How warm was the last interglacial? new model–data comparisons. *Philosophical Transactions of the Royal Society A: Mathematical, Physical and Engineering Sciences*, **371**, 20130097, doi:10.1098/rsta.2013.0097.

Ourbak, T. and A. K. Magnan, 2018: The Paris Agreement and climate change negotiations: Small Islands, big players. *Regional environmental change*, **18**, 2201–2207, doi:10.1007/s10113-017-1262-x.

Paillard, D., 2015: Quaternary glaciations: from observations to theories. *Quaternary Science Reviews*, **107**, 11–24, doi:10.1016/j.quascirev.2014.10.002.

Paillard, D. and F. Parrenin, 2004: The Antarctic ice sheet and the triggering of deglaciations. *Earth and Planetary Science Letters*, **227**, 263–271, doi:10.1016/j.epsl.2004.08.023.

Paolo, F., L. Padman, H. Fricker, S. Adusumilli, S. Howard, and M. Siegfried, 2018: Response of Pacific-sector Antarctic ice shelves to the El Niño/Southern Oscillation. *Nature geoscience*, **11**, 121, doi:10.1038/s41561-017-0033-0.

Paolo, F. S., H. A. Fricker, and L. Padman, 2015: Volume loss from antarctic ice shelves is accelerating. *Science*, **348**, 327–331, doi:10.1126/science.aaa0940.

Pattyn, F., 2017: Sea-level response to melting of Antarctic ice shelves on multi-centennial timescales with the fast Elementary Thermomechanical Ice Sheet model (f. ETISh v1. 0). *The Cryosphere*, **11**, 1851–1878, doi:10.5194/tc-11-1851-2017.

— 2018: The paradigm shift in Antarctic ice sheet modelling. *Nature communications*, **9**, 2728, doi:10.1038/s41467-018-05003-z.

Pattyn, F. and G. Durand, 2013: Why marine ice sheet model predictions may diverge in estimating future sea level rise. *Geophysical research letters*, **40**, 4316–4320, doi:10.1002/grl.50824.

Pattyn, F. and M. Morlighem, 2020: The uncertain future of the Antarctic Ice Sheet. *Science*, **367**, 1331–1335, doi:10.1126/science.aaz5487.

Pattyn, F., C. Ritz, E. Hanna, X. Asay-Davis, R. DeConto, G. Durand, L. Favier, X. Fettweis, H. Goelzer, N. R. Golledge, P. K. Munneke, J. T. Lenaerts, S. Nowicki, A. J. Payne, A. Robinson, H. Seroussi, L. D. Trusel, and M. van den

Broeke, 2018: The Greenland and Antarctic ice sheets under 1.5 C global warming. *Nature climate change*, **8**, 1053–1061, doi:10.1038/s41558-018-0305-8.

Pattyn, F., C. Schoof, L. Perichon, R. Hindmarsh, E. Bueler, B. De Fleurian, G. Durand, O. Gagliardini, R. Gladstone, D. Goldberg, G. Gudmundsson, P. Huybrechts, V. Lee, F. Nick, A. Payne, D. Pollard, O. Rybak, F. Saito, and A. Vieli, 2012: Results of the marine ice sheet model intercomparison project, MISMIP. *The Cryosphere*, **6**, 573–588, doi:10.5194/tc-6-573-2012.

Pearson, P. N., G. L. Foster, and B. S. Wade, 2009: Atmospheric carbon dioxide through the eocene–oligocene climate transition. *Nature*, **461**, 1110, doi:10.1038/nature08447.

Pedro, J. B., M. Jochum, C. Buizert, F. He, S. Barker, and S. O. Rasmussen, 2018: Beyond the bipolar seesaw: Toward a process understanding of interhemispheric coupling. *Quaternary Science Reviews*, **192**, 27–46, doi:10.1016/j.quascirev.2018.05.005.

Pelle, T., M. Morlighem, and J. H. Bondzio, 2019: Brief communication: PICOP, a new ocean melt parameterization under ice shelves combining PICO and a plume model. *The Cryosphere*, **13**, 1043–1049, doi:10.5194/tc-13-1043-2019.

Peltier, W., D. Argus, and R. Drummond, 2015: Space geodesy constrains ice age terminal deglaciation: The global ICE-6G_C (VM5a) model. *J. Geophys. Res. Solid Earth*, **120**, 450–487, doi:10.1002/2014JB011176.

— 2018: Comment on "An Assessment of the ICE-6G_C (VM5a) Glacial Isostatic Adjustment Model" by Purcell et al. *J. Geophys. Res. Solid Earth*, **123**, doi:10.1002/2016JB013844.

Peltier, W. and R. G. Fairbanks, 2006: Global glacial ice volume and Last Glacial Maximum duration from an extended Barbados sea level record. *Quaternary Science Reviews*, **25**, 3322–3337, doi:10.1016/j.quascirev.2006.04.010.

Petersen, S. V., D. P. Schrag, and P. U. Clark, 2013: A new mechanism for dansgaard-oeschger cycles. *Paleoceanography*, **28**, 24–30, doi:10.1029/2012PA002364.

Peyaud, V., C. Ritz, and G. Krinner, 2007: Modelling the Early Weichselian Eurasian Ice Sheets: role of ice shelves and influence of ice-dammed lakes. *Climate of the Past Discussions*, **3**, 221–247, doi:10.5194/cp-3-375-2007.

Philippon, G., G. Ramstein, S. Charbit, M. Kageyama, C. Ritz, and C. Dumas, 2006: Evolution of the Antarctic ice sheet throughout the last deglaciation: A study with a new coupled climate—north and south hemisphere ice sheet model. *Earth and Planetary Science Letters*, **248**, 750–758, doi:10.1016/j.epsl.2006.06.017.

Pollard, D. and R. DeConto, 2012a: A simple inverse method for the distribution of basal sliding coefficients under ice sheets, applied to Antarctica. *The Cryosphere*, **6**, 953, doi:10.5194/tc-6-953-2012.

— 2012b: Description of a hybrid ice sheet-shelf model, and application to Antarctica. *Geoscientific Model Development*, **5**, 1273–1295, doi:10.5194/gmd-5-1273-2012.

Pollard, D. and R. M. DeConto, 2009: Modelling west antarctic ice sheet growth and collapse through the past five million years. *Nature*, **458**, 329, doi:10.1038/nature07809.

Pritchard, H., S. R. Ligtenberg, H. A. Fricker, D. G. Vaughan, M. R. van den Broeke, and L. Padman, 2012: Antarctic ice-sheet loss driven by basal melting of ice shelves. *Nature*, **484**, 502–505, doi:10.1038/nature10968.

Quiquet, A., C. Dumas, C. Ritz, V. Peyaud, and D. M. Roche, 2018: The GRISLI ice sheet model (version 2.0): calibration and validation for multi-millennial changes of the Antarctic ice sheet. *Geoscientific Model Development*, **11**, 5003, doi:10.5194/gmd-11-5003-2018.

Rahmstorf, S., 2002: Ocean circulation and climate during the past 120,000 years. *Nature*, **419**, 207, doi:10.1038/nature01090.

Rashid, H., R. Hesse, and D. J. Piper, 2003: Evidence for an additional Heinrich event between H5 and H6 in the Labrador Sea. *Paleoceanography*, **18**, doi:10.1029/2003PA000913.

Reeh, N., 1989: Parameterization of melt rate and surface temperature on the Greenland ice sheet. *J. Geophys. Res.-Sol. Ea.*, **59**, 113–128, doi:10013/epic.13107.

Reese, R., T. Albrecht, M. Mengel, X. Asay-Davis, and R. Winkelmann, 2018: Antarctic sub-shelf melt rates via PICO. *The Cryosphere*, **12**, 1969–1985, doi:10.5194/tc-12-1969-2018.

Rignot, E., G. Casassa, P. Gogineni, W. Krabill, A. Rivera, and R. Thomas, 2004: Accelerated ice discharge from the antarctic peninsula following the collapse of larsen b ice shelf. *Geophysical Research Letters*, **31**, doi:10.1029/2004GL020697.

Rignot, E., S. Jacobs, J. Mouginot, and B. Scheuchl, 2013: Ice-shelf melting around antarctica. *Science*, **341**, 266–270, doi:10.1126/science.1235798.

Rignot, E. and S. S. Jacobs, 2002: Rapid bottom melting widespread near Antarctic ice sheet grounding lines. *Science*, **296**, 2020–2023, doi:10.1126/science.1070942.

Rignot, E., J. Mouginot, M. Morlighem, H. Seroussi, and B. Scheuchl, 2014: Widespread, rapid grounding line retreat of Pine Island, Thwaites, Smith, and Kohler glaciers, West Antarctica, from 1992 to 2011. *Geophysical Research Letters*, **41**, 3502–3509, doi:10.1002/2014GL060140.

Rignot, E., J. Mouginot, and B. Scheuchl, 2011: Ice flow of the Antarctic ice sheet. *Science*, **333**, 1427–1430, doi:10.1126/science.1208336.

Rignot, E., J. Mouginot, B. Scheuchl, M. van den Broeke, M. J. van Wessem, and M. Morlighem, 2019: Four decades of Antarctic Ice Sheet mass balance from 1979–2017. *Proceedings of the National Academy of Sciences*, **116**, 1095–1103, doi:10.1073/pnas.1812883116.

Ritz, C., T. L. Edwards, G. Durand, A. J. Payne, V. Peyaud, and R. C. Hindmarsh, 2015: Potential sea-level rise from Antarctic ice-sheet instability constrained by observations. *Nature*, **528**, 115, doi:10.1038/nature16147.

Ritz, C., A. Fabre, and A. Letréguilly, 1996: Sensitivity of a Greenland ice sheet model to ice flow and ablation parameters: consequences for the evolution through the last climatic cycle. *Climate Dynamics*, **13**, 11–23, doi:10.1007/s003820050.

Ritz, C., V. Rommelaere, and C. Dumas, 2001: Modeling the evolution of Antarctic ice sheet over the last 420,000 years: Implications for altitude changes in the Vostok region. *Journal of Geophysical Research: Atmospheres*, **106**, 31943–31964, doi:10.1029/2001JD900232.

Robel, A. A., H. Seroussi, and G. H. Roe, 2019: Marine ice sheet instability amplifies and skews uncertainty in projections of future sea-level

rise. *Proceedings of the National Academy of Sciences*, **116**, 14887–14892, doi:10.1073/pnas.1904822116.

Robinson, A., J. Alvarez-Solas, M. Montoya, H. Goelzer, R. Greve, and C. Ritz, 2020: Description and validation of the ice-sheet model Yelmo (version 1.0). *Geoscientific Model Development*, **13**, 2805–2823, doi:10.5194/gmd-13-2805-2020.

Robinson, A., R. Calov, and A. Ganopolski, 2011: Greenland ice sheet model parameters constrained using simulations of the Eemian Interglacial. *Climate of the Past*, **7**, 381–396, doi:10.5194/cp-7-381-2011.

Rohling, E., G. L. Foster, K. Grant, G. Marino, A. Roberts, M. E. Tamisiea, and F. Williams, 2014: Sea-level and deep-sea-temperature variability over the past 5.3 million years. *Nature*, **508**, 477, doi:10.1038/nature13230.

Rohling, E. J., K. Grant, M. Bolshaw, A. Roberts, M. Siddall, C. Hemleben, and M. Kucera, 2009: Antarctic temperature and global sea level closely coupled over the past five glacial cycles. *Nature Geoscience*, **2**, 500, doi:10.1038/NGEO557.

Sadatzki, H., T. M. Dokken, S. M. Berben, F. Muschitiello, R. Stein, K. Fahl, L. Menviel, A. Timmermann, and E. Jansen, 2019: Sea ice variability in the southern norwegian sea during glacial dansgaard-oeschger climate cycles. *Science advances*, **5**, eaau6174, doi:10.1126/sciadv.aau6174.

Sallée, J.-B., 2018: Southern ocean warming. *Oceanography*, **31**, 52–62, doi:10.5670/oceanog.2018.215.

Scambos, T. A., J. Bohlander, C. u. Shuman, and P. Skvarca, 2004: Glacier acceleration and thinning after ice shelf collapse in the larsen b embayment, antarctica. *Geophysical Research Letters*, **31**, doi:10.1029/2004GL020670.

Scambos, T. A., C. Hulbe, M. Fahnestock, and J. Bohlander, 2000: The link between climate warming and break-up of ice shelves in the Antarctic Peninsula. *Journal of Glaciology*, **46**, 516–530, doi:10.3189/172756500781833043.

Schaffer, J., R. Timmermann, J. E. Arndt, S. S. Kristensen, C. Mayer, M. Morlighem, and D. Steinhage, 2016: A global, high-resolution data set of ice sheet topography, cavity geometry, and ocean bathymetry. *Earth System Science Data*, **8**, 543, doi:10.5194/essd-8-543-2016.

Schellnhuber, H. J., S. Rahmstorf, and R. Winkelmann, 2016: Why the right climate target was agreed in Paris. *Nature Climate Change*, **6**, 649, doi:10.1038/nclimate3013.

Scherer, R. P., A. Aldahan, S. Tulaczyk, G. Possnert, H. Engelhardt, and B. Kamb, 1998: Pleistocene collapse of the west antarctic ice sheet. *Science*, **281**, 82–85, doi:10.1126/science.281.5373.82.

Schiermeier, Q., 2019: Antarctic project to drill for oldest-ever ice core. *Nature*, **567**, 442, doi:10.1038/d41586-018-07588-3.

Schlegel, N.-J., H. Seroussi, M. P. Schodlok, E. Y. Larour, C. Boening, D. Limonadi, M. M. Watkins, M. Morlighem, and M. R. Van Den Broeke, 2018: Exploration of Antarctic Ice Sheet 100-year contribution to sea level rise and associated model uncertainties using the ISSM framework. *The Cryosphere*, **12**, 3511–3534.

Schmidtko, S., K. J. Heywood, A. F. Thompson, and S. Aoki, 2014: Multidecadal warming of antarctic waters. *Science*, **346**, 1227–1231, doi:10.1126/science.1256117.

Schmitt, J., R. Schneider, J. Elsig, D. Leuenberger, A. Lourantou, J. Chappellaz, P. Köhler, F. Joos, T. F. Stocker, M. Leuenberger, et al., 2012: Carbon isotope constraints on the deglacial co2 rise from ice cores. *Science*, **336**, 711–714, doi:10.1126/science.1217161.

Schoof, C., 2007: Ice sheet grounding line dynamics: Steady states, stability, and hysteresis. *Journal of Geophysical Research: Earth Surface*, **112**, doi:10.1029/2006JF000664.

— 2010: Ice-sheet acceleration driven by melt supply variability. *Nature*, **468**, 803, doi:10.1038/nature09618.

Schulz, M., 2002: On the 1470-year pacing of dansgaard-oeschger warm events. *Paleoceanography*, **17**, 4–1, doi:10.1029/2000PA000571.

Seroussi, H. and M. Morlighem, 2018: Representation of basal melting at the grounding line in ice flow models. *The Cryosphere*, **12**, 3085–3096, doi:10.5194/tc-12-3085-2018.

Seroussi, H., M. Morlighem, E. Larour, E. Rignot, and A. Khazendar, 2014: Hydrostatic grounding line parameterization in ice sheet models. *The Cryosphere*,

8, 2075–2087, doi:10.5194/tc-8-2075-2014.

Seroussi, H., S. Nowicki, A. J. Payne, H. Goelzer, W. H. Lipscomb, A. Abe Ouchi, C. Agosta, T. Albrecht, X. Asay-Davis, A. Barthel, R. Calov, R. Cullather, C. Dumas, R. Gladstone, N. Golledge, J. M. Gregory, R. Greve, T. Hatterman, M. J. Hoffman, A. Humbert, P. Huybrechts, N. C. Jourdain, T. Kleiner, E. Larour, G. R. Leguy, D. P. Lowry, C. M. Little, M. Morlighem, F. Pattyn, T. Pelle, S. F. Price, A. Quiquet, R. Reese, N.-J. Schlegel, A. Shepherd, E. Simon, R. S. Smith, F. Straneo, S. Sun, L. D. Trusel, J. Van Breedam, R. S. W. van de Wal, R. Winkelmann, C. Zhao, T. Zhang, and T. Zwinger, 2020: ISMIP6 Antarctica: a multi-model ensemble of the Antarctic ice sheet evolution over the 21st century. *The Cryosphere Discussions*, doi:10.5194/tc-2019-324.

Seroussi, H., S. Nowicki, E. Simon, A. Abe-Ouchi, T. Albrecht, J. Brondex, S. Cornford, C. Dumas, F. Gillet-Chaulet, H. Goelzer, N. R. Golledge, J. M. Gregory, R. Greve, M. J. Hoffman, A. Humbert, P. Huybrechts, T. Kleiner, E. Larour, G. Leguy, W. H. Lipscomb, D. Lowry, M. Mengel, M. Morlighem, F. Pattyn, A. J. Payne, D. Pollard, S. F. Price, A. Quiquet, T. J. Reerink, R. Reese, C. B. Rodehacke, N.-J. Schlegel, A. Shepherd, S. Sun, J. Sutter, J. Van Breedam, R. S. W. van de Wal, R. Winkelmann, and T. Zhang, 2019: initMIP-Antarctica: an ice sheet model initialization experiment of ISMIP6. *The Cryosphere*, **13**, 1441–1471, doi:10.5194/tc-13-1441-2019.

Shackleton, N. J., M. A. Hall, and E. Vincent, 2000: Phase relationships between millennial-scale events 64,000–24,000 years ago. *Paleoceanography*, **15**, 565–569, doi:10.1029/2000PA000513.

Shaffer, G., S. M. Olsen, and C. J. Bjerrum, 2004: Ocean subsurface warming as a mechanism for coupling dansgaard-oeschger climate cycles and ice-rafting events. *Geophysical Research Letters*, **31**, doi:10.1029/2004GL020968.

Shakun, J. D., P. U. Clark, F. He, S. A. Marcott, A. C. Mix, Z. Liu, B. Otto-Bliesner, A. Schmittner, and E. Bard, 2012: Global warming preceded by increasing carbon dioxide concentrations during the last deglaciation. *Nature*, **484**, 49, doi:10.1038/nature10915.

Shapiro, N. M. and M. H. Ritzwoller, 2004: Inferring surface heat flux distributions guided by a global seismic model: particular applica-

tion to Antarctica. *Earth and Planetary Science Letters*, **223**, 213–224, doi:10.1016/j.epsl.2004.04.011.

Shepherd, A., E. Ivins, E. Rignot, B. Smith, M. Van Den Broeke, I. Velicogna, P. Whitehouse, K. Briggs, I. Joughin, G. Krinner, et al., 2018: Mass balance of the antarctic ice sheet from 1992 to 2017. *Nature*, **558**, 219–222, doi:10.1038/s41586-018-0179-y.

Sherif, M. M. and V. P. Singh, 1999: Effect of climate change on sea water intrusion in coastal aquifers. *Hydrological Processes*, **13**, 1277–1287, doi:10.1002/(SICI)1099-1085(19990615)13:8¡1277::AID-HYP765¿3.0.CO;2-W.

Siddall, M., E. J. Rohling, A. Almogi-Labin, C. Hemleben, D. Meischner, I. Schmelzer, and D. Smeed, 2003: Sea-level fluctuations during the last glacial cycle. *Nature*, **423**, 853, doi:10.1038/nature01690.

Siddall, M., E. J. Rohling, W. G. Thompson, and C. Waelbroeck, 2008: Marine isotope stage 3 sea level fluctuations: Data synthesis and new outlook. *Reviews of Geophysics*, **46**, doi:10.1029/2007RG000226.

Simms, A. R., L. Lisiecki, G. Gebbie, P. L. Whitehouse, and J. F. Clark, 2019: Balancing the last glacial maximum (lgm) sea-level budget. *Quaternary Science Reviews*, **205**, 143–153, doi:10.1016/j.quascirev.2018.12.018.

Steig, E. J., 2008: Sources of uncertainty in ice core data.

Steig, E. J., Q. Ding, D. Battisti, and A. Jenkins, 2012: Tropical forcing of Circumpolar Deep Water inflow and outlet glacier thinning in the Amundsen Sea Embayment, West Antarctica. *Annals of Glaciology*, **53**, 19–28, doi:10.3189/2012AoG60A110.

Stocker, T. F., 1998: The seesaw effect. *Science*, **282**, 61–62, doi:10.1126/science.282.5386.61.

— 2003: Global change: South dials north. *Nature*, **424**, 496, doi:10.1038/424496a.

Stocker, T. F. and S. J. Johnsen, 2003: A minimum thermodynamic model for the bipolar seesaw. *Paleoceanography*, **18**, doi:10.1029/2003PA000920.

Stockhecke, M., M. Sturm, I. Brunner, H.-U. Schmincke, M. Sumita, R. Kipfer, D. Cukur, O. Kwiecien, and F. S. Anselmetti, 2014: Sedimentary evolution

and environmental history of lake van (turkey) over the past 600 000 years. *Sedimentology*, **61**, 1830–1861, doi:10.1111/sed.12118.

Stolldorf, T., H.-W. Schenke, and J. B. Anderson, 2012: LGM ice sheet extent in the Weddell Sea: evidence for diachronous behavior of Antarctic Ice Sheets. *Quaternary Science Reviews*, **48**, 20–31, doi:10.1016/j.quascirev.2012.05.017.

Sun, S., F. Pattyn, E. G. Simon, T. Albrecht, S. Cornford, R. Calov, C. Dumas, F. Gillet-Chaulet, H. Goelzer, N. R. Golledge, et al., 2020: Antarctic ice sheet response to sudden and sustained ice-shelf collapse (ABUMIP). *Journal of Glaciology*, 1–14, doi:10.1017/jog.2020.67.

Sutter, J., H. Fischer, K. Grosfeld, N. B. Karlsson, T. Kleiner, B. Van Liefferinge, and O. Eisen, 2019: Modelling the Antarctic Ice Sheet across the mid-Pleistocene transition–implications for Oldest Ice. *The Cryosphere*, **13**, 2023–2041, doi:10.5194/tc-13-2023-2019.

Sutter, J., P. Gierz, K. Grosfeld, M. Thoma, and G. Lohmann, 2016: Ocean temperature thresholds for last interglacial west antarctic ice sheet collapse. *Geophysical Research Letters*, **43**, 2675–2682, doi:10.1002/2016GL067818.

Tabone, I., J. Blasco, A. Robinson, J. Alvarez-Solas, and M. Montoya, 2018: The sensitivity of the Greenland Ice Sheet to glacial–interglacial oceanic forcing. *Climate of the Past*, **14**, 455–472, doi:10.5194/cp-14-455-2018.

Tabone, I., A. Robinson, J. Alvarez-Solas, and M. Montoya, 2019: Impact of millennial-scale oceanic variability on the Greenland ice-sheet evolution throughout the last glacial period. *Climate of the Past*, **15**, 593–609, doi:10.5194/cp-15-593-2019.

Taylor, K. E., R. J. Stouffer, and G. A. Meehl, 2012: An overview of CMIP5 and the experiment design. *Bulletin of the American Meteorological Society*, **93**, 485–498, doi:10.1175/BAMS-D-11-00094.1.

The RAISED Consortium, 2014: A community-based geological reconstruction of Antarctic Ice Sheet deglaciation since the Last Glacial Maximum. *Quaternary Science Reviews*, **100**, 1–9, doi:10.1016/j.quascirev.2014.06.025.

Thoma, M., A. Jenkins, D. Holland, and S. Jacobs, 2008: Modelling circumpolar deep water intrusions on the Amundsen Sea continental shelf, Antarctica. *Geophysical Research Letters*, **35**, doi:10.1029/2008GL034939.

Thornalley, D. J., I. N. McCave, and H. Elderfield, 2010: Freshwater input and abrupt deglacial climate change in the North Atlantic. *Paleoceanography*, **25**, doi:10.1029/2009PA001772.

Tsai, V. C., A. L. Stewart, and A. F. Thompson, 2015: Marine ice-sheet profiles and stability under Coulomb basal conditions. *Journal of Glaciology*, **61**, 205–215, doi:10.3189/2015JoG14J221.

Turney, C. S. M., C. J. Fogwill, N. R. Golledge, N. P. McKay, E. van Sebille, R. T. Jones, D. Etheridge, M. Rubino, D. P. Thornton, S. M. Davies, C. B. Ramsey, Z. A. Thomas, M. I. Bird, N. C. Munksgaard, M. Kohno, J. Woodward, K. Winter, L. S. Weyrich, C. M. Rootes, H. Millman, P. G. Albert, A. Rivera, T. van Ommen, M. Curran, A. Moy, S. Rahmstorf, K. Kawamura, C.-D. Hillenbrand, M. E. Weber, C. J. Manning, J. Young, and A. Cooper, 2020: Early Last Interglacial ocean warming drove substantial ice mass loss from Antarctica. *Proceedings of the National Academy of Sciences*, doi:10.1073/pnas.1902469117.

van den Broeke, M., 2005: Strong surface melting preceded collapse of Antarctic Peninsula ice shelf. *Geophysical Research Letters*, **32**, doi:10.1029/2005GL023247.

Van Wessem, J., C. Reijmer, M. Morlighem, J. Mouginot, E. Rignot, B. Medley, I. Joughin, B. Wouters, M. Depoorter, J. Bamber, J. Lenaerts, W. van der Berg, M. van den Broeke, and E. van Meijgaard, 2014: Improved representation of East Antarctic surface mass balance in a regional atmospheric climate model. *Cambridge University Press*, **60**, 761–770, doi:10.3189/2014JoG14J051.

Vasskog, K., P. M. Langebroek, J. T. Andrews, J. E. Ø. Nilsen, and A. Nesje, 2015: The greenland ice sheet during the last glacial cycle: Current ice loss and contribution to sea-level rise from a palaeoclimatic perspective. *Earth-Science Reviews*, **150**, 45–67, doi:10.1016/j.earscirev.2015.07.006.

Vieli, A. and A. J. Payne, 2005: Assessing the ability of numerical ice sheet models to simulate grounding line migration. *Journal of Geophysical Research: Earth Surface*, **110**, doi:10.1029/2004JF000202.

WAIS Divide Project Members, 2015: Precise interpolar phasing of abrupt climate change during the last ice age. *Nature*, **520**, 661, doi:10.1038/nature14401.

Weaver, A. J., O. A. Saenko, P. U. Clark, and J. X. Mitrovica, 2003: Meltwater pulse 1a from antarctica as a trigger of the bølling-allerød warm interval. *Science*, **299**, 1709–1713, doi:10.1126/science.1081002.

Weber, M., P. Clark, G. Kuhn, A. Timmermann, D. Sprenk, R. Gladstone, X. Zhang, G. Lohmann, L. Menviel, M. Chikamoto, et al., 2014: Millennial-scale variability in antarctic ice-sheet discharge during the last deglaciation. *Nature*, **510**, 134, doi:10.1038/nature13397.

Weber, M., G. Kuhn, D. Sprenk, C. Rolf, C. Ohlwein, and W. Ricken, 2012: Dust transport from patagonia to antarctica–a new stratigraphic approach from the scotia sea and its implications for the last glacial cycle. *Quaternary Science Reviews*, **36**, 177–188, doi:10.1016/j.quascirev.2012.01.016.

Weertman, J., 1974: Stability of the junction of an ice sheet and an ice shelf. *Journal of Glaciology*, **13**, 3–11, doi:10.3189/S0022143000023327.

Whitehouse, P. L., 2018: Glacial isostatic adjustment modelling: historical perspectives, recent advances, and future directions. *Earth surface dynamics.*, **6**, 401–429, doi:10.5194/esurf-6-401-2018.

Whitehouse, P. L., M. J. Bentley, and A. M. Le Brocq, 2012a: A deglacial model for Antarctica: geological constraints and glaciological modelling as a basis for a new model of Antarctic glacial isostatic adjustment. *Quaternary Science Reviews*, **32**, 1–24, doi:10.1016/j.quascirev.2011.11.016.

Whitehouse, P. L., M. J. Bentley, G. A. Milne, M. A. King, and I. D. Thomas, 2012b: A new glacial isostatic adjustment model for Antarctica: calibrated and tested using observations of relative sea-level change and present-day uplift rates. *Geophysical Journal International*, **190**, 1464–1482, doi:10.1111/j.1365-246X.2012.05557.x.

Whitehouse, P. L., N. Gomez, M. A. King, and D. A. Wiens, 2019: Solid Earth change and the evolution of the Antarctic Ice Sheet. *Nature communications*, **10**, 503, doi:10.1038/s41467-018-08068-y.

Wilson, D. J., R. A. Bertram, E. F. Needham, T. van de Flierdt, K. J. Welsh, R. M. McKay, A. Mazumder, C. R. Riesselman, F. J. Jimenez-Espejo, and C. Escutia, 2018: Ice loss from the east antarctic ice sheet during late pleistocene interglacials. *Nature*, **561**, 383, doi:10.1038/s41586-018-0501-8.

Winkelmann, R., A. Levermann, M. A. Martin, and K. Frieler, 2012: Increased future ice discharge from antarctica owing to higher snowfall. *Nature*, **492**, 239, doi:10.1038/nature11616.

Winkelmann, R., M. A. Martin, M. Haseloff, T. Albrecht, E. Bueler, C. Khroulev, and A. Levermann, 2011: The Potsdam parallel ice sheet model (PISM-PIK)– Part 1: Model description. *The Cryosphere*, **5**, 715–726, doi:10.5194/tc-5-715-2011.

Wolovick, M. J. and J. C. Moore, 2018: Stopping the flood: could we use targeted geoengineering to mitigate sea level rise? *The Cryosphere*, **12**, 2955–2967, doi:10.5194/tc-12-2955-2018.

Wright, A. and M. Siegert, 2012: A fourth inventory of Antarctic subglacial lakes. *Antarctic Science*, **24**, 659–664, doi:10.1017/S095410201200048X.

Wunsch, C., 2006: Abrupt climate change: An alternative view. *Quaternary Research*, **65**, 191–203, doi:10.1016/j.yqres.2005.10.006.

Yokoyama, Y., T. M. Esat, W. G. Thompson, A. L. Thomas, J. M. Webster, Y. Miyairi, C. Sawada, T. Aze, H. Matsuzaki, J. Okuno, et al., 2018: Rapid glaciation and a two-step sea level plunge into the last glacial maximum. *Nature*, **559**, 603, doi:10.1038/s41586-018-0335-4.

Yu, H., E. Rignot, H. Seroussi, M. Morlighem, and Y. Choi, 2019: Impact of iceberg calving on the retreat of Thwaites Glacier, West Antarctica over the next century with different calving laws and ocean thermal forcing. *Geophysical Research Letters*, doi:10.1029/2019GL084066.

Zachos, J. C., T. M. Quinn, and K. A. Salamy, 1996: High-resolution (104 years) deep-sea foraminiferal stable isotope records of the eocene-oligocene climate transition. *Paleoceanography*, **11**, 251–266, doi:10.1029/96PA00571.

Zhang, X., G. Knorr, G. Lohmann, and S. Barker, 2017: Abrupt north atlantic circulation changes in response to gradual co2 forcing in a glacial climate state. *Nature Geoscience*, **10**, 518, doi:10.1038/ngeo2974.

Zhang, X., G. Lohmann, G. Knorr, and C. Purcell, 2014: Abrupt glacial climate shifts controlled by ice sheet changes. *Nature*, **512**, 290, doi:10.1038/nature13592.

Zoet, L. and N. Iverson, 2020: A slip law for glaciers on deformable beds. *Science*, **368**, 76–78, doi:10.1126/science.aaz1183.

Zwally, H., M. B. Jay, M. A. B. Giovinetto, and J. L. Saba, 2012: Antarctic and greenland drainage systems, gsfc cryospheric sciences laboratory.
URL http://icesat4.gsfc.nasa.gov/cryo_data/ant_grn_drainage_systems.php